Small-Angle Scattering by Cellulose

Structural changes in cellulosic materials under chemical and mechanical treatments

Velichko, Evgenii

DOI
10.4233/uuid:5383f365-fd5d-47ff-8826-e4d557c6e082

Publication date
2019

Document Version
Final published version

SMALL-ANGLE SCATTERING BY CELLULOSE

STRUCTURAL CHANGES IN CELLULOSIC MATERIALS UNDER CHEMICAL AND MECHANICAL TREATMENTS

SMALL-ANGLE SCATTERING BY CELLULOSE

STRUCTURAL CHANGES IN CELLULOSIC MATERIALS UNDER CHEMICAL AND MECHANICAL TREATMENTS

Proefschrift

ter verkrijging van de graad van doctor
aan de Technische Universiteit Delft,
op gezag van de Rector Magnificus prof. dr. ir. T. H. J. J. van der Hagen,
voorzitter van het College voor Promoties,
in het openbaar te verdedigen op woensdag 16 oktober 2019 om 12:30 uur

door

Evgenii VELICHKO

Master of Science in Chemistry,
Ural Federal University, Yekaterinburg, Russia,
geboren te Nizhny Tagil, Sovjet-Unie.

Dit proefschrift is goedgekeurd door de promotoren.

Samenstelling promotiecommissie:

Rector Magnificus,	voorzitter
Prof. dr. C. Pappas,	Technische Universiteit Delft, promotor
Dr. W. G. Bouwman,	Technische Universiteit Delft, copromotor

Onafhankelijke leden:

Prof. dr. S. J. Picken	Technische Universiteit Delft
Prof. dr. J. van Duynhoven	Wageningen University and Research
Prof. dr. E. van der Linden	Wageningen University and Research
Dr. M. Schooneveld-Bergmans	DSM Biotechnology Center
Dr. A. Petoukhov	Universiteit Utrecht
Prof. dr. E. H. Brück	Technische Universiteit Delft, reservelid

This work is part of the research program Open Technology with project number 13386 which is financed by the Netherlands Organization for Scientific Research (NWO).

Keywords: Cellulose, mesostructure, SAXS, SANS

Printed by: Ipskamp Printing

Front & Back: ...

ISBN/EAN 978-94-028-1720-1

An electronic version of this dissertation is available at
http://repository.tudelft.nl/.

Give me six hours to chop down a tree and
I will spend the first four sharpening the axe

Abraham Lincoln

The world will not be destroyed by those who do evil,
but by those who watch them without doing anything.

Albert Einstein

CONTENTS

PROPOSTIONS

1. In order to understand the multi-level hierarchical structure of cellulose one has to apply a broad range of research techniques.
2. Even measured in a limited range of momentum transfers, small-angle scattering of X-rays can provide a good indication for the specific surface area of the material under investigation.
3. A possibility to use the same sample environment for both neutron and X-ray experiments can substantially improve the reproducibility of the experiments.
4. In contrast to microcrystalline cellulose, a microfibrillated one does not align under shear rates below 300 s^{-1}.
5. The internal structure of microfibrillated citrus fiber flocs under shear rates below 300 s^{-1} at 20°C and atmospheric pressure can be considered constant.
6. Stable suspensions with a constant structure in a broad range of experimental conditions might be good for the final application, but incredibly boring to investigate.
7. The life of a PhD candidate is guided by the Pareto principle and steered by Murphy's law.
8. Obtaining a PhD degree is a lot like a marathon: you have to spread your resources for the whole distance; there is a finish line, but you don't see it most of the time; the last 20% of the distance is as hard as the first 80; and it is a very lonely journey.
9. Success in teaching new tricks to old cats does not justify the necessary investment of time and energy.
10. The most important relationship in one's life is the relationship with oneself.

STELLINGEN

1. Om de hiërarchische structuur op meerdere niveaus van cellulose te begrijpen, moet men een breed scala aan onderzoekstechnieken toepassen.

2. Zelfs als de metingen een klein bereik van het mogelijke momentumoverdracht beslaan, kan kleine hoek Röntgenverstrooiing een goede indicatie geven voor het specifieke oppervlak van het onderzochte materiaal.

3. Een mogelijkheid om dezelfde monsteromgeving te gebruiken voor zowel neutronen- als Röntgenexperimenten kan de reproduceerbaarheid van de experimenten aanzienlijk verbeteren.

4. In tegenstelling tot microkristallijne cellulose, lijnt een microgefibrilleerde cellulose niet uit onder afschuifsnelheden van minder dan 300 s^{-1}.

5. De interne structuur van microgefibrilleerde citrusvezelvlokken onder afschuifsnelheden van minder dan 300 s^{-1} bij 20 °C en atmosferische druk kan als constant worden beschouwd.

6. Stabiele suspensies met een constante structuur in een breed gebied van experimentele omstandigheden kunnen goed zijn voor de uiteindelijke toepassing, maar zijn ongelooflijk saai om te onderzoeken.

7. Het leven van een promovendus wordt geleid door het Pareto-principe en gestuurd door de wet van Murphy.

8. Het behalen van een doctoraat is vergelijkbaar met een marathon: je moet je middelen over de hele afstand spreiden; er is een finishlijn, maar die zie je meestal niet; de laatste 20% van de afstand is even moeilijk als de eerste 80; en het is een zeer eenzame reis.

9. Het succes in het aanleren van nieuwe trucen aan oude katten is geen rechtvaardiging voor de noodzakelijke investering van tijd en energie.

10. De belangrijkste relatie in je leven is de relatie met jezelf.

FOREWORD

We live in a strange world, where children must sacrifice their own education in order to protest against the destruction of their future

Greta Thunberg

History repeats itself. Any innovation goes through stages of pre-contemplation, contemplation, preparation, action, maintenance, relapse and back to pre-contemplation. In favorable circumstances, the innovation leads to improvement and the spiral progresses upward. Most of the time is spent in the pre-contemplation stage when everything seems fine and no problems hinder the horizon. The time necessary for the rest of the stages depends on the severity of the problem and desire to solve it. The fastest turns of the spiral were made in the most dramatic times of crisis, such as war. In such circumstances, nations seem to be able to mobilize most of their resources to solve the problem.

It is well scientifically established and proven that climate changes adversely and the change accelerated dramatically in the last century. The source of the change is also well established and agreed upon. However, little progress has been made in resolving the problem. Moreover, some of the contributors to greenhouse gas emissions are simply denying the facts, pretending the problem does not exist, and even aggravating the issue.

Mankind is capable of great accomplishments. However, it is important to keep in mind that mankind consist of individuals, and most of the accomplishments are due to the compound effect. It is, therefore, up to everyone to take an individual bit of responsibility and to contribute one's mite to the solution of climate change. Some examples of such individual contributions could be reductions in meat consumption, disposable cutlery, and plastic bags, and use of bicycle instead of cars for personal transportation up to 10 km.

The manuscript you read is another example of such a contribution. In the course of four years, the author had studied various kinds of cellulose and had become convinced that cellulose can and should be one of the major components of modern energy and materials mixes. The main intent of this book is to inspire the reader to step on the route towards a sustainable future and make a feasible contribution into achieving this goal. Although, with low probability, a butterfly can extinguish the fire.

Evgenii Velichko
Delft, October 2019

1

INTRODUCTION

THE ever–increasing world population demands an even faster increase in materials and energy production [1]. This demand not only rapidly diminishes the natural resources of our planet, but also leads to some adversary changes in our environment, such as global warming. Fossilized organic materials, used for production of lubricants, plastics, robbers, and fuels, can be exhausted in just over a century from now [2]. However, the scarcity of resources is not quite as dangerous as potential environmental damage of their accelerated consumption.

A comprehensive study of Arctic climate [3] clearly shows worldwide implications of the Arctic warming: glacial melt leads to rising sea level and slowing ocean circulation; increasing sea levels lead to increased exposure of coastal communities to storms and floods; a shift in vegetation zones caused by global warming is likely to cause increase in frequency, severity, and duration of forest fires.

Global problems require global solutions. Therefore, in 2016 in Paris 195 member states of the United Nations signed an agreement aimed at keeping the global average temperature increase below 2°C above pre-industrial levels. Under the agreement, each country must define and reach individual goal contributing towards the common aim of confinement of climate change.

Although every agreement participant can define their own route and means to conquer it, some basic requirements are common for everyone. It is clear, that the amount of greenhouse gases released into the atmosphere should be substantially decreased. Such decrease requires a fundamentally new approach to energy generation, recycling, and management of resources. Renewable sources of energy and chemicals will play an important role in such a new approach [4–8].

Biomass is one of the most obvious and abundant renewable resources [6]. Every year we can see fresh leaves and grass growing in the spring and dying out in the fall to form a nourishing substrate for the next generation. One of the main components of biomass is cellulose – a biopolymer responsible for mechanical properties and protection of plants from the environment. Let us consider this remarkable material in more detail in the following sections.

1

1.1. CELLULOSE AS A RENEWABLE POLYMER MATERIAL

Cellulose is the most abundant biopolymer on our planet. About 10^{10} to 10^{11}t of cellulose is produced globally every year[9]. Less than a tenth part of it is used by paper, textile, material and chemical industries [10]. Since its discovery in 1838 by Payen, physical and chemical characteristics of cellulose were thoroughly investigated [11].

On the molecular level, cellulose is a linear homopolysaccharide of β-1.4-linked anhydro-D-glucose units[12, 13] with a degree of polymerization varying between approximately 10000 and 15000 [9]. Due to the presence of hydroxyl groups in each monomer, cellulose chains tend to agglomerate already during the synthesis process and form elementary fibrils with alternating crystalline and amorphous regions along the cellulose chain [12].

The crystalline parts of cellulose exist in four different polymorph forms: cellulose I, II, III and IV. In nature native cellulose if found in form I with two allomorphs, I_α and I_β. After re-crystallization or mercerization of the cellulose I with aqueous sodium hydroxide, one obtains cellulose II, also known as regenerated cellulose. It is the most stable crystalline form of cellulose [13]. By ammonia treatment of cellulose I or II, one arrives to cellulose III_I or III_{II}, respectively. With the glycerol treatment of cellulose III one can produce cellulose IV.

The elementary fibrils of cellulose consist of about 36 individual cellulose macromolecules [12] and are about 5 nm in diameter. Agglomeration of the elementary fibrils during biosynthesis of cellulose leads to the formation of larger units called microfibrillated cellulose, which have diameters in the range of 20 to 50 nm. The micrifibrillated cellulose, in turn, agglomerates further to form cellulose fibers with the diameters in the micrometer domain.

Cellulose can be produced by plants [14], algae [15] and bacteria [16]. In plants and algae, cellulose is present in the walls of individual cells and is responsible for the plant's growth and form. In the case of bacteria, cellulose does not form a part of the organism but is extracted as a waste product. As a result of this difference in function, plant and algal cellulose is usually present in a highly agglomerated form mixed with several other biopolymers. Bacterial cellulose, on the other hand, usually present in much less aggregated state and pure of the other biopolymers.

Depending on the desired application, different forms of cellulose are required. In our quest towards more sustainable sources of energy and materials, we will take a closer look at two forms of cellulose, namely lignocellulosic biomass and microfibrillated cellulose.

1.1.1. LIGNOCELLULOSIC BIOMASS

Energy demand has more than doubled in the last decades and it is predicted to double once more in the coming decades. Most of the energy consumed worldwide comes from fossil fuels. Many alternatives to fossil fuels exist, including hydro, wind and solar energy. However, all of these alternatives generate energy only at the right environmental conditions and require batteries to store energy for the rest of the time. Biofuels, derived from biomass, can easily be stored in ready to use form. Moreover, most of the existing infrastructure and internal-combustion engines could be used with little to no modifications for biofuels.

First generation biofuels were known already in the 1880s when Henry Ford designed

early model Ts that ran on "farm ethanol". The biofuels are based on crops such as sugar cane and corn. However, the appearance of petroleum-derived fuels (fossil fuels) in the early twentieth century, has quickly changed the trend and fossil fuels dominated the market. It took the "oil crisis" of the 1970s for global leaders to realize the importance of alternative energy sources. Thanks to the National Alcohol Program, which started shortly after the crisis, Brazil has become the world leader in the development of bioethanol.

Ethanol has some advantages in comparison to gasoline, such as a higher octane number, leading to a superior net performance of the combustion engine running on ethanol [17], and increased power outputs due to the high vapor pressure and heat of vaporization. On the other hand, due to oxygen content, has about 33% less energy than gasoline [18]. Nevertheless, the vital advantage of ethanol is its small impact on the environment[19] in comparison to the hazardous effects of fossil fuels [20].

However, the first generation biofuels are not sustainable in the long-run, as they require fertile land and compete with traditional agriculture [21]. This competition also drives up the cost of raw materials, which can reach 40% of the bioethanol cost [22]. Therefore, recent developments in biofuels have focused on the second generation of biofuels, which are nonfood materials available from plants, also known as lignocellulosic biomass.

Lignocellulosic biomass is a cheap and abundant natural material, which can be found in the agricultural waste(wheat straw, corn stalks, soybean residues, sugar cane bagasse), industrial waste (pulp and paper industry), forestry residues, municipal solid waste, etc. [23]. According to Claassen et al. [24], lignocellulose accounts for about 50% of the annual production of biomass in the world ($1-5\cdot10^{11}$t), which could potentially cover yearly global energy demand. However, the efficiency of lignocellulose conversion into ethanol is still very low.

In order to turn bioethanol production into a sustainable process, one has to pay attention to various steps therein. The steps include synthesis of biomaterials, separation of valuable high-value chemicals from biomass feedstock, and generation of biofuels from the feedstock [6]. The challenge in biomass production is the development of crops with a suite of desirable physical and chemical traits while increasing biomass yields by a factor of 2 or more. One of the possible solutions would be to increase the initial capture of light energy above the current level of 2%. It was achieved, for example by overexpressing of the cyanobacterial versions of rate-limiting enzymes in the chrloroplast's carbon-fixing "dark reaction" in tobacco [25]. The experiment resulted in an elevated photosynthesis rate and increased plant dry weight. Another approach is to manipulate the plant's genes involved in nitrogen metabolism. Such an approach has led to a 41% increase in height of transgenetic poplar [26]. Genetic modification can also increase the plant's resistance to adverse environmental conditions and pathogens [27].

Once the biomass is collected it has to be converted into valuable biofuels and biomaterials. This conversion consists of several steps, including separation, refining, and transformation into chemicals and fuels. Firstly, high-value chemicals present in biomass should be extracted, such as fragrances, flavoring agents, food-related products, and high-value nutraceuticals, providing health and medical benefits [28]. Next, the remaining biomass has to go through further separation and depolymerization to convert plant

saccharides into feedstock for bio-derived materials and fuels. A range of solvents and conditions can be used for this purpose. Among them, supercritical CO_2, near-critical water and gas-expanded liquids [29, 30].

Once the biomass is reduced to biopolymers and lignin, the biofuel production starts. The key challenge in the process is recalcitrance of lignocellulose, present on multiple levels. Pretreatment of lignocellulosics is an important tool in facilitating the biomass conversion [31, 32]. A broad range of pretreatment techniques has been proposed for overcoming the recalcitrance and increasing the efficiency of biomass conversion [33]. The methods include mechanical[34], thermal[35–37], and thermo-chemical[38–45]. The methods have different working mechanisms and effect on various parameters of biomass [46, 47].

A deep understanding of the complex multi-level structure of biomass is necessary to establish a connection between pretreatment parameters and the biomass conversion efficiency. In solving the puzzle, one has to take into account as many structural characteristics of biomass as possible. In doing so, it is important to observe the changes in a broad range of length-scales. It is why in this work we applied a broad range of experimental techniques to cover 7 orders of magnitude in length-scales, from Å up to mm scale.

1.1.2. MICROFIBRILLATED CELLULOSE

Another form of cellulosic materials studied in this work is microfibrillated cellulose (MFC). It can be obtained by high-pressure disintegration of cellulosic fibers into fibrils [48, 49]. Quickly after its first description in 1983, it gained the attention of scientific community due to some very peculiar properties, such as high theoretical strength and modulus [50, 51], high surface area and water absorption [52], gelation at very low concentrations [53, 54].

A broad range of potential applications is proposed for MFC, ranging from protective coatings [55], and packaging [52] to food and cosmetics [56]. Most of the MFC-containing materials require shear conditions during preparation or application. Let us consider an application of MFC in low-caloric foods, as was suggested by Turbak in his pioneering work [48]. In the food production process MFC has to be mixed with other ingredients, and in the consecutive consumption process the food being sheared in the mouth and in the bowels of a consumer. In order to ascertain consistent and pleasant customer experience, the food producer has to ascertain the consistency of properties and performance of the product. This goal requires a deep understanding of the rheological behavior of MFC.

Already at very low solid content, microfibrillated cellulose forms network structures. Nechyporchuc et al. [57] have applied oscillatory shear to investigate the viscoelastic properties of TEMPO-oxidized MFC. They found that MFC suspensions remain stable at strain values up to 1%, after which the elastic network is destroyed, which was observed in nonlinear behavior of the storage and loss moduli. Strength of the elastic network was found to be dependent on the production conditions of MFC [58, 59]. The stronger network was linked to the higher specific surface area and a higher degree of entanglements of cellulose microfibrils. Saarinen et al. [60] have shown that storage modulus of mechanically disintegrated cellulose suspensions is inversely proportional to the degree

of cellulose fibrillation. Moreover, Naderi and Linstrom [58] have shown that the network strength of the enzymatically pretreated suspensions increases with the severity of fibrillation conditions when a preshear protocol is applied followed by rest. Without preshear the trend was reversed.

Independently of the way of production, all types of microfibrillated cellulose suspensions show shear-thinning behavior. Furthermore, the suspensions are thixotropic [61]. Due to these properties, the suspension properties are strongly time-dependent and the measurements should be performed at steady-state flow. Flow measurements were applied to indicate the degree of fibrillation of MFC. Herrick et al. [49] have shown the gradual increase of viscosity of mechanically fibrillated MFC with the increase in the number of passes in a homogenizer. Similar results were obtained by other groups [55, 62].

Reduction in the pH from 10 to 2 has been shown to increase the viscosity of enzymatically pretreated and disintegrated in a microfluidizer MFC suspensions [63]. The effect was explained by neutralization of the surface negative charge by protons and enhancement of interfibrillar interactions. Increase in temperature leads to decrease in viscosity of MFC [49, 64]. Yet another parameter, i.e. concentration, was found to increase the viscosity [64–69]. In a number of studies, a hysteresis loop was observed upon increasing-decreasing (or vice versa) of the shear rate [58, 64, 70]. This phenomenon was associated with the formation and breakdown of shear-induced structures in MFC suspensions.

In order to investigate those structures, Saarikoski et al.[71] and Karppinen et al. [72] have designed and applied a visualization setup based on a transparent Couette geometry. They have shown the presence of flocs of cellulose fibrils in the MFC suspensions and their evolution into rolls elongated along the Couette height under low apparent shear rates. A flow of detached flocs with flow sizes proportional to the shear rate was consequently observed under high shear rates. Martoia et al. [73] also applied a visualization approach to investigate the flow behavior of MFC suspensions, produced employing either enzymatic pretreatment or TEMPO-mediated oxidation. These materials showed behavior similar to described above: suspensions were in the form of floc chains (100-300μm), which split into individual flocs (< 100μm) with an increase of the shear rate.

Local flow properties of MFC suspensions were studied by combinations of flow measurements with an optical coherence tomography [74, 75], ultrasonic speckle velocimetry [73], and magnetic resonance imaging [76]. All of the measurements have shown appearance of the flocculated flow of MFC with decreasing in the floc sizes as a result of increasing shear rate.

Although many peculiar properties of MFC were already discovered and explained, the system still holds several mysteries. Many of these mysteries appear in the nm - μm length-scale domain. It is unknown how does the high-pressure homogenization affect the structure and sizes of elementary fibrils of cellulose, or how crowded the neighborhood of a typical cellulose fibril is. Flocculation of microfibrillated cellulose under shear is fascinating by itself, but even more interesting is the internal arrangement of the flocks and its evolution with the shear. In order to tackle these questions, we have employed small-angle X-ray scattering technique to the investigation of the microfibrillated cellulose based on citrus fiber.

1

SCOPE AND OUTLINE OF THE THESIS

By applying small angle scattering of X-rays, the mesostructure of cellulose-based materials has been investigated. The knowledge of structural changes happening in the material's structure during different chemical and mechanical treatments promotes its sustainable applications. This thesis is focused on two types of cellulosic materials, namely, lignocellulosic biomass (poplar) and MFC based on citrus fiber.

Firstly, the complex hierarchical structure and recalcitrance of lignocellulose are discussed in Chapter 2. A broad range of experimental techniques was applied to investigate changes happening to poplar biomass under acid pretreatment. The combination of techniques covers 7 orders of magnitude in length-scales, ranging from Å up to mm scale, which allowed to indicate the key structural parameters responsible for the efficiency of biomass conversion.

The next two chapters discuss the connection between the mesostructure of microfibrillated cellulose (MFC) and its rheological properties. In order to asses the mesostructure of MFC under shear, a special flexible geometry shear-SAS cell was created. The cell design and several applications are described in Chapter 3.

Chapter 4 describes an investigation of microfibrillated cellulose suspensions based on citrus fiber by means of rheology, rheo-MRI, SAXS, and shear-SAXS. All of the experimental results suggest that the materials are stable and consistent. Although flocculated flow is formed in the suspensions under shear, the process is completely reversible. Moreover, the flocs consist of randomly oriented intertwined microfibrils.

Chapter 5 describes an investigation of mesostructure of bacterial cellulose studied by small-angle neutron scattering. It was found that mesostructure of hydrogenated bacterial cellulose from different sources is very similar. However, deuteration of the cellulose leads to substantial changes in its mesostructure and rheological properties.

REFERENCES

[1] V. Smil, *Energy Transitions: Global and National Perspectives.* (2017).

[2] BP, *Statistical Review of World Energy*, Tech. Rep. 65 (2016).

[3] ACIA, *Impacts of a Warming Arctic - Arctic Climate Impact Assessment*, edited by C. Symon (Cambridge University Press, Cambridge, UK, 2004) p. 144.

[4] R. J. P. Schmitt, N. Kittner, G. M. Kondolf, and D. M. Kammen, *Deploy diverse renewables to save tropical rivers,* Nature **569**, 330 (2019).

[5] M. A. J. Huijbregts, S. Hellweg, R. Frischknecht, K. Hungerbühler, and A. J. Hendriks, *Ecological footprint accounting in the life cycle assessment of products,* Ecological Economics **64**, 798 (2008).

[6] A. J. Ragauskas, *The Path Forward for Biofuels and Biomaterials,* Science **311**, 484 (2006).

[7] D. J. C. Mackay, *Sustainable Energy — without the hot air*, Vol. 78 (2009) p. 383.

[8] S. Chu and A. Majumdar, *Opportunities and challenges for a sustainable energy future,* Nature **488**, 294 (2012).

[9] M. A. S. Azizi Samir, F. Alloin, and A. Dufresne, *Review of Recent Research into Cellulosic Whiskers, Their Properties and Their Application in Nanocomposite Field,* Biomacromolecules **6**, 612 (2005).

[10] J. Simon, H. Müller, R. Koch, and V. Müller, *Thermoplastic and biodegradable polymers of cellulose,* Polymer Degradation and Stability **59**, 107 (1998).

[11] M. Poletto, V. Pistor, and A. J., *Structural Characteristics and Thermal Properties of Native Cellulose,* in *Cellulose - Fundamental Aspects* (InTech, 2013) pp. 45–68.

[12] Y. Habibi, L. A. Lucia, and O. J. Rojas, *Cellulose nanocrystals: chemistry, self-assembly, and applications.* Chemical reviews **110**, 3479 (2010).

[13] G. Siqueira, J. Bras, and A. Dufresne, *Cellulosic Bionanocomposites: A Review of Preparation, Properties and Applications,* Polymers **2**, 728 (2010).

[14] M. Brown, I. Saxena, and K. Kudlicka, *Cellulose biosynthesis in higher plants,* Trends in Plant Science **1**, 149 (1996).

[15] I. Tsekos, *The sites of cellulose synthesis in algae:diversity and evolution of cellulose-synthesizing enzyme complexes,* Journal of Phycology **35**, 635 (1999).

[16] R. M. Brown, J. H. Willison, and C. L. Richardson, *Cellulose biosynthesis in Acetobacter xylinum: visualization of the site of synthesis and direct measurement of the in vivo process.* Proceedings of the National Academy of Sciences **73**, 4565 (1976).

[17] C. E. Wyman, *Ethanol Production from Lignocellulosic Biomass: Overview,* in *Handbook on Bioethanol: Production and Utilization*, edited by C. Wyman (Taylor & Francis, Washington, DC, 1996) Chap. 1, pp. 1–18.

[18] N. Kosaric, *Ethanol– Potential Source of Energy and Chemical Products,* in *Biotechnology*, edited by H. Rehm and G. Reed (Wiley-VCH Verlag GmbH, Weinheim, Germany, 2008) Chap. 4, pp. 121–203.

[19] M. A. Brown, M. D. Levine, J. P. Romm, A. H. Rosenfeld, and J. G. Koomey, *Engineering-economic studies of energy technologies to reduce greenhouse gas emissions: Opportunities and Challenges,* Annual Review of Energy and the Environment **23**, 287 (1998).

[20] OFD, *Review of the Research Strategy for Biomass-Derived Transportation Fuels* (National Academies Press, Washington, D.C., 1999).

[21] S. Naik, V. V. Goud, P. K. Rout, and A. K. Dalai, *Production of first and second generation biofuels: A comprehensive review,* Renewable and Sustainable Energy Reviews **14**, 578 (2010).

[22] M. von Sivers, G. Zacchi, L. Olsson, and B. Hahn-Haegerdal, *Cost Analysis of Ethanol Production from Willow Using Recombinant Escherichia coli,* Biotechnology Progress **10**, 555 (1994).

[23] A. Wiselogel, S. Tyson, and D. Johnson, *Biomass feedstock resources and composition,* in *Handbook on bioethanol: production and utilization*, edited by C. Wyman (Taylor and Francis, Washington, DC, 1996) Chap. 6, pp. 105–118.

[24] P. A. M. Claassen, J. B. van Lier, A. M. Lopez Contreras, E. W. J. van Niel, L. Sijtsma, A. J. M. Stams, S. S. de Vries, and R. A. Weusthuis, *Utilisation of biomass for the supply of energy carriers,* Applied Microbiology and Biotechnology **52**, 741 (1999).

[25] W. Van Camp, *Yield enhancement genes: seeds for growth,* Current Opinion in Biotechnology **16**, 147 (2005).

[26] Z. P. Jing, F. Gallardo, M. B. Pascual, R. Sampalo, J. Romero, A. T. De Navarra, and F. M. Cánovas, *Improved growth in a field trial of transgenic hybrid poplar overexpressing glutamine synthetase,* New Phytologist **164**, 137 (2004).

[27] B. Vinocur and A. Altman, *Recent advances in engineering plant tolerance to abiotic stress: achievements and limitations,* Current Opinion in Biotechnology **16**, 123 (2005).

[28] P. Morandini, F. Salamini, and P. Gantet, *Engineering of Plant Metabolism for Drug and Food,* Current Medicinal Chemistry-Immunology, Endocrine & Metabolic Agents **5**, 103 (2005).

[29] S. a. Nolen, C. L. Liotta, C. a. Eckert, and R. Gläser, *The catalytic opportunities of near-critical water: a benign medium for conventionally acid and base catalyzed condensations for organic synthesis,* Green Chem. **5**, 663 (2003).

[30] C. A. Eckert, C. L. Liotta, D. Bush, J. S. Brown, and J. P. Hallett, *Sustainable Reactions in Tunable Solvents,* The Journal of Physical Chemistry B **108**, 18108 (2004).

[31] N. MOSIER, *Features of promising technologies for pretreatment of lignocellulosic biomass,* Bioresource Technology **96**, 673 (2005).

[32] M. Foston and A. J. Ragauskas, *Biomass Characterization: Recent Progress in Understanding Biomass Recalcitrance,* Industrial Biotechnology **8**, 191 (2012).

[33] A. T. W. M. Hendriks and G. Zeeman, *Pretreatments to enhance the digestibility of lignocellulosic biomass,* Bioresource Technology **100**, 10 (2009), arXiv:1579-4377 .

[34] Z. Lin, H. Huang, H. Zhang, L. Zhang, L. Yan, and J. Chen, *Ball Milling Pretreatment of Corn Stover for Enhancing the Efficiency of Enzymatic Hydrolysis,* Applied Biochemistry and Biotechnology **162**, 1872 (2010).

[35] O. Bobleter, *Hydrothermal degradation of polymers derived from plants,* Progress in Polymer Science **19**, 797 (1994).

[36] G. Garrote, H. Domínguez, and J. C. Parajó, *Hydrothermal processing of lignocellulosic materials,* Holz als Roh- und Werkstoff **57**, 191 (1999).

[37] C. Liu and C. E. Wyman, *The Effect of Flow Rate of Compressed Hot Water on Xylan, Lignin, and Total Mass Removal from Corn Stover,* Industrial & Engineering Chemistry Research **42**, 5409 (2003).

[38] M. a. Kabel, G. Bos, J. Zeevalking, A. G. J. Voragen, and H. a. Schols, *Effect of pretreatment severity on xylan solubility and enzymatic breakdown of the remaining cellulose from wheat straw.* Bioresource technology **98**, 2034 (2007).

[39] M. Foston and A. J. Ragauskas, *Changes in lignocellulosic supramolecular and ultrastructure during dilute acid pretreatment of Populus and switchgrass,* Biomass and Bioenergy **34**, 1885 (2010).

[40] Q. Sun, M. Foston, X. Meng, D. Sawada, S. V. Pingali, H. M. O'Neill, H. Li, C. E. Wyman, P. Langan, A. J. Ragauskas, and R. Kumar, *Effect of lignin content on changes occurring in poplar cellulose ultrastructure during dilute acid pretreatment,* Biotechnology for Biofuels **7**, 150 (2014).

[41] G. Brodeur, E. Yau, K. Badal, J. Collier, K. B. Ramachandran, and S. Ramakrishnan, *Chemical and Physicochemical Pretreatment of Lignocellulosic Biomass: A Review,* Enzyme Research **2011**, e787532 (2011), arXiv:787532 .

[42] J. S. Kim, Y. Lee, and T. H. Kim, *A review on alkaline pretreatment technology for bioconversion of lignocellulosic biomass,* Bioresource Technology **199**, 42 (2016).

[43] P.-L. Tang, P. M. Abdul, N. S. Engliman, and O. Hassan, *Effects of pretreatment and enzyme cocktail composition on the sugars production from oil palm empty fruit bunch fiber (OPEFBF),* Cellulose (2018), 10.1007/s10570-018-1894-0.

[44] G. Bali, X. Meng, J. I. Deneff, Q. Sun, and A. J. Ragauskas, *The effect of alkaline pretreatment methods on cellulose structure and accessibility,* ChemSusChem **8**, 275 (2015).

[45] S. V. Pingali, V. S. Urban, W. T. Heller, J. McGaughey, H. O'Neill, M. B. Foston, H. Li, C. E. Wyman, D. A. Myles, P. Langan, A. Ragauskas, B. Davison, and B. R. Evans, *Understanding Multiscale Structural Changes During Dilute Acid Pretreatment of Switchgrass and Poplar,* ACS Sustainable Chemistry & Engineering **5**, 426 (2017).

[46] P. Harmsen, W. Huigen, L. Bermudez, and R. Bakker, *Literature Review of Physical and Chemical Pretreatment Processes for Lignocellulosic Biomass*, September (2010) pp. 1–54.

[47] L. J. Jönsson and C. Martín, *Pretreatment of lignocellulose: Formation of inhibitory by-products and strategies for minimizing their effects,* Bioresource Technology **199**, 103 (2016).

[48] A. F. Turbak, F. W. Snyder, and K. R. Sandberg, *Microfibrillated cellulose, a new cellulose product: properties, uses, and commercial potential,* (United States, 1983).

[49] F. W. Herrick, R. L. Casebier, J. K. Hamilton, and K. R. Sandberg, *Microfibrillated cellulose: morphology and accessibility,* (United States, 1983).

[50] D. G. Hepworth and D. M. Bruce, *Method of calculating the mechanical properties of nanoscopic plant cell wall components from tissue properties,* Journal of Materials Science **35**, 5861 (2000).

[51] Y.-C. Hsieh, H. Yano, M. Nogi, and S. J. Eichhorn, *An estimation of the Young's modulus of bacterial cellulose filaments,* Cellulose **15**, 507 (2008).

[52] K. L. Spence, R. A. Venditti, O. J. Rojas, Y. Habibi, and J. J. Pawlak, *The effect of chemical composition on microfibrillar cellulose films from wood pulps: water interactions and physical properties for packaging applications,* Cellulose **17**, 835 (2010).

[53] A. Naderi, T. Lindström, and T. Pettersson, *The state of carboxymethylated nanofibrils after homogenization-aided dilution from concentrated suspensions: a rheological perspective,* Cellulose **21**, 2357 (2014).

[54] S. J. Veen, A. Kuijk, P. Versluis, H. Husken, and K. P. Velikov, *Phase Transitions in Cellulose Microfibril Dispersions by High-Energy Mechanical Deagglomeration,* Langmuir **30**, 13362 (2014).

[55] F. Grüneberger, T. Künniger, T. Zimmermann, and M. Arnold, *Rheology of nanofibrillated cellulose/acrylate systems for coating applications,* Cellulose **21**, 1313 (2014).

[56] D. Klemm, E. D. Cranston, D. Fischer, M. Gama, S. A. Kedzior, D. Kralisch, F. Kramer, T. Kondo, T. Lindström, S. Nietzsche, K. Petzold-Welcke, and F. Rauchfuß, *Nanocellulose as a natural source for groundbreaking applications in materials science: Today's state,* Materials Today **21**, 720 (2018).

[57] O. Nechyporchuk, M. N. Belgacem, and F. Pignon, *Concentration effect of TEMPO-oxidized nanofibrillated cellulose aqueous suspensions on the flow instabilities and small-angle X-ray scattering structural characterization,* Cellulose **22**, 2197 (2015).

[58] A. Naderi and T. Lindstrom, *Rheological Measurements on Nanofibrillated Cellulose Systems: A Science in Progress,* in *Cellulose and Cellulose Derivatives: Synthesis, Modification and Applications*, edited by I. H. Mondal (Nova Science Publishers, Inc., New York, 2015) Chap. 10, pp. 187–204.

[59] O. Nechyporchuk, M. N. Belgacem, and F. Pignon, *Rheological properties of micro-/nanofibrillated cellulose suspensions: Wall-slip and shear banding phenomena,* Carbohydrate Polymers **112**, 432 (2014).

[60] T. Saarinen, M. Lille, and J. Seppälä, *Technical Aspects on Rheological Characterization of Microfibrillar Cellulose Water Suspensions,* Annual Transaction of the Nordic Rheology Society **17**, 121 (2009).

[61] J. Mewis and N. J. Wagner, *Thixotropy,* Advances in Colloid and Interface Science **147-148**, 214 (2009).

[62] H. Taheri and P. Samyn, *Effect of homogenization (microfluidization) process parameters in mechanical production of micro- and nanofibrillated cellulose on its rheological and morphological properties,* Cellulose **23**, 1221 (2016).

[63] M. Pääkkö, M. Ankerfors, H. Kosonen, A. Nykänen, S. Ahola, M. Österberg, J. Ruokolainen, J. Laine, P. T. Larsson, O. Ikkala, and T. Lindström, *Enzymatic Hydrolysis Combined with Mechanical Shearing and High-Pressure Homogenization for Nanoscale Cellulose Fibrils and Strong Gels,* Biomacromolecules **8**, 1934 (2007).

[64] M. Iotti, Ø. W. Gregersen, S. Moe, and M. Lenes, *Rheological Studies of Microfibrillar Cellulose Water Dispersions,* Journal of Polymers and the Environment **19**, 137 (2011).

[65] E. Lasseuguette, D. Roux, and Y. Nishiyama, *Rheological properties of microfibrillar suspension of TEMPO-oxidized pulp,* Cellulose **15**, 425 (2008).

[66] G. Agoda-Tandjawa, S. Durand, S. Berot, C. Blassel, C. Gaillard, C. Garnier, and J.-L. Doublier, *Rheological characterization of microfibrillated cellulose suspensions after freezing,* Carbohydrate Polymers **80**, 677 (2010).

[67] I. Besbes, M. R. Vilar, and S. Boufi, *Nanofibrillated cellulose from Alfa, Eucalyptus and Pine fibres: Preparation, characteristics and reinforcing potential,* Carbohydrate Polymers **86**, 1198 (2011).

[68] E. Dinand, H. Chanzy, and M. R. Vignon, *Parenchymal cell cellulose from sugar beet pulp: preparation and properties,* Cellulose **3**, 183 (1996).

[69] M. Mohtaschemi, K. Dimic-Misic, A. Puisto, M. Korhonen, T. Maloney, J. Paltakari, and M. J. Alava, *Rheological characterization of fibrillated cellulose suspensions via bucket vane viscometer,* Cellulose **21**, 1305 (2014).

[70] F. Bettaieb, O. Nechyporchuk, R. Khiari, M. F. Mhenni, A. Dufresne, and M. N. Belgacem, *Effect of the oxidation treatment on the production of cellulose nanofiber suspensions from Posidonia oceanica : The rheological aspect,* Carbohydrate Polymers **134**, 664 (2015).

[71] E. Saarikoski, T. Saarinen, J. Salmela, and J. Seppälä, *Flocculated flow of microfibrillated cellulose water suspensions: An imaging approach for characterisation of rheological behaviour,* Cellulose **19**, 647 (2012).

[72] A. Karppinen, T. Saarinen, J. Salmela, A. Laukkanen, M. Nuopponen, and J. Seppälä, *Flocculation of microfibrillated cellulose in shear flow,* Cellulose **19**, 1807 (2012).

[73] F. Martoïa, C. Perge, P. J. J. Dumont, L. Orgéas, M. A. Fardin, S. Manneville, and M. N. Belgacem, *Heterogeneous flow kinematics of cellulose nanofibril suspensions under shear,* Soft Matter **11**, 4742 (2015).

[74] T. Saarinen, S. Haavisto, A. Sorvari, J. Salmela, and J. Seppälä, *The effect of wall depletion on the rheology of microfibrillated cellulose water suspensions by optical coherence tomography,* Cellulose **21**, 1261 (2014).

[75] S. Haavisto, A. I. Koponen, and J. Salmela, *New insight into rheology and flow properties of complex fluids with Doppler optical coherence tomography,* Frontiers in Chemistry **2**, 1 (2014).

[76] D. de Kort, S. Veen, H. Van As, D. Bonn, K. Velikov, and J. van Duynhoven, *Yielding and flow of cellulose microfibril dispersions in the presence of a charged polymer,* Soft Matter (2016), 10.1039/c1sm05495c.

2

EFFECTS OF DILUTE ACID PRETREATMENT ON THE STRUCTURE OF POPLAR BIOMASS

Effects of dilute acid pretreatment on the structure of poplar biomass have been investigated by a variety of techniques: microscopy, small angle scattering and diffraction of X-rays. The pretreatment consists of exposure to 0.2% H_2SO_4 for 12 minutes (a mild pretreatment), or to 0.5% H_2SO_4 for 8 minutes (a severe pretreatment). The effectiveness of the pretreatment is measured as the glucose yield after 72 hours of enzymatic hydrolysis of the feedstock before and after pretreatment. The pretreatment results in the increase of the yield from 1% for initial poplar material to 50% after mild pretreatment and up to 70% after severe pretreatment. XRD has shown decrease of cellulose crystallinity in poplar from 50% in the initial material to 26% and 24% after the mild and severe pretreatments, respectively. SAXS analysis has allowed us to estimate the specific surface area of the materials in wet state. It has shown more than sevenfold increase of specific surface area after the mild pretreatment and almost ninefold increase after the severe pretreatment. Our findings suggest that the crystallinity index of cellulose and the specific surface area of the material are the main structural features responsible for optimum cellulose conversion; increase of pretreatment severity does not affect crystallinity index, but facilitates the conversion via increase in specific surface area of feedstock.

This chapter, by Evgenii Velichko, Margot Schooneveld-Bergmans, and Wim G. Bouwman, has been submitted to the scientifi journal: Cellulose

2.1. INTRODUCTION

Renewable sources of energy have attracted considerable attention from governments worldwide. It is widely recognized that the human civilization overuses fossil fuel resources and has almost exhausted them [1]. Moreover, this overuse has led to an enormous greenhouse gas release into the atmosphere and is one of the main causes of the global warming [2]. Biofuel is a viable alternative to fossil fuels [3]. It can be produced from starch or sugar sources; however, exploiting food sources requires expansion of fertile lands, which is not feasible. As an alternative, biofuel can be derived from lignocellulosic biomass, which includes agricultural and forestry residues, herbaceous and woody crops [4]. The main advantages of this source are abundance, carbon-neutrality and renewability. Therefore, lignocellulosic biomass is considered one of the most promising renewable energy sources. Cellulose, which is the main component of the lignocellulosic biomass, has a complex hierarchical structure [5–13]. On the molecular level, it is a long chain of glucose molecules. These macromolecules are bound together by hydrogen bonds and form alternating crystalline and amorphous regions of cellulose. To produce biofuel, cellulose has to be converted into glucose by enzymes, so-called enzymatic hydrolysis [14]. However, this process is hindered by various structural and compositional factors [15–17]. Several pretreatments have been proposed to make biomass more susceptible to hydrolysis, including mechanical [18–21], chemical [22–27] and thermochemical methods [25, 27–29]. Acidic pretreatment is one of the most promising and widely used among these. Researchers have reported a decrease in crystallinity and improved enzymatic digestibility of cellulose as a result of this pretreatment [30–35]. Therefore, recalcitrance of cellulose is attributed to its crystal structure. However, it is hard to imagine that changes of the most basic units of cellulose are happening without changes on the larger length scale. For alteration of crystallinity to take place, changes on the nanometer length scale should take place, so that crystallites become more accessible to acid for interaction. However, very little is known about the effect of pretreatment on nanometer and micrometer scales of cellulose.

Small angle scattering of X-rays and neutrons gives access to intermediate length scale, the mesostructure. It is commonly accepted that cellulose has several levels of organization in the nano- and micrometer length scale: elementary fibrils with diameters of several nm, microfibrils with diameters in the order of tens of nm and bundles of microfibrils with diameters in micrometer range [36, 37]. In recent years small angle scattering techniques were applied to a multitude of cellulosic materials, ranging from bacterial cellulose, to switchgrass and poplar [5, 7, 35, 38–41]. A core-shell cylinder model with absolute power law for fitting of the SAS data, proposed by a group of Gilbert [5] was recently successfully applied to bacterial cellulose and cotton materials [38, 42]. In combination with the XRD data, this model gives valuable insights into the hierarchical structure fo cellulosic materials. A recent small-angle neutron scattering research of switchgrass and poplar by Pingali *et al.* gave valuable insights into structural changes in cellulosic materials and concluded that "cellulose accessibility is the decisive factor in increasing glucose yields, while cellulose crystallinity and lignin aggregation play lesser roles." However, the researchers were using a multilevel unified fit, which is considerably ambiguous.

In this study we have applied a multi-technique approach based on microscopy,

small-angle scattering and X-ray diffraction to study structural changes in poplar biomass. This combination allowed us to assess structural changes in cellulose over a wide range of length scales (from Ångström scale up to millimeter scale). Moreover, the link between the changes in mesostructure and enzymatic digestibility of the cellulose material was established with the help of high performance liquid chromatography. By comparing the structural parameters with the cellulose digestibility, we outlined the key structural features responsible for optimum cellulose digestion. This approach can be used to evaluate the effects of pretreatment on the mesostructure of biomass, thus facilitating the development of a sustainable process for the production of the biofuel.

2.2. MATERIALS AND METHODS

2.2.1. MATERIALS AND PRETREATMENT

The initial poplar material was pretreated with two different concentrations of sulfuric acid: 0.2% (mildly treated poplar, MP) and 0.5% (severely treated poplar, SP). Firstly, chipped poplar feedstock was mixed with diluted sulfuric acid to reach 40% feedstock dry matter and required concentration of sulfuric acid. After soaking for 16 hours the mixtures were transferred to a bench scale reactor and heated with steam to 180°C for 12 minutes (MP), or to 190°C for 8 minutes (SP). At the end of the reaction time, the temperature and pressure were instantly dropped by opening a valve of the reactor, and the pretreated feedstock and liquid were collected. After acid treatment feedstock was separated from liquid, washed with demineralized water and used for further analysis. The dry matter content was approximately 30%. 2 ml of each sample were kept in the wet state for SAXS experiments and were stored in a fridge at 4°C. The rest of the samples were dried at 50° C till constant weight and were stored at room temperature in closed beakers.

2.2.2. FEEDSTOCK COMPOSITION

Total sugar composition was determined based on NMR analysis of acid hydrolyzed feedstock according to the method of Carvalho de Souza *et al.* [43].

2.2.3. MICROSCOPY

Bright field and fluorescence microscopy were performed using the Keyence BZ8000 Fluorescence microscope (Biozero). The exposure time settings of the microscope for optimal fluorescent signal were determined automatically by the software of the microscope. The image size of an image is 680 x 512 pixels. Samples under investigation were placed in silicone isolators from Grace Biolabs (Press-to-seal Silicone isolator) with a depth of 0.5 mm and a diameter of 20 mm (Sigma GBL666505).

2.2.4. X-RAY DIFFRACTION ANALYSIS

The X-ray diffraction (XRD) measurements were carried out at the Reactor Institute Delft using a PANalytical X'Pert pro X-ray diffractometer with Cu-Kα radiation ($5^\circ \leq 2\theta \leq 80^\circ$ with a step size of 0.008° (2θ); total measuring time was 1 h per sample). All the samples were dried prior to XRD measurements. All measurements were performed at room temperature and atmospheric pressure.

The crystallinity indexes (X_C) were determined by the method proposed by Teeäär, Serlmaa and Paakkari [44], and successfully applied by several groups [38, 45–47]:

$$X_C(\%) = \frac{\Sigma A_{Crystal}}{A_{Total}} \times 100, \tag{2.1}$$

where A_{Total} is the sum of the areas under all the diffraction peaks and $\Sigma A_{Crystal}$ is the sum of the areas corresponding to the three crystalline peaks.

The apparent crystallite sizes ($\tau_{(hkl)}$) were calculated using the Scherrer's equation [48]:

$$\tau_{(hkl)} = \frac{K \times \lambda}{\beta_{(hkl)} \times \cos(\theta_{(hkl)})}, \tag{2.2}$$

where K is a constant of value 0.9, λ is the X-ray wavelength (0.1542 nm), β is the half-height width of the diffraction band in radians, and 2θ is the Bragg angle corresponding to the (hkl) plane.

2.2.5. SMALL ANGLE X-RAY SCATTERING (SAXS)

Small angle X-ray scattering experiments were performed at the high-brilliance ID02 beamline of the European Synchrotron Radiation Facility (ESRF) in Grenoble, France. Details of the experimental setup are given elsewhere [49]. Data were collected in the range 3×10^{-4}Å$\leq q \leq 0.7$Å, where $q = \frac{4\pi}{\lambda}\sin(2\theta)$ is the momentum transfer, where θ is a scattering angle and λ the wavelength of the used X-rays (in our experiments λ=0.0996 nm). Measurements were performed in transmission mode. All samples were in the form of a suspension in water with a dry material content of about 30 %. Each sample was placed in a 30 position temperature stage with aluminum sample holders between mica windows, and the temperature of the sample cell kept constant at 20°C. A scattering pattern of 2 mm of water between two mica windows was used for background subtraction for all the measurements. The scattering intensities were scaled to absolute units [cm^{-1}] using a water reference ($I_{H_2O,20°C} = 1.641 \cdot 10^{-2} cm^{-1}$).

2.2.6. SAXS DATA ANALYSIS

Two-step analysis was performed to describe SAXS data. Firstly, from Porod law [50] and scattering invariant we determined the fraction of water absorbed by the particles, their effective scattering length density contrast, effective density and volume fraction, as well as specific surface areas.

The scattering invariant is defined as

$$Q^* = \int_{-\infty}^{\infty} q^2 \Delta I(q) dq, \tag{2.3}$$

and can be calculated for a 2 phase system as

$$Q^* = 2\pi^2 \varphi (1-\varphi)(\Delta\rho)^2, \tag{2.4}$$

where φ is the volume fraction of the scattering particles and $\Delta\rho$ is their scattering length density contrast with the solvent.

The specific surface area can be determined from the invariant as

$$S_I = \frac{2\pi\varphi(1-\varphi)K_p}{Q^* D}, \tag{2.5}$$

where K_p is the Porod scale factor, and D is the mass density of the particle. Some more details on the evaluation of specific surface area are provided in section 2.3.4.

In case if the particles can soak in the solvent, we can modify the Eq. 2.4 as

$$Q^* = 2\pi^2(\varphi+c)(1-(\varphi+c))\left(\frac{\Delta\rho\cdot\varphi}{\varphi+c}\right)^2 = 2\pi^2\cdot\varphi_{ef}\cdot(1-\varphi_{ef})\cdot\Delta\rho_{ef}^2, \tag{2.6}$$

where c is the fraction of the solvent absorbed by the particles, and $\varphi_{ef} = \varphi + c$ and $\Delta\rho_{ef} = \frac{\Delta\rho\cdot\varphi}{\varphi+c}$ are effective volume fraction and scattering length density contrast. As the second step in the analysis of SAXS data, all of the scattering curves were fitted using SASView [51] software and applying the core-shell model described in [7, 52]. The model consists of a power-law and a core-shell cylinder form-factor:

$$I(q) = \frac{sf}{V}\cdot\sum_{R_{core}} n(R_{core},\sigma_{core})\cdot P(q,R_{core},R_{shell},L, \tag{2.7}$$
$$\rho_{core},\rho_{shell},\rho_{solv}) + A\cdot q^{-m} + bckg,$$

where the first term corresponds to the form factor of a core-shell cylinder with polydisperse core radii, multiplied by the number density of particles (sf/V), where V is the total volume of the particle, the second term accounts for the power-law scattering of large clusters, and the third term corresponds to the incoherent background remaining after solvent background subtraction. A detailed description of the form factor function and the parameters defining the model can be found elsewhere [7].

2.2.7. SURFACE AREA

The specific surface area for all the samples was measured by nitrogen adsorption according to Brunauer-Emmett-Teller (BET) theory [53] using Micromeritics Tristar 3000 analyzer at Ural Federal University in Yekaterinburg, Russia.

2.2.8. GLUCOSE RELEASE

All of the powder samples were suspended in an acetate buffer at pH of 4.5 and 2% weight concentration of dry material. Resulting slurries were stirred for 16 hours in order to assure sufficient wetting of the material. After stirring, two aliquots of 950 μL of each slurry were transported into 2 mL Eppendorf tubes. One tube of each material, indicated as t=0, was filled with water to make 1000 μL of 1.9% material and stored in a freezer at -20°C for further analysis. The remaining tubes were preheated to 60°C in a thermomixer. Following preheating, an overdose of cellulase cocktail was added to each tube, making concentrations of 1.9% in each tube. All of the tubes were left in Thermomixer at 60°C and shaking at 1000 rpm and were taken away and set on ice 72 hours after addition of enzymes. The pH of all samples was checked after hydrolysis and was 4.45. The samples were centrifuged and filtered to remove all solids.

The monosugars profile of the samples after enzymatic hydrolysis was analyzed using high-performance anion exchange chromatography (HPLC) with pulsed amperometric detection (Dionex ICS-500 with AS-AP autosampler). The samples were separated on a CarboPac PA-20 column preceded by a CarboPac PA-20 guard-column, by elution for 19 minutes in 5 mM NaOH at a flow rate of 0.5 ml/min. The column was washed by solutions of NaOH with gradually increasing concentration up to 380 mM, and 6 minutes with 380 mM NaOH solution. Subsequently, the column was equilibrated to 5 mM NaOH. Quantification of glucose was done using the response factor of the glucose standard.
The glucose yield is calculated in the following way:

$$Yield(\%) = \frac{C_{meas}}{C_{max}} \cdot 100\% = \frac{C_{meas}}{C_{cell} \cdot C_{DM} \cdot C_{slurry}} \cdot 100\%, \tag{2.8}$$

where C_{meas} is the measured concentration of glucose, C_{max} is the potential maximal concentration of glucose in the sample, C_{cell} is the concentration of cellulose in the dry material, C_{DM} is the concentration of dry matter in the material, and C_{slurry} is the concentration of material in the slurry with the enzyme cocktail.

2.3. RESULTS

2.3.1. FEEDSTOCK COMPOSITION

According to NMR analysis of the of acid hydrolyzed feedstock, the initial poplar material contains 45.9% wt. of glucan (cellulose), 10.8% wt. of xylan, 3.8% wt. water, and the remaining 39.5% wt. are attributed primarily lignin and some other hemicellulose sugars. The values obtained are in a good agreement with the typical composition of poplar [54].

Table 2.1: Densities and X-ray SLDs for the components of poplar biomass, based on [7, 55]

Component	Density (g/cm^3)	X-ray SLD (10^{10} cm^{-2})
Cellulose (crystalline)	1.60	14.46
Cellulose (amorphous)	1.48	13.38
Xylan	1.40	12.71
Lignin	1.40	12.59
H_2O	1.00	9.47

2.3.2. MICROSCOPY

Bright field and fluorescent light microscopy images of all the investigated samples are shown in Fig. 2.1. As can be seen from Fig. 2.1(a), initial poplar material is composed of rather big particles with typical dimensions above 1.1 mm (horizontal dimension of the field of view of the images). Evidently, pretreatment resulted in smaller particle sizes. On Fig. 2.1(c) one can see two kinds of particles: one with sizes of some 100 μm and the other with sizes of some 10 μm. The sizes of poplar particle after severe pretreatment

are more homogeneously distributed in the 10 μm size domain. Fig. 2.1(b,d,f) show a homogeneous distribution of lignin on the surface of the particles.

2.3.3. X-RAY DIFFRACTION ANALYSIS

X-ray diffractograms are presented in the Fig. 2.2. Three distinct peaks at ca. 2θ = 16°,22.5° and 35° can be observed for the initial and treated poplar materials. These diffraction peaks were attributed to the (110), (200) and (040) crystalline planes of the highly recalcitrant cellulose I allomorph. Although, cellulose I is a mixture of two crystalline forms: I_α (triclinic) and I_β (monoclinic) [56, 57] with slightly different d-spacings, and, therefore, positions of the diffraction peaks, in this study we did not make the distinction between the two, as the complexity and inhomogeneity of the studied material did not allow for a thorough profile analysis of the diffractograms. They were normalized by their respective areas under the curve. In this way we can directly quantify the impact of different sample components on the total diffractogram, as the total area under the curve after normalization is equal to 1 and corresponds to the sum of all the components present in the material.

The crystallinity indexes (X_C) and average crystallite sizes and d-spacings are presented in Tab. 2.2. Crystallinity index defined by the deconvolution method has decreased almost twice in the course of pretreatment, but there is a small difference between crystallinity of mildly and severely treated materials. The average crystallite sizes in the direction perpendicular to the (200) plane (τ_{200}) are increasing in the course of pretreatment and the more severe pretreatment results in the bigger crystallites. A similar effect was observed previously for switchgrass[35], where authors have suggested a coalescence of neighboring crystalline fibrils as an underlying mechanism for this change. Another possible explanation for this phenomenon could be a preferential destruction of the smaller crystallites in the course of the acidic pretreatment. It could lead to the shift of average crystallite sizes towards higher values.

Based on the values for the composition and crystallinity of the studied materials, we have calculated the maximal values for the density, scattering length density contrast, and minimal volume fractions of the particles (assuming, no pores are present and the materials consists only of the components listed in the Tab. 2.1). The calculated values are listed in Tab. 2.3).

Table 2.2: Crystallinity indexes (X_C), average crystallite sizes (τ), and the corresponding d-spacing for the (200) crystalline plane of the poplar biomass samples

Material	Poplar, initial material	Poplar, mildly treated	Poplar, severely treated
X_C (%)	23(1)	12(1)	11(1)
d_{200} (Å)	3.9(4)	3.8(8)	3.9(2)
τ_{200} (nm)	5.2(2)	6.9(8)	7.9(2)

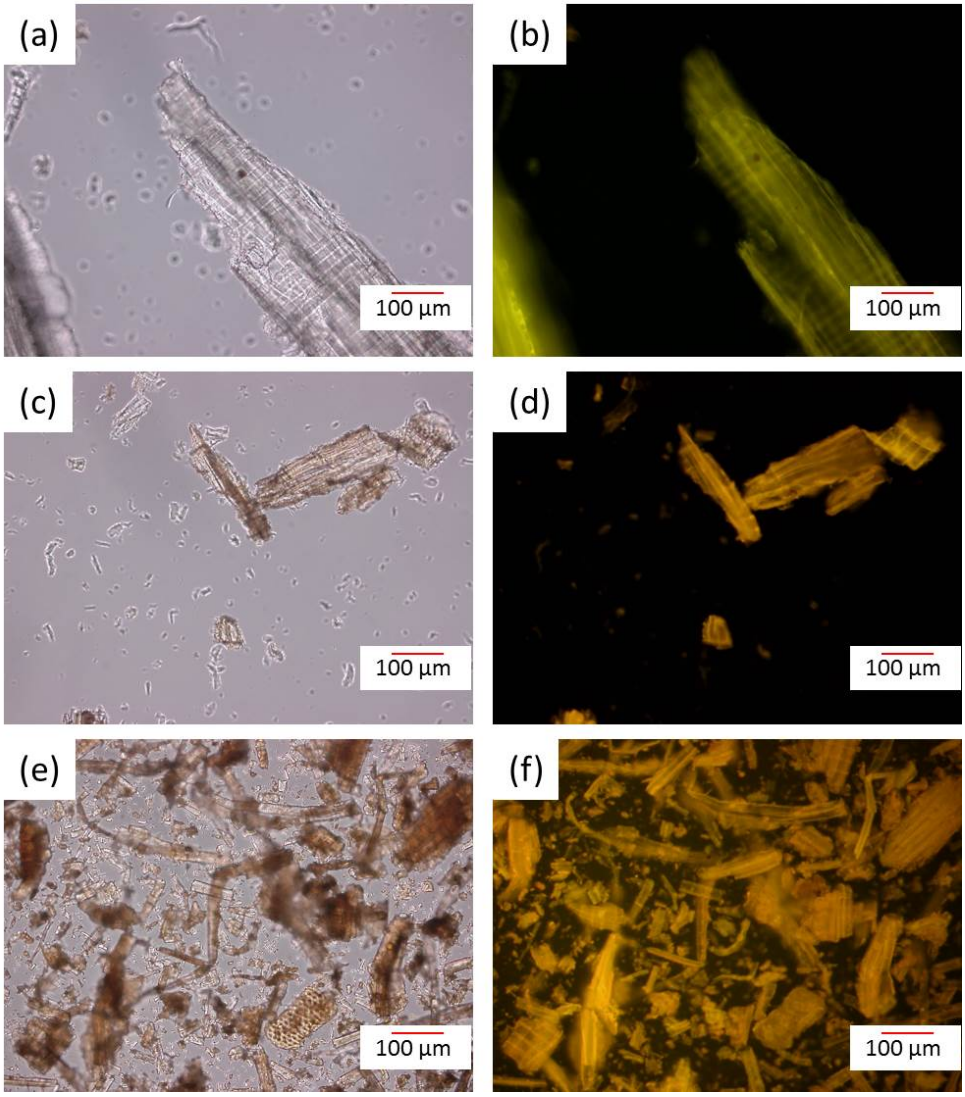

Figure 2.1: Bright field (a, c, e) and fluorescent (b, d, f) light microscopy of the samples before and after pretreatment: (a) typical image of the initial poplar material with (b) respective luminescent image, (c) poplar material after a mild treatment with (d) respective luminescent image,(e) poplar material after the severe treatment with (f) respective luminescent image

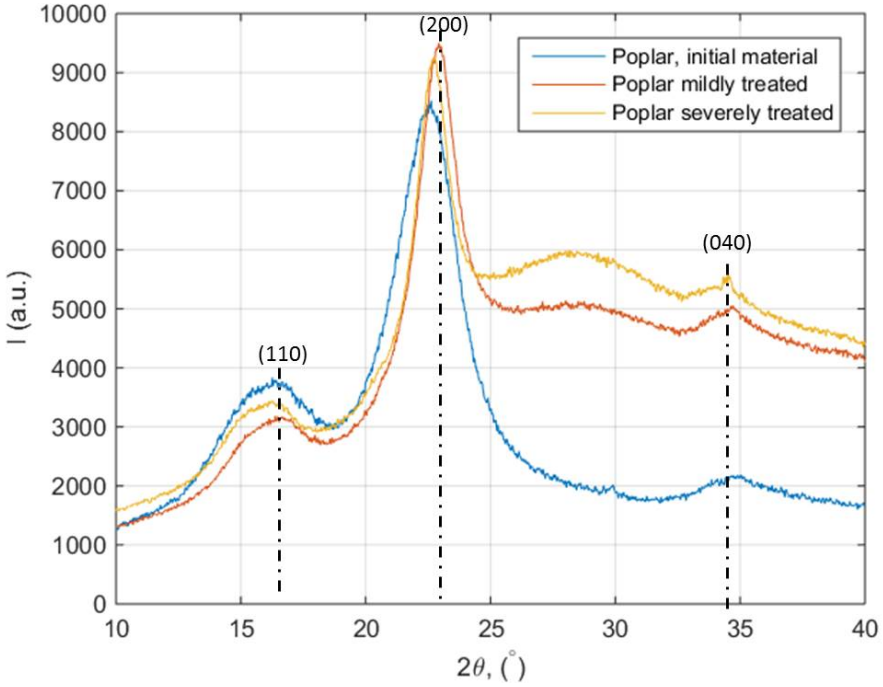

Figure 2.2: XRD patterns of poplar materials before and after acidic pretreatment

2.3.4. SMALL ANGLE X-RAY SCATTERING (SAXS)

All of the data related to the analysis of the scattering invariant are collected in Tab. 2.3. Firstly, we have determined the background level from the Porod plots for all of the scattering curves. Once we knew the exact value of background, we could calculate the invariants for each of the curves. It should be noted, that no extrapolations were made in low- or high q regions, only the measured q region was used for the invariant calculations. The measured and calculated values for the invariant, maximal $\Delta\rho$ and minimal φ were filled in Eq. 2.6 and the equation was solved for the fraction of absorbed water c. Based on the c values we could calculate values for $D_{ef}, \Delta\rho_{ef}$, and φ_{ef} values. It should be noted that for the dry sample of the initial poplar material the volume fraction could not be well estimated from the sample thickness and density as the particle of the material are not uniform and the beam size was about 8000 μm^2. However, we could calculate the volume fraction from the scattering invariant.

Table 2.3: Data relevant for the SAXS analysis

Material	Poplar dry, initial material	Poplar wet, initial material	Poplar, mildly treated	Poplar, severely treat
Background (cm^{-1})	0.008	0.037	0.014	0.0147
Scattering invariant Q^* (cm^{-1}Å^{-3})	0.00376	0.00118	0.00109	0.00117
Maximal density D (g/cm^3)	1.4491	1.4491	1.4359	1.4347
Maximal ρ (10^{10} cm^{-2})	13.089	13.089	12.970	12.959
Maximal $\Delta\rho$ (10^{10} cm^{-2})	13.089	3.619	3.500	3.489
Minimal φ	n.a.	0.228(1)	0.229(1)	0.229(1)
Fraction of absorbed water c	n.a.	0.305(1)	0.310(1)	0.290(1)
Effective density D_{ef} (g/cm^3)	n.a	1.312(1)	1.301(1)	1.309(1)
Effective ρ_{ef} (10^{10} cm^{-2})	n.a.	11.019(1)	10.960(1)	11.013(1)
Effective $\Delta\rho_{ef}$ (10^{10} cm^{-2})	n.a.	1.549(1)	1.490(1)	1.543(1)
Effective φ_{ef}	0.989(1)	0.533(1)	0.539(1)	0.519(1)

Small-angle X-ray scattering curves with the fitting results are presented in Fig. 2.3. Tab. 2.4 shows all of the fitting parameters of the model.

2.3.5. SPECIFIC SURFACE AREA

Results of specific surface area measurements are presented in Tab. 2.5. It is clear that treatment of poplar biomass has resulted in substantial increase of the specific surface area and higher severity of pretreatment resulted in higher increase.

2.3.6. GLUCOSE RELEASE

The glucose yield after enzymatic hydrolysis is presented in Tab. 2.6. Acidic pretreatment leads to much higher levels of glucose conversion and the more severe pretreatment results in the higher glucose yield.

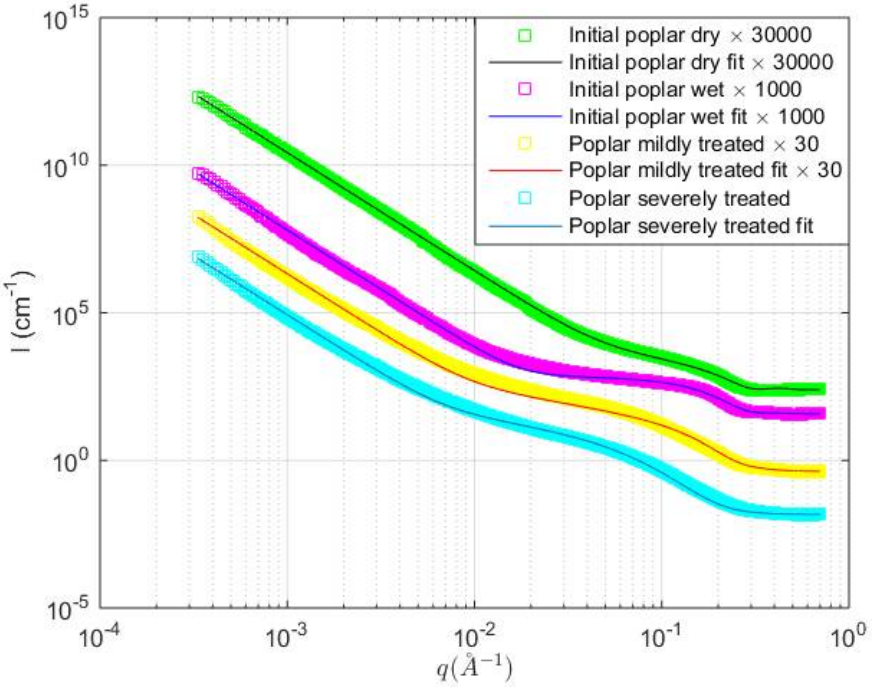

Figure 2.3: Small-angle X-ray scattering curves for all of the samples and the corresponding fits

Table 2.4: Parameters of the model for the mesostructure of poplar biomass

Parameter	Poplar, dry	Poplar wet	Poplar, mild treated	Poplar, severe treated
Scale factor	0.080(1)	0.027(3)	0.020(1)	0.018(1)
Length (Å) *	21000	30.5(1)	21000	21000
Core radius (Å)	11.0(1)	9.0(1)	12.1(1)	14.2(1)
Polydispersity	0.10(1)	0.20(1)	0.35(1)	0.40(1)
Shell thickness (Å)	2.0(1)	1.3(1)	2.0(1)	2.0(1)
ρ_{core}, (10^{10} cm^{-2}) *	14.46	14.46	14.46	14.46
ρ_{shell}, (10^{10} cm^{-2})	12.60(1)	12.60(1)	12.60(1)	12.60(1)
ρ_{solv}, (10^{10} cm^{-2}) *	13.089	9.47	9.47	9.47
Power-law coefficient (K_{APL})	$8.9(1)\cdot10^{-7}$	$6.3(1)\cdot10^{-8}$	$7.0(1)\cdot10^{-8}$	$8.6(1)\cdot10^{-8}$
Power-law exponent (m) *	4	4	4	4

* parameters which were fixed in the fitting process

Table 2.5: Specific surface area for all of the materials, determined by the N2-BET adsorption method, and derived from the SAXS data

Material	SSA (m^2/g) from BET*	SSA (m^2/g) from SAXS
Poplar, dry	0.07(1)	0.10(1)
Poplar, mildly treated	0.38(1)	0.77(1)
Poplar, severely treated	0.64(1)	0.88(1)
Poplar, wet	n.a.	0.64(1)

2.4. DISCUSSION

The crystallinity of the poplar materials has been determined from XRD characterization. The crystallinity index X_C of the material decreases in the course of the pretreatment decreases from 23% in the initial poplar material to 12% in the mildly- and even to 11% in the severely treated samples. In terms of cellulose crystallinity (normalizing X_C by the content of cellulose in the material), this means: from 50% to 26% and 24%, respectively. It should be noted, that in publications on crystallinity of lignocellulosic biomass, XRD peak height method [58] is the most used up until now. However, it gives substantially higher crystallinity values in comparison with other techniques [31], moreover, in our analysis, values obtained by this method were significantly higher than total cellulose content in the material, which simply could not be true. Average crystallite sizes,also obtained from the XRD analysis, have shown a slight increase in the course of acidic pretreatment.

Water holding capacity and specific surface area were determined from the scattering invariant analysis of the SAXS data. Since the scattering exponent in the low q region was always equal to 4, we can conclude that particles of all studied materials have a sharp interface with the solvent and do not show any fractal properties. All materials are

Table 2.6: Glucose yields for all of the studied materials after 72 hours of enzymatic hydrolysis

Material	Glucose yield after 72 hours of enzymatic hydrolysis (%)
Poplar, initial material	1.0(5)
Poplar, mildly treated	50(4)
Poplar, severely treated	70(4)

able to hold 1.5 volume of water per volume of the dry material. Specific surface area of the materials has increased as the result of the pretreatment, with the higher increase corresponding to the higher severity of the pretreatment. Since no change in the topological dimension of the particle surface (scattering exponent) was observed as a result of the pretreatment, the only possible explanation for the increase of the specific surface area of the materials is the decrease in average particle sizes. This decrease is outlined in the results of light microscopy. The specific surface area values obtained from SAXS analysis were compared to ones from BET analysis. The values for the dry initial material, obtained by both methods are in good agreement, however, for the materials which were in wet state during SAXS analysis, the values obtained by BET method are considerably lower than ones obtained from SAXS analysis. We assume that as a result of the necessary drying step before BET analysis, the particle surface shrinks and open pores collapse. Since, in the industrial applications enzymatic hydrolysis of biomass happens in the wet state, it is very useful to be able to determine specific surface area for the materials in this state, and the SAXS method seems to be the right tool for doing it.

Fitting SAXS data with the core-shell cylinder and absolute power law model gives several insights into affect of acidic pretreatment on the mesostructure of lignocellulosic biomass. Firstly, the core radii of the fibers are increasing in the course of pretreatment, however their volume fractions (scale factor) are decreasing. It appears that small fibers are disrupted much easier than bigger ones during the pretreatment. On the other hand, the coefficient of the power law K_{APL} is steadily increasing as a result of pretreatment. Therefore, we can conclude that disrupted fibrils do not dissolve completely, but become amorphous and stay around the preserved ones, forming part of the big agglomerates of lignocellulose. The increase in sizes of crystalline cores in the course of pretreatment correlates with the XRD results and agree with the previous findings published in [35]. Moreover, the average crystallite sizes obtained from XRD are approximately 3 times larger than diameters of crystalline cores for all of the studied materials. One of the possible explanations for this effect is the coalescence of the neighboring elementary fibrils in the drying process preceding the XRD measurements. On the other hand, the almost constant ratio between crystallite sizes and diameters of elementary fibrils can indicate that SAXS and XRD are sensitive to different levels of cellulose organization. Crystallite sizes determined from XRD could be attributed to cross-sections of microfibrils, formed by hexagonal organization of elementary fibrils as was previously shown for the maize cell wall [11]. Then, assuming that the smaller fibers are preferentially destructed, we could simultaneously explain the average core radius and the average crystallite size increase. It should be also noted that obtained value for the fiber length of the initial poplar

material in wet state considerably deviates from the other materials.

For the initial poplar material we could not match the SAXS curve with the fixed fiber length; we had to fit it as free parameter. The only possible explanation is that the material contains closed elongated pores. Since the pores would have scattering contrast with the average scattering length density of the material ($\Delta\rho_{pore} \approx 11 \times 10^{10}\text{cm}^{-2}$), a volume fraction as low as 0.005 would be sufficient to cause this effect.

2.5. CONCLUSIONS

We have successfully applied small-angle scattering and X-ray diffraction, combined with nitrogen absorption and light microscopy, to investigate changes in the structure of poplar biomass due to pretreatment by sulfuric acid of two different concentrations ("mild" and "severe" pretreatment). During the pretreatment we observe a decrease in particle size, crystalline core radius of elementary fibrils, and about twofold decrease in cellulose crystallinity index. Simultaneously, from nitrogen absorption measured according to the Brunauer-Emmett-Teller method, we see an increase of the specific surface area; it agrees with our findings from light microscopy and small-angle X-ray scattering. The glucose yield after enzymatic hydrolysis following the pretreatment, improves from 1% to 50% after mild pretreatment and up to 70% after the severe pretreatment.

Our results suggest that the main structural features responsible for optimum cellulose digestion are the crystallinity index of cellulose and the specific surface area of the material. An acidic pretreatment gives a decrease in crystallinity by a factor of about 2; the severity of the pretreatment hardly affects it. However, the severity of the pretreatment does affect the specific surface area: we have seen that the more severe treatment gives a higher specific surface area of the cellulose feedstock, attributed to a lower overall particle size. It agrees with our findings from light microscopy. The reduction in particle size makes it better accessible to enzymes, giving a higher glucose yield. We believe that the method of estimating specific surface area from the SAXS data on the materials in their native wet state could facilitate the sustainable applications of lignocellulosic biomass.

REFERENCES

[1] J. Hill, E. Nelson, D. Tilman, S. Polasky, and D. Tiffany, *Environmental, economic, and energetic costs and benefits of biodiesel and ethanol biofuels,* Proceedings of the National Academy of Sciences **103**, 11206 (2006).

[2] M. Hoel and S. Kverndokk, *Depletion of fossil fuels and the impacts of global warming,* Resource and Energy Economics **18**, 115 (1996).

[3] A. J. Ragauskas, *The Path Forward for Biofuels and Biomaterials,* Science **311**, 484 (2006).

[4] C. Wyman, S. Decker, M. Himmel, J. Brady, C. Skopec, and L. Viikari, *Hydrolysis of Cellulose and Hemicellulose,* in *Polysaccharides*, Chapter 43 (CRC Press, 2004) pp. 994–1033.

[5] M. Martínez-Sanz, P. Lopez-Sanchez, M. J. Gidley, and E. P. Gilbert, *Evidence for differential interaction mechanism of plant cell wall matrix polysaccharides in hierarchically-structured bacterial cellulose,* Cellulose **22**, 1541 (2015).

[6] T. Cui, J. Li, Z. Yan, M. Yu, and S. Li, *The correlation between the enzymatic saccharification and the multidimensional structure of cellulose changed by different pretreatments,* Biotechnology for Biofuels **7**, 134 (2014).

[7] M. Martínez-Sanz, M. J. Gidley, and E. P. Gilbert, *Hierarchical architecture of bacterial cellulose and composite plant cell wall polysaccharide hydrogels using small angle neutron scattering,* Soft Matter **12**, 1534 (2016).

[8] D. Klemm, B. Heublein, H.-P. Fink, and A. Bohn, *Cellulose: Fascinating Biopolymer and Sustainable Raw Material,* Angewandte Chemie International Edition **44**, 3358 (2005), arXiv:0402594v3 [arXiv:cond-mat] .

[9] A. Mittal, R. Katahira, M. E. Himmel, and D. K. Johnson, *Effects of alkaline or liquid-ammonia treatment on crystalline cellulose: changes in crystalline structure and effects on enzymatic digestibility,* Biotechnology for Biofuels **4**, 41 (2011).

[10] R. E. Quiroz-Castañeda and J. L. Folch-Mallol, *Hydrolysis of biomass mediated by cellulases for the production of sugars,* Sustainable Degradation of Lignocellulosic Biomass - Techniques, Applications and Commercialization , 119 (2013).

[11] S.-Y. Ding and M. E. Himmel, *The maize primary cell wall microfibril: a new model derived from direct visualization.* J Agric Food Chem **54**, 597 (2006).

[12] S.-Y. Ding, Y.-S. Liu, Y. Zeng, M. E. Himmel, J. O. Baker, and E. A. Bayer, *How Does Plant Cell Wall Nanoscale Architecture Correlate with Enzymatic Digestibility?* Science **338**, 1055 (2012).

[13] M. Foston and A. J. Ragauskas, *Biomass Characterization: Recent Progress in Understanding Biomass Recalcitrance,* Industrial Biotechnology **8**, 191 (2012).

[14] L. Hu, L. Lin, Z. Wu, S. Zhou, and S. Liu, *Chemocatalytic hydrolysis of cellulose into glucose over solid acid catalysts,* Applied Catalysis B: Environmental **174-175**, 225 (2015).

[15] P. Gilna, L. R. Lynd, D. Mohnen, M. F. Davis, and B. H. Davison, *Progress in understanding and overcoming biomass recalcitrance: a BioEnergy Science Center (BESC) perspective,* Biotechnology for Biofuels **10**, 285 (2017).

[16] Q. Sun, M. Foston, X. Meng, D. Sawada, S. V. Pingali, H. M. O'Neill, H. Li, C. E. Wyman, P. Langan, A. J. Ragauskas, and R. Kumar, *Effect of lignin content on changes occurring in poplar cellulose ultrastructure during dilute acid pretreatment,* Biotechnology for Biofuels **7**, 150 (2014).

[17] M. E. Himmel, S.-Y. Ding, D. K. Johnson, W. S. Adney, M. R. Nimlos, J. W. Brady, and T. D. Foust, *Biomass Recalcitrance: Engineering Plants and Enzymes for Biofuels Production,* Science **315**, 804 (2007).

[18] C. C. Kwan, M. Ghadiri, D. G. D. Papadopoulos, A. C. Bentham, B. Chih, C. C. Kwan, M. Ghadiri, D. G. D. Papadopoulos, and A. C. Bentham, *The Effects of Operating Conditions on the Milling of Microcrystalline Cellulose,* Chemical Engineering & Technology **26**, 185 (2003).

[19] R. Sun, L. Mott, and J. Bolton, *Isolation and Fractional Characterization of Ball-Milled and Enzyme Lignins from Oil Palm Trunk,* J. Agric. Food Chem. **46**, 718 (1998).

[20] X.-F. Sun, Sun, P. Fowler, and M. S. Baird, *Extraction and Characterization of Original Lignin and Hemicelluloses from Wheat Straw,* Journal of Agricultural and Food Chemistry **53**, 860 (2005).

[21] H. Zhao, J. H. Kwak, Y. Wang, J. A. Franz, J. M. White, and J. E. Holladay, *Effects of Crystallinity on Dilute Acid Hydrolysis of Cellulose by Cellulose Ball-Milling Study,* Energy & Fuels **20**, 807 (2006).

[22] M. a. Kabel, H. van den Borne, J.-P. Vincken, A. G. J. Voragen, and H. a. Schols, *Structural differences of xylans affect their interaction with cellulose,* Carbohydrate Polymers **69**, 94 (2007).

[23] P. Kumar, D. M. Barrett, M. J. Delwiche, and P. Stroeve, *Methods for Pretreatment of Lignocellulosic Biomass for Efficient Hydrolysis and Biofuel Production,* Industrial & Engineering Chemistry Research **48**, 3713 (2009), arXiv:787532 .

[24] G. Bali, X. Meng, J. I. Deneff, Q. Sun, and A. J. Ragauskas, *The effect of alkaline pretreatment methods on cellulose structure and accessibility,* ChemSusChem **8**, 275 (2015).

[25] Y. Pu, F. Hu, F. Huang, B. H. Davison, and A. J. Ragauskas, *Assessing the molecular structure basis for biomass recalcitrance during dilute acid and hydrothermal pretreatments.* Biotechnology for biofuels **6**, 15 (2013).

[26] M. Pedersen and A. S. Meyer, *Lignocellulose pretreatment severity - relating pH to biomatrix opening,* New Biotechnology **27**, 739 (2010).

[27] A. T. W. M. Hendriks and G. Zeeman, *Pretreatments to enhance the digestibility of lignocellulosic biomass,* Bioresource Technology **100**, 10 (2009), arXiv:1579-4377 .

[28] B. S. Donohoe, S. R. Decker, M. P. Tucker, M. E. Himmel, and T. B. Vinzant, *Visualizing lignin coalescence and migration through maize cell walls following thermochemical pretreatment,* Biotechnology and Bioengineering **101**, 913 (2008).

[29] P.-L. Tang, P. M. Abdul, N. S. Engliman, and O. Hassan, *Effects of pretreatment and enzyme cocktail composition on the sugars production from oil palm empty fruit bunch fiber (OPEFBF),* Cellulose (2018), 10.1007/s10570-018-1894-0.

[30] P. Bansal, M. Hall, M. J. Realff, J. H. Lee, and A. S. Bommarius, *Multivariate statistical analysis of X-ray data from cellulose: A new method to determine degree of crystallinity and predict hydrolysis rates,* Bioresource Technology **101**, 4461 (2010).

[31] S. Park, J. O. Baker, M. E. Himmel, P. A. Parilla, and D. K. Johnson, *Cellulose crystallinity index: measurement techniques and their impact on interpreting cellulase performance*. Biotechnology for biofuels **3**, 10 (2010).

[32] C. Cateto, G. Hu, and A. Ragauskas, *Enzymatic hydrolysis of organosolv Kanlow switchgrass and its impact on cellulose crystallinity and degree of polymerization,* Energy & Environmental Science **4**, 1516 (2011).

[33] Y. Sun, L. Lin, H. Deng, J. Li, B. He, R. Sun, and P. Ouyang, *Structural Changes of Bamboo CelluloseE in Formic Acid,* BioResources **3**, 297 (2008).

[34] D. N. Thompson, H. C. Chen, and H. E. Grethlein, *Comparison of pretreatment methods on the basis of available surface area,* Bioresource Technology **39**, 155 (1992).

[35] S. V. Pingali, V. S. Urban, W. T. Heller, J. McGaughey, H. O'Neill, M. B. Foston, H. Li, C. E. Wyman, D. A. Myles, P. Langan, A. Ragauskas, B. Davison, and B. R. Evans, *Understanding Multiscale Structural Changes During Dilute Acid Pretreatment of Switchgrass and Poplar,* ACS Sustainable Chemistry & Engineering **5**, 426 (2017).

[36] Y. Habibi, L. A. Lucia, and O. J. Rojas, *Cellulose nanocrystals: chemistry, self-assembly, and applications*. Chemical reviews **110**, 3479 (2010).

[37] N. Lavoine, I. Desloges, A. Dufresne, and J. Bras, *Microfibrillated cellulose – Its barrier properties and applications in cellulosic materials: A review,* Carbohydrate Polymers **90**, 735 (2012).

[38] M. Martínez-Sanz, F. Pettolino, B. Flanagan, M. J. Gidley, and E. P. Gilbert, *Structure of cellulose microfibrils in mature cotton fibres,* Carbohydrate Polymers **175**, 450 (2017).

[39] K. Leppänen, S. Andersson, M. Torkkeli, M. Knaapila, N. Kotelnikova, and R. Serimaa, *Structure of cellulose and microcrystalline cellulose from various wood species, cotton and flax studied by X-ray scattering,* Cellulose **16**, 999 (2009).

[40] F. Xu, Y.-C. Shi, and D. Wang, *X-ray scattering studies of lignocellulosic biomass: A review,* Carbohydrate Polymers **94**, 904 (2013).

[41] P. A. Penttilä, T. Imai, M. Capron, M. Mizuno, Y. Amano, R. Schweins, and J. Sugiyama, *Multimethod approach to understand the assembly of cellulose fibrils in the biosynthesis of bacterial cellulose,* Cellulose **25**, 2771 (2018).

[42] M. Martínez-Sanz, D. Mikkelsen, B. M. Flanagan, C. Rehm, L. de Campo, M. J. Gidley, and E. P. Gilbert, *Investigation of the micro- and nano-scale architecture of cellulose hydrogels with plant cell wall polysaccharides: A combined USANS/SANS study,* Polymer **105**, 449 (2016).

[43] A. C. de Souza, T. Rietkerk, C. G. Selin, and P. P. Lankhorst, *A robust and universal NMR method for the compositional analysis of polysaccharides,* Carbohydrate Polymers **95**, 657 (2013).

[44] R. Teeeer, R. Serimaa, and T. Paakkarl, *Crystallinity of cellulose, as determined by CP/MAS NMR and XRD methods,* Polymer Bulletin **17**, 231 (1987), arXiv:bk-31 .

[45] N. Wang, E. Ding, and R. Cheng, *Thermal degradation behaviors of spherical cellulose nanocrystals with sulfate groups,* Polymer **48**, 3486 (2007).

[46] M. Poletto, A. J. Zattera, M. M. C. Forte, and R. M. C. Santana, *Thermal decomposition of wood: Influence of wood components and cellulose crystallite size,* Bioresource Technology **109**, 148 (2012).

[47] M.-C. Popescu, C.-M. Popescu, G. Lisa, and Y. Sakata, *Evaluation of morphological and chemical aspects of different wood species by spectroscopy and thermal methods,* Journal of Molecular Structure **988**, 65 (2011).

[48] A. L. Patterson, *The Scherrer Formula for X-Ray Particle Size Determination,* Physical Review **56**, 978 (1939), arXiv:arXiv:1011.1669v3 .

[49] T. Narayanan, O. Diat, and P. Bösecke, *SAXS and USAXS on the high brilliance beamline at the ESRF,* Nuclear Instruments and Methods in Physics Research Section A: Accelerators, Spectrometers, Detectors and Associated Equipment **467-468**, 1005 (2001).

[50] G. Porod, *Die Röntgenkleinwinkelstreuung von dichtgepackten kolloiden Systemen,* Colloid & Polymer Science **2** (1951).

[51] M. Doucet, J. H. Cho, G. Alina, J. Bakker, W. Bouwman, P. Butler, K. Campbell, M. Gonzales, R. Heenan, A. Jackson, P. Juhas, S. King, P. Kienzle, J. Krzywon, A. Markvardsen, T. Nielsen, L. O'Driscoll, W. Potrzebowski, R. Ferraz Leal, T. Richter, P. Rozycko, T. Snow, and A. Washington, *Sasview version 4.2,* (2018).

[52] M. Martínez-Sanz, M. J. Gidley, and E. P. Gilbert, *Application of X-ray and neutron small angle scattering techniques to study the hierarchical structure of plant cell walls: A review,* Carbohydrate Polymers **125**, 120 (2015).

[53] S. Brunauer, P. H. Emmett, and E. Teller, *Adsorption of Gases in Multimolecular Layers,* Journal of the American Chemical Society **60**, 309 (1938), arXiv:arXiv:1011.1669v3 .

[54] P. Sannigrahi, A. J. Ragauskas, and G. A. Tuskan, *Poplar as a feedstock for biofuels: A review of compositional characteristics,* Biofuels, Bioproducts and Biorefining **4**, 209 (2010), arXiv:bk-16a .

[55] U. Vainio, N. Maximova, B. Hortling, J. Laine, P. Stenius, L. K. Simola, J. Gravitis, and R. Serimaa, *Morphology of Dry Lignins and Size and Shape of Dissolved Kraft Lignin Particles by X-ray Scattering,* Langmuir **20**, 9736 (2004).

[56] R. H. Atalla and D. L. Vanderhart, *Native Cellulose: A Composite of Two Distinct Crystalline Forms,* Science **223**, 283 (1984).

[57] M. Wada, T. Okano, and J. Sugiyama, *Allomorphs of native crystalline cellulose I evaluated by two equatoriald-spacings,* Journal of Wood Science **47**, 124 (2001).

[58] L. Segal, J. Creely, A. Martin, and C. Conrad, *An Empirical Method for Estimating the Degree of Crystallinity of Native Cellulose Using the X-Ray Diffractometer,* Textile Research Journal **29**, 786 (1959).

3

A VERSATILE SHEAR CELL FOR INVESTIGATION OF STRUCTURE OF FOOD MATERIALS UNDER SHEAR

A versatile cell for X-ray and neutron scattering experiments on samples under shear has been designed. To our knowledge, it is the first shear cell which can be used for both SAXS and SANS in respectively synchrotron or reactor beamlines. The cell is mainly intended for scattering experiments in so-called "1-2 plane geometry", but can also be modified into cone-plate and plate-plate rheological geometries, giving access to the 1-3 scattering plane. The latter two geometries, however, can only be used with neutron scattering. The final cell design is compact, which allows it to be used even with lab-based X-ray sources. A special thermostatic shell allows for the temperature control of the samples under investigation in the range from 5 up to 100° C. Several X-ray and neutron scattering experiments performed with the cell have helped in better understanding of the structuring under shear of food materials, such as: cellulose suspensions, fat crystal networks and milk proteins.

This chapter has been published in Colloids and Surfaces A 566, 21-28 (2019) [1].

3.1. INTRODUCTION

A major challenge for food science is to reconcile the societal drive towards sustainable food production with the consumers demand for natural, stable and superior tasting foods [2]. Conventional routes for food manufacturing have been optimized over decades and have reached their limits. The required radical redesign of food formulation and processing routes requires deepened insights in relationships between product structure and functionality [3]. When processing raw materials to final consumer food products, their structures undergo changes at multiple length scales [4, 5]. A prerequisite for rational redesign of food processing routes is to have insights in how these hierarchical multiscale structures evolve under dynamic condition [4].

Small-angle scattering (SAS) of X-rays (SAXS) and neutrons (SANS) is widely utilized to study structures of food colloids ([6–11]). A number of works has also been done on application of these techniques on materials under shear or flow conditions [12, 13]. Both methods, SAXS and SANS [14] are capable of investigations on nano- and mesoscale size range, moreover, by utilizing a spin-echo principle for SANS encoding (SESANS [15]), the range can be extended up to 20 μm. However, these methods have certain advantages and disadvantages related to the employed type of radiation. X-rays interact with electron clouds of atoms, which leads to linear dependency of scattering power on the atomic number of the element. Neutrons interact with atom nuclei, which causes different scattering power for different isotopes of the same chemical element. This effect is widely employed in experiments with contrast variation. Moreover, due to the weak interaction of neutrons with matter, rather bulky samples can be studied with neutron scattering. Since X-rays are easy to generate, a multitude of laboratory-scale plug-and-play SAXS instruments came to the market in recent years. Compact neutron sources are still under development and SANS experiments still require large-facilities like nuclear reactors, or spallation sources. Synchrotrons, large-facilities generating X-ray are also open for SAXS experiments. One of the great advantages of synchrotrons is their high flux of X-rays, which is 6-7 orders of magnitude higher than average flux of neutrons at neutron large-facilities. Such a high flux allows for a very high time resolution, as well as high spatial resolution of the experiment, as X-ray beam at synchrotron can easily be focused to 100 μm, or, with special optics, even to a few nm. However, such high flux might be a considerable disadvantage in studies of soft matter, as samples can easily get radiation damage or even destroyed within a fraction of a second. Taking into account compatibility of X-rays and neutrons, we decided to make our shear-cell suitable for both kind of radiation, so that we could perform (SE)SANS and SAXS experiments on complex fluids under the same conditions. In the following the cells, suitable for either SANS or SAXS on the samples under shear, will be called shear-SAS cells.

Table 3.1 gives an overview of the shear-SAS cells described in the literature. As can be seen, the most popular cell geometry is Taylor-Couette, which allows for radial and tangential passage of the beam along the cell (for more details of various cell geometries as well as scattering planes see the review [13]). Depending on the direction of the beam relative to the shear cell, three different scattering geometries are possible. Figure 3.1 shows three possible scattering geometries based on the Taylor-Couette cell. AntonPaar was the first company able to combine a rheometer with a suitable Taylor-Couette cell with small-angle scattering of X-rays [16], a few years later simultaneous

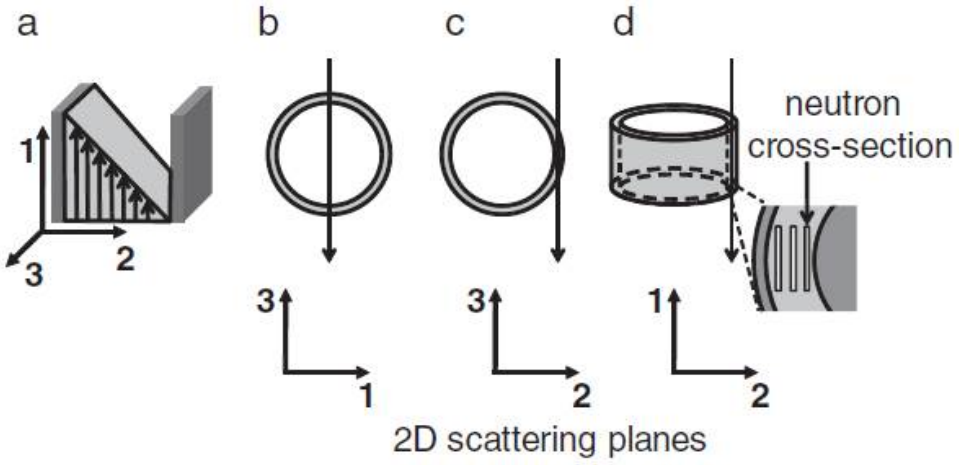

Figure 3.1: The common Taylor-Couette flow cell geometries with accessible scattering planes. (a) Rectilinear coordinate frame where the 1-, 2-, and 3-directions are defined as the velocity (V), velocity gradient (ΔV), and vorticity (ω) directions, respectively. (b), (c), and (d) are the radial, tangential, and 1–2 plane flow cell geometries that allow for scattering along the 1–3, 2–3, and 1–2 planes, respectively. In the latter, an incident beam cross-section smaller than the fluid gap allows for spatial resolution along the gap. **The Figure is adopted from [13]**

SANS and torque measurements were performed with a rheometer of Rheowis-Fluid (Labplus, Jona, Switzerland) [17]. Another way of evolution of shear-SAS cells was a development of so-called "1-2 plane shear cell"[18, 19]. As such a cell allows spatial resolution along the shear-gradient direction across the gap, it is very attractive for investigation of materials showing shear-banding [18, 20–23]. However, this geometry does not allow for a simultaneous torque measurement, as the cell is placed horizontally, while all of the existing rheometers are vertical. For our design we decided to omit possibility for a simultaneous torque measurement and chose for horizontal cell geometry.

In this article we present detailed design of the versatile shear-cell suitable for SAXS, SANS and SESANS measurements. Three examples of shear-SAS cell application for studies of food colloids are presented in the experimental section. Although in our research we focused mostly on application of the shear-SAS cell for investigation of food colloidal dispersions, the applications can be extended to the much broader field of soft matter.

Figure 3.2 shows a schematic drawing of the developed shear-SAS cell and Figure 3.9 shows an image of the cell mounted at the SAXS DUBBLE (BM-26) beamline at ESRF [37, 38]. As can be seen from Figure 3.9, the cell with its drive and motor is rather compact (it can fit in a box of $25 \times 25 \times 25$ cm^3), which makes it easy in transportation, it even has been transported as hand luggage on an airplane. The compactness made it possible to mount it on various beamlines and even laboratory X-ray sources (see section 3.2.1). The cell consists of an inner rotating disk (rotor) and an outer stable container (stator), leaving a gap which is filled up with the material under investigation. Rotor and stator are both made of aluminum.

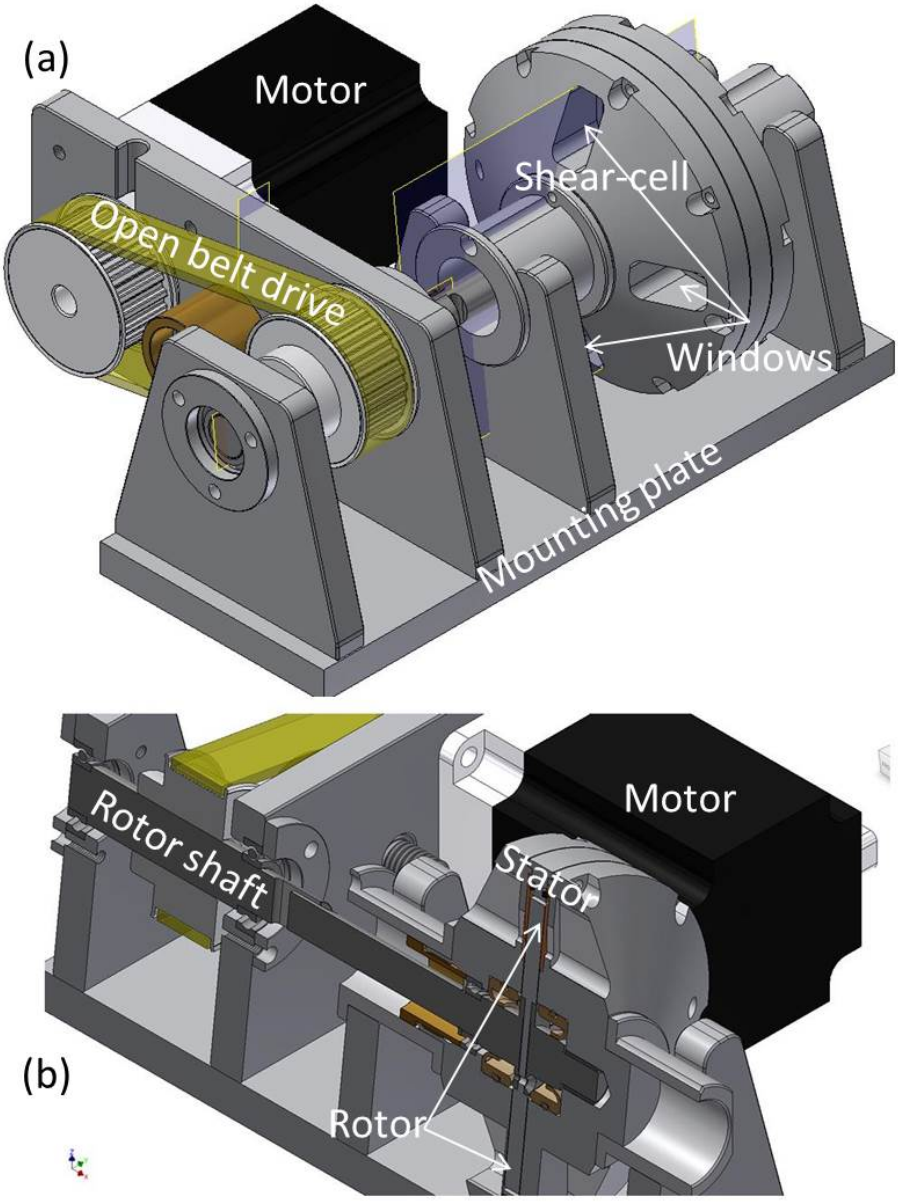

Figure 3.2: A schematic 3D drawing of the developed shear-cell (a) and a vertical cross section of it along the rotation axis of the cell.

Table 3.1: Shear-SAS cells described in the literature.

Source	Simultaneous torque meausurement	Type of radiation	Cell geometry	Scattering plane(s)
[24]	-	neutrons	Taylor-Couette	1-3
[25]	-	neutrons	Taylor-Couette	1-3
[26]	-	neutrons	Taylor-Couette	1-3
[27]	-	neutrons	Taylor-Couette	1-3
[28]	-	X-rays	plate-plate	1-2
[29]	-	neutrons	plate-plate	1-2
[30]	-	neutrons	plate-plate	1-3
[31]	-	X-rays	Taylor-Couette	1-3, 2-3
[32]	-	neutrons	Taylor-Couette	1-2
[16]	+	X-rays	Taylor-Couette	1-3, 2-3
[18, 19]	-	neutrons	Taylor-Couette	1-2
[17]	+	neutrons	Taylor-Couette	1-3, 2-3
[33]	+	X-rays	plate-plate	1-3
[34]	+	neutrons	Taylor-Couette	1-3, 2-3
[35]	+	X-rays	Sliding plate	1-2
[36]	+	neutrons	Taylor-Couette	1-3, 2-3

3.1.1. FIT FOR NEUTRONS AND X-RAYS

In order to make the cell suitable for X-rays and neutrons, special types of windows were necessary for each type of radiation. In case of neutrons 0.4 mm thick aluminum windows with accessible area 10×17 mm^2 are integrated in the cell design. Figure 3.3 shows a 2D (a) and 1D (b) SANS patterns from the empty shear cell. For X-rays two circular diamond windows with 0.2 mm thickness and 6 mm diameter were created, which give hardly any background scattering (see Figure 3.3(c,d)). For visual inspection of the sample and potential light scattering applications, 1 mm thick quartz windows with accessible area 8×15 mm^2 were added to the cell design. Figure 3.10 shows the windows positions on the cell. It should be noted, that in order to obtain the most homogeneous sample flow at the measurement position, the cell should be positioned in such a way that required window appears on the side of the cell (on the Figure 3.10(a) Quartz and Diamond windows are in the right position).
As the cell is also intended to be used for SESANS measurement, we had to minimize magnetic fields appearing due to motor driving the cell. At the current distance between the aluminum window of the cell and the motor (20 cm) we did not observe any effects of the motor magnetic field on the neutron beam polarization.

3.1.2. SHEAR-SAS CELL GEOMETRIES

The cell is mainly intended to probe the so-called 1-2 scattering plane of the complex fluids. The Taylor-Couette cell geometry for this application is similar to one described in [19] with the additional possibility for the SAXS experiments. This geometry in com-

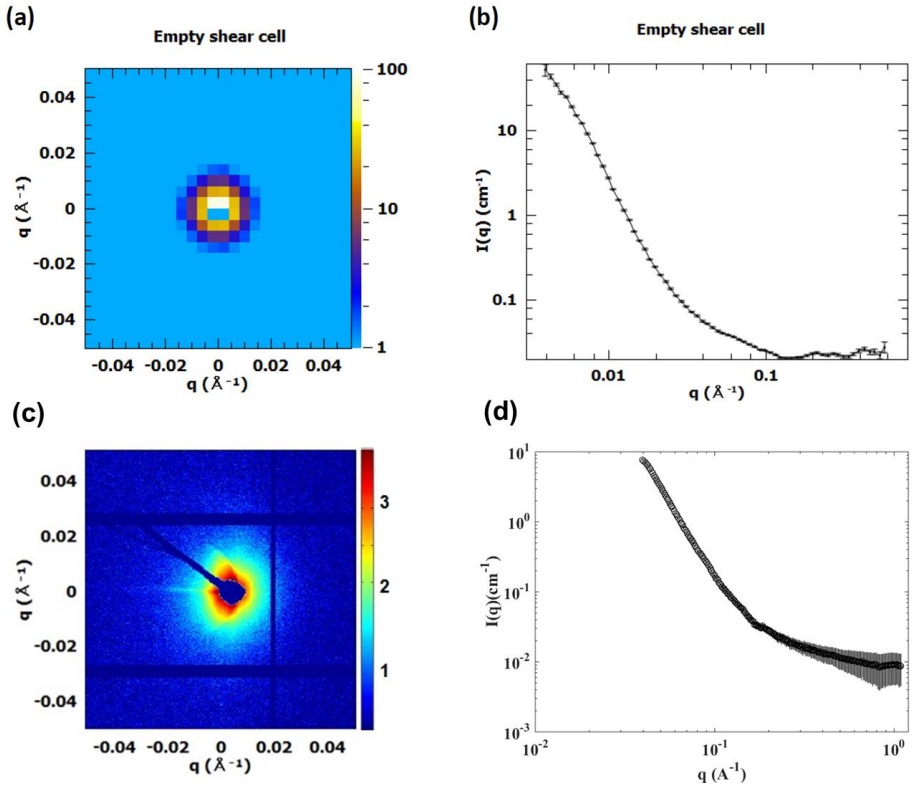

Figure 3.3: 2D (a) and 1D (b) SANS patterns from the empty shear cell in cone-plate configuration. 2D (c) and 1D (d) SAXS patterns from the empty shear cell in Taylor-Couette cell geometry. The scattering was collected at LARMOR beamline of ISIS neutron source (a,b) and at BM26 (DUBBLE) beamline of ESRF (c,d)

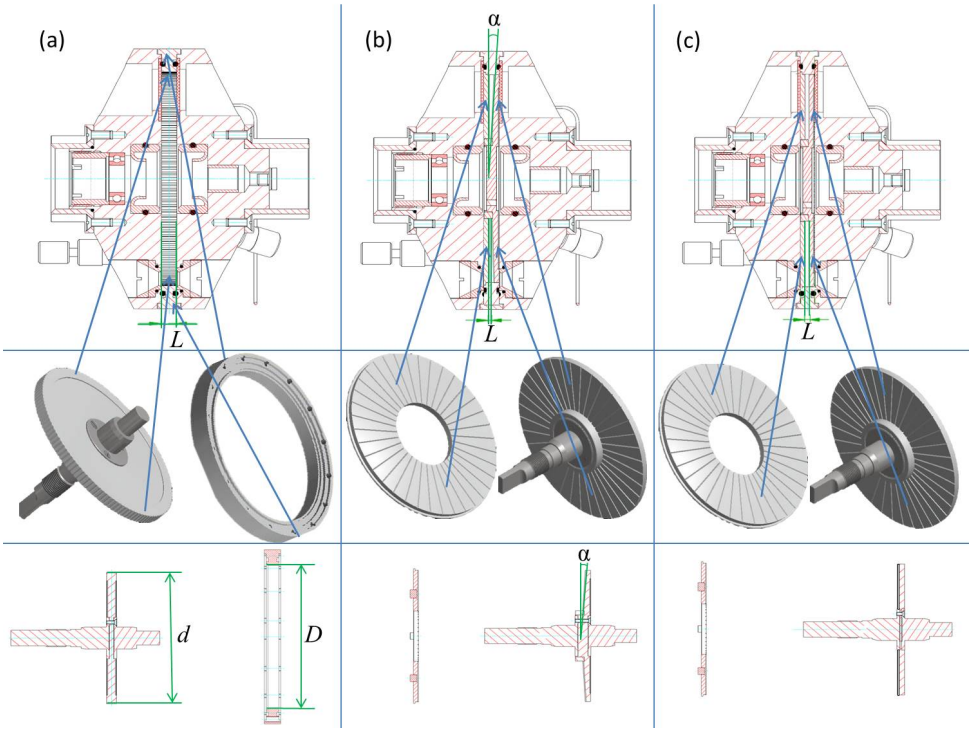

Figure 3.4: Geometries of the cell: (a) Taylor-Couette geometry, (b) cone-plate geometry, and (c) plate-plate geometry. The top row shows a cross section of the entire cell, the stators and rotors for respective geometries are shown in the middle row with their respective cross sections in the bottom row. Blue arrows show where the stators and rotors appear on the drawings of the cross sections. L is a sample thickness on the beam, d is a diameter of the rotor, D is an inner diameter of the housing ring, and α is the cone angle

bination with intensive neutron or X-ray beam allows for spatially-resolved SAXS/SANS measurements across the gap. Moreover, since the cell is made of aluminum, which is relatively transparent for neutrons, we decided to use this advantage and extend the cell design to two more geometries, namely cone-plate and plate-plate. All three geometries are shown in Figure 3.4.

In the Taylor-Couette geometry, the shear-SAS cell allows access to so-called 1-2 scattering plane, which in combination with intensive beams allows for spatially-resolved SAXS/SANS measurements across the gap. Therefore, it is possible to locally probe structure of the material under investigation. By varying thicknesses of the rotor and outer ring, it is possible to achieve different sample thicknesses along the beam L. However, the minimal value of L is 4 mm due to mechanical limitations. The gap size between the rotor and the ring also can be varied by varying the rotor diameter d. In our experiments we were using a gap size of 1 mm. It can be increased up to 6 mm for x-ray experiments and up to 15 mm for experiments with neutrons.

In plate-plate or cone-plate geometry the scattering pattern appears in 1-3 scattering plane. In this case the beam is going through the sample along the shear-gradient direction and the scattering pattern is integrated over all shear rates present in the system. In this case the sample thickness along the beam can be varied either by changing the thickness of the rotor or by changing the cone angle α. The cone angle can be varied between 1 and 10°. In our experiments we were using $\alpha = 3°$.

In all three geometries, the surfaces of the rotor and the stator can be made smooth, sand-blasted, or serrated, depending on roughness desired for the planned experiment.

3.1.3. TEMPERATURE CONTROL

Since rheology and structure of food is highly dependent on temperature and temperature history of the material, we included a special housing for temperature control of the cell in our design. A thermostatic shell was designed for this purpose. The shell is made of 1 mm thick nylon 12 with copper insertions for better temperature exchange. The nylon parts of the cell were 3D-printed and the copper insertions were glued to them with a temperature-resistant glue. The internal surface of the shell follows the shape of the shear cell and has maximal available contact surface area with the cell. The shell is hollow, which allows for the flow of a cooling or heating liquid with desired temperature through it. For temperature measurements a K-type thermocouple is used. Figure 3.11 shows a cross section of the cell in the thermostatic shell as well as the internal surface of the shell with copper insertions.

3.2. EXPERIMENTAL RESULTS AND DISCUSSION

A couple of in-situ experiments were conducted so far: one at the DUBBLE beamline at ESRF [37, 38] and one at the LARMOR instrument at ISIS. In the first case the Taylor-Cuette geometry was used in combination with X-ray scattering for investigation of cellulose dispersions and fat crystal dispersions. In the second experiment protein dispersions were studied in plate-plate and cone-plate geometry with aid of neutron scattering.

3.2.1. X-RAYS: MICROFIBRILLATED CELLULOSE DISPERSIONS

So-called non-local flow behaviour of microfibrillated cellulose was observed by Rheo-MRI [39]: the viscosity of the sample was dependent on the position across the cell gap. This can be explained by a formation of flocks of microfibrills, or a formation of an aligned liquid crystal phase.

In order to check these two models, we have performed a shear-SAXS experiment at the BM-26 (DUBBLE) beamline at ESRF [1]. Figure 3.5 shows typical scattering patterns for a sample of microfibrillated bacterial cellulose stabilized by carboxymethylcellulose (BC-CMC) at high and low shear rates. The scattering patterns appear to be isotropic at both shear rates. This result indicates absence of aligned liquid crystal phase, and sustaines the flocculation model as the explanation for the position dependent viscosity.

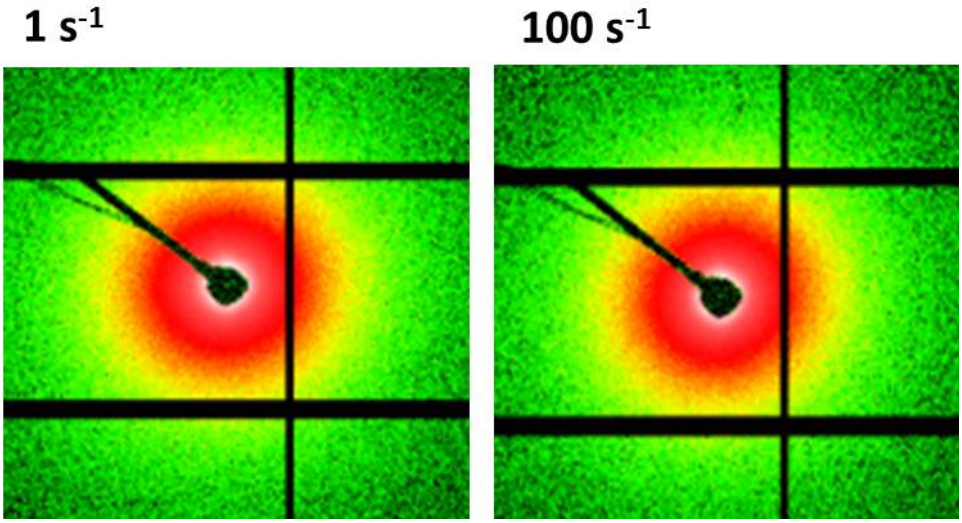

Figure 3.5: 2D SAXS patterns for a sample of microfibrillated bacterial cellulose (BC) with carboxymethylcellulose (CMC) with a concentration of BC 0.2 % wt. and ratio BC:CMC = 4:1 at 1 (left) and 100 (right) s^{-1}. The patterns are shown for a point in the middle of the cell gap

3.2.2. X-RAYS: *in situ* VIEW ON FAT CRYSTAL NETWORK FORMATION

Stability and sensorial quality of fat-based products, such as butter and margarine, are defined by the underlying multiscale structure of fat crystal networks [8]. A novel route to design the fat crystal structure is based on dispersing micronized fat crystal (MFC) nanoplatelets in oil [11, 40]. In this way, the crystallisation of the fat crystal nanoplatelets can be decoupled from the aggregation of fat crystals into larger structures, which could radically simplify manufacturing of food manufacturing routes. However, rational design of these routes is challenging, since kinetics of multiscale network formation is strongly determined by temperature and shear [41]. The developed shear cell was employed to assess kinetics of fat crystal mesoscale networks in well-controlled shear stress fields at different temperatures [11, 42].

Figure 3.6(a) shows the 2D SAXS pattern and an radial integration of the first order diffraction peak obtained under imposed shear 0.1 s^{-1} at the BM-26 (DUBBLE) beamline at ESRF. The rheo-SAXS experiment revealed the alignment of the dispersed MFC nanoplatelets under shear. As most of the information about individual MFC nanoplatelets lies in the first diffraction peak at scattering vectors q=1.6 nm^{-1}, it was also possible to perform experiments at a lab-scale X-ray diffractometer Bruker D8-Discover (3.12) . Even though the obtained 2D pattern (3.6(b)) had a different signal to noise ratio, the effect of shear on the alignment of MFC nanoplatelets could clearly be observed.

The presence of a well resolved first order diffraction peak allowed real-time assessment of the increase in average crystal thickness (ACT) of the dispersed MFC nanoplatelets under shear. The ACT was estimated based on the Scherrer line shape analysis [11, 43]. Figure 3.7(a) shows the ACT as a function of time under imposed constant shear of 0.1 s^{-1}

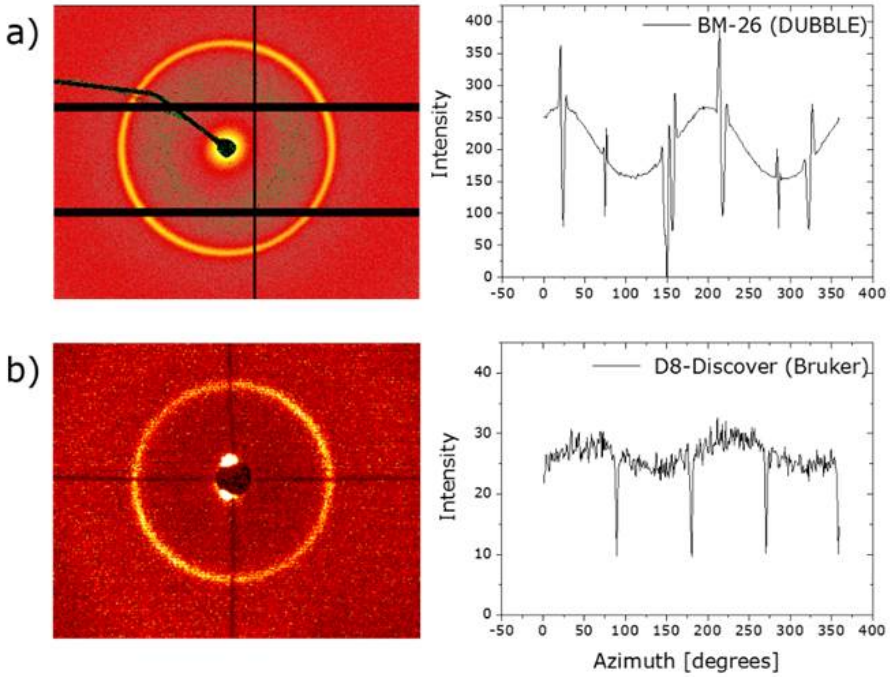

Figure 3.6: 2D SAXS patterns and their radial averages presented in the Intensity vs Azimuth angle plots for MFC nanoplatelets dispersed in sunflower oil obtained at the BM-26 (DUBBLE) beamline at ESRF (a) and at the lab-scale Bruker D8-Discover X-ray diffractometer (b). Both experiments were performed in the developed Couette geometry with serrated walls at an imposed shear rate of 0.1 s^{-1} and ambient temperatures

at ambient temperature. The scattering patterns were obtained at the BM-26 (DUBBLE) beamline at ESRF. The increase in ACT during 8-13 hours of shear points toward shear induced recrystallisation of the MFC nanoplatelets. This recrystallisation effect was also observed in a shear-SAXS experiment at D8-Discover diffractometer, albeit with lower signal to noise ratio (see Figure 3.7(a)).

The performance of the variable temperature capability of the shear cell is illustrated by Figure 3.7(b). MFC dispersions were measured at 20 and 26°C with the shear cell mounted in a lab scale Discover D8 diffractometer for 13 hours under constant shear of 1 s^{-1}. Even with this lab scale instrument kinetic curves could be obtained that allow observation of two recrystallisation stages of which one is clearly temperature dependent (see Figure 3.7(b)) [11, 42]. The availability of the rheo-SAXS cell with variable temperature capability which can versatile be mounted in both synchrotron beamlines and labscale instruments has been an important enabler of studies investigated fat crystal network formation [11, 42]. In future work we expect that the cell will also be deployed in combination with Ultra Small Angle X-rays Scattering (USAXS) to provide unprecedented views on network formation in the micronscale domain.

3.2.3. NEUTRONS: PROTEIN DISPERSIONS

Manski.et al [44] found a way to produce fibrous structure from calcium caseinate dispersion by applying simple shear, heat and enzyme transglutaminase. In order to investigate the structuring of calcium caseinate dispersions under shear, we have designed and performed a small-angle neutron scattering experiment [45]. The experiment was conducted at the LARMOR instrument at ISIS.

Figure 3.8a shows the typical scattering patterns of the sample. All data were reduced with their corresponding background, for the shear-cell, the background is the cell filled with H_2O. A nearly perfect overlap between the sample measured ex-situ and at 0 s^{-1} inside the shear-cell confirmed the shear-cell did not interfere with the sample. Surprisingly, the scattering pattern obtained at a shear rate as high as 100 s^{-1} also overlapped perfectly with the others, indicating shear had no influence on the sample structure at the length scale studied. Moreover, the scattering is isotropic at all shear rates, as the radially averaged scattering intensity in Figure 3.8b shows.

3.3. CONCLUSIONS

We have designed and built a versatile compact shear cell to perform SAXS, SANS and SESANS measurements with temperature control. The experimental section of the article has shown applications of the designed shear cell in studies of food materials. Each of the obtained results provides a valuable insight into structuring of the soft matter under shear, relevant to both fundamental and applied sciences.

REFERENCES

[1] E. Velichko, B. Tian, T. Nikolaeva, J. Koning, J. van Duynhoven, and W. G. Bouwman, *A versatile shear cell for investigation of structure of food materials under shear*, Colloids and Surfaces A: Physicochemical and Engineering Aspects **566**, 21 (2019).

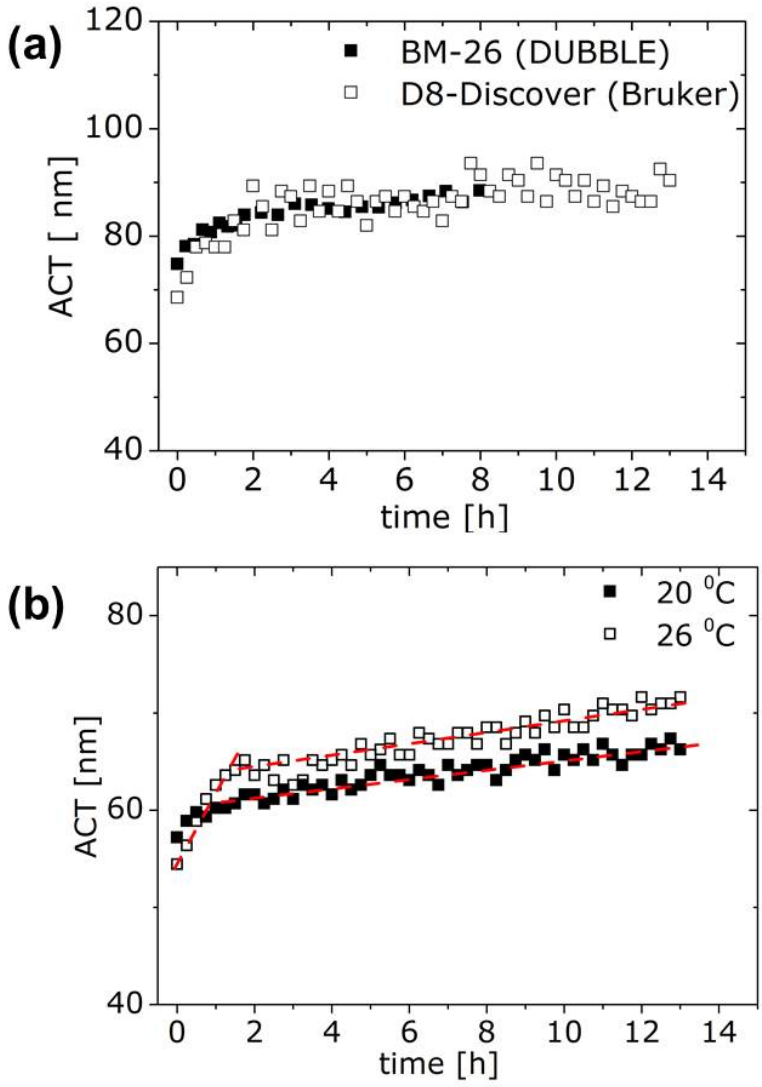

Figure 3.7: (a) A comparison of the ACT data as a function of time obtained at the BM-26 (DUBBLE) beamline at ESRF (solid symbols) and at the lab-scale X-ray diffractometer Bruker D8-Discover (empty symbols). Both experiments were done for MFC nanoplatelets dispersed in sunflower oil in the developed Couette geometry with serrated walls at an imposed shear rate of 0.1 s^{-1} and ambient temperatures. (b) ACT as a function of time for MFC nanoplatelets dispersed in bean oil at an imposed shear rate of 1 s^{-1} and temperatures of 20°C (solid symbols) and 26°C (empty symbols). The measurements were performed in a rheo-SAXS Couette cell geometry (1 mm gap) at the D8-Discover

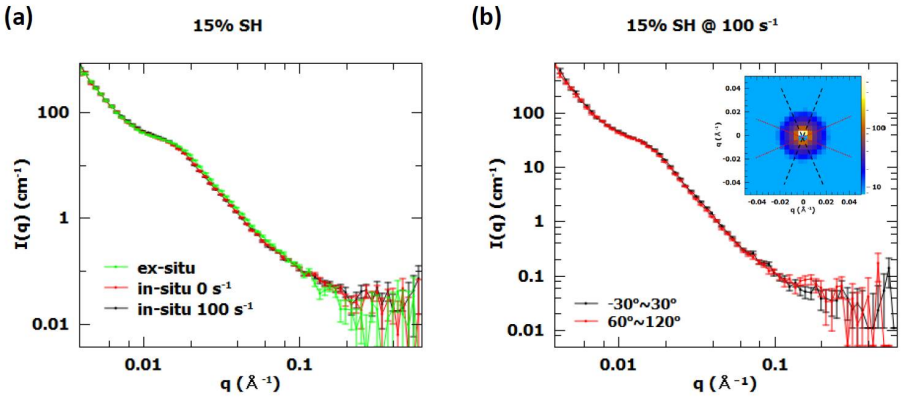

Figure 3.8: Scattering patterns of 15% w/w calcium caseinate dissolved in H_2O (SH). (a): 1D scattering patterns of the sample sheared at 0, 100 $^{-1}$ and ex-situ; (b) Intensities of sector-cut from the 2D patterns of the sample sheared at 100 $^{-1}$ (inset).

[2] A. J. van der Goot, P. J. Pelgrom, J. A. Berghout, M. E. Geerts, L. Jankowiak, N. A. Hardt, J. Keijer, M. A. Schutyser, C. V. Nikiforidis, and R. M. Boom, *Concepts for further sustainable production of foods,* Journal of Food Engineering **168**, 42 (2016).

[3] M. A. Augustin, M. Riley, R. Stockmann, L. Bennett, A. Kahl, T. Lockett, M. Osmond, P. Sanguansri, W. Stonehouse, I. Zajac, and L. Cobiac, *Role of food processing in food and nutrition security,* Trends in Food Science & Technology **56**, 115 (2016).

[4] J. Ubbink, *Soft matter approaches to structured foods: from "cook-and-look" to rational food design?* Faraday Discussions **158**, 9 (2012).

[5] R. Mezzenga, P. Schurtenberger, A. Burbidge, and M. Michel, *Understanding foods as soft materials,* Nature Materials **4**, 729 (2005).

[6] J. Doutch and E. P. Gilbert, *Characterisation of large scale structures in starch granules via small-angle neutron and X-ray scattering,* Carbohydrate Polymers **91**, 444 (2013).

[7] A. Lopez-Rubio, B. M. Flanagan, A. K. Shrestha, M. J. Gidley, and E. P. Gilbert, *Molecular Rearrangement Of Starch During In Vitro Digestion: Toward A Better Understanding Of Enzyme Resistant Starch Formation In Processed Starches,* Biomacromolecules **9**, 1951 (2008).

[8] P. R. R. Ramel, F. Peyronel, and A. G. Marangoni, *Characterization of the nanoscale structure of milk fat,* Food Chemistry **203**, 224 (2016).

[9] F. Peyronel, B. Quinn, A. G. Marangoni, and D. a. Pink, *Ultra small angle x-ray scattering in complex mixtures of triacylglycerols,* Journal of Physics: Condensed Matter **26**, 464110 (2014).

[10] M. Nieuwland, W. G. Bouwman, M. L. Bennink, E. Silletti, and H. H. J. de Jongh, *Characterizing Length Scales that Determine the Mechanical Behavior of gels from Crosslinked Casein Micelles,* Food Biophysics (2015), 10.1007/s11483-015-9399-y.

[11] T. Nikolaeva, R. den Adel, E. Velichko, W. G. Bouwman, D. Hermida-Merino, H. Van As, A. Voda, and J. van Duynhoven, *Networks of micronized fat crystals grown under static conditions,* Food & Function **9**, 2102 (2018).

[12] J. Vermant and M. J. Solomon, *Flow-induced structure in colloidal suspensions,* Journal of Physics: Condensed Matter **17**, R187 (2005).

[13] A. P. R. Eberle and L. Porcar, *Flow-SANS and Rheo-SANS applied to soft matter,* Current Opinion in Colloid & Interface Science **17**, 33 (2012).

[14] A. Lopez-Rubio and E. P. Gilbert, *Neutron scattering: a natural tool for food science and technology research,* Trends in Food Science & Technology **20**, 576 (2009).

[15] M. T. Rekveldt, J. Plomp, W. G. Bouwman, W. H. Kraan, S. Grigoriev, and M. Blaauw, *Spin-echo small angle neutron scattering in Delft,* Review of Scientific Instruments **76**, 033901 (2005).

[16] P. Panine, M. Gradzielski, and T. Narayanan, *Combined rheometry and small-angle x-ray scattering,* Review of Scientific Instruments **74**, 2451 (2003).

[17] J. Stellbrink, B. Lonetti, G. Rother, L. Willner, and D. Richter, *Shear induced structures of soft colloids: Rheo-SANS experiments on kinetically frozen PEP–PEO diblock copolymer micelles,* Journal of Physics: Condensed Matter **20**, 404206 (2008).

[18] M. W. Liberatore, F. Nettesheim, N. J. Wagner, and L. Porcar, *Spatially resolved small-angle neutron scattering in the 1-2 plane: A study of shear-induced phase-separating wormlike micelles,* Physical Review E **73**, 020504 (2006).

[19] A. K. Gurnon, P. D. Godfrin, N. J. Wagner, A. P. R. Eberle, P. Butler, and L. Porcar, *Measuring material microstructure under flow using 1-2 plane flow-small angle neutron scattering,* Journal of Visualized Experiments **84**, e51068 (2014).

[20] M. W. Liberatore, F. Nettesheim, P. A. Vasquez, M. E. Helgeson, N. J. Wagner, E. W. Kaler, L. P. Cook, L. Porcar, and Y. T. Hu, *Microstructure and shear rheology of entangled wormlike micelles in solution,* Journal of Rheology **53**, 441 (2009).

[21] M. E. Helgeson, M. D. Reichert, Y. T. Hu, and N. J. Wagner, *Relating shear banding, structure, and phase behavior in wormlike micellar solutions,* Soft Matter **5**, 3858 (2009).

[22] M. E. Helgeson, L. Porcar, C. Lopez-Barron, and N. J. Wagner, *Direct Observation of Flow-Concentration Coupling in a Shear-Banding Fluid,* Physical Review Letters **105**, 084501 (2010).

[23] K. M. Weigandt, L. Porcar, and D. C. Pozzo, *In situ neutron scattering study of structural transitions in fibrin networks under shear deformation,* Soft Matter **7**, 9992 (2011).

[24] P. Lindner and R. Oberthür, *Apparatus for the investigation of liquid systems in a shear gradient by small angle neutron scattering (SANS),* Revue de Physique Appliquée **19**, 759 (1984).

[25] G. C. Straty, *Apparatus for Neutron Scattering Measurements,* Journal of Research of the National Institute of Standards and Technology Apparatus **94**, 259 (1989).

[26] B. Cummins, P G, Staple, E, Millen and P. J, *A Couette shear flow cell for small-angle neutron scattering studies,* Measurement Science and Technology **1**, 179 (1990).

[27] G. C. Straty, H. J. M. Hanley, and C. J. Glinka, *Shearing apparatus for neutron scattering studies on fluids: Preliminary results for colloidal suspensions,* Journal of Statistical Physics **62**, 1015 (1991).

[28] S. Okamoto, K. Saijo, and T. Hashimoto, *Dynamic SAXS Studies of Sphere-Forming Block Copolymers under Large Oscillatory Shear Deformation,* Macromolecules **27**, 3753 (1994).

[29] L. Noirez and A. Lapp, *Shear Flow Induced Transition from Liquid-Crystalline to Polymer Behavior in Side-Chain Liquid Crystal Polymers,* Physical Review Letters **78**, 70 (1997).

[30] C. Dux, S. Musa, V. Reus, H. Versmold, D. Schwahn, and P. Lindner, *Small angle neutron scattering experiments from colloidal dispersions at rest and under sheared conditions,* The Journal of Chemical Physics **109**, 2556 (1998).

[31] F. Molino, J.-F. Berret, G. Porte, O. Diat, and P. Lindner, *Identification of flow mechanisms for a soft crystal,* The European Physical Journal B **3**, 59 (1998).

[32] L. Porcar, W. A. Hamilton, P. D. Butler, and G. G. Warr, *A vapor barrier Couette shear cell for small angle neutron scattering measurements,* Review of Scientific Instruments **73**, 2345 (2002).

[33] B. Struth, K. Hyun, E. Kats, T. Meins, M. Walther, M. Wilhelm, and G. Grübel, *Observation of new states of liquid crystal 8CB under nonlinear shear conditions as observed via a novel and unique rheology/small-angle X-ray scattering combination,* Langmuir **27**, 2880 (2011).

[34] L. Porcar, D. Pozzo, G. Langenbucher, J. Moyer, and P. D. Butler, *Rheo–small-angle neutron scattering at the National Institute of Standards and Technology Center for Neutron Research,* Review of Scientific Instruments **82**, 083902 (2011).

[35] P. Pfleiderer, S. J. Baik, Z. Zhang, G. Vleminckx, M. P. Lettinga, E. Grelet, J. Vermant, and C. Clasen, *X-ray scattering in the vorticity direction and rheometry from confined fluids,* Review of Scientific Instruments **85**, 065108 (2014).

[36] J. J. Richards, N. J. Wagner, and P. D. Butler, *A strain-controlled RheoSANS instrument for the measurement of the microstructural, electrical, and mechanical properties of soft materials,* Review of Scientific Instruments **88**, 105115 (2017).

[37] M. Borsboom, W. Bras, I. Cerjak, D. Detollenaere, D. Glastra van Loon, P. Goedtkindt, M. Konijnenburg, P. Lassing, Y. K. Levine, B. Munneke, M. Oversluizen, R. van Tol, and E. Vlieg, *The Dutch–Belgian beamline at the ESRF,* Journal of Synchrotron Radiation **5**, 518 (1998).

[38] W. Bras, I. Dolbnya, D. Detollenaere, R. van Tol, M. Malfois, G. Greaves, A. Ryan, and E. Heeley, *Recent experiments on a small-angle/wide-angle X-ray scattering beam line at the ESRF,* Journal of Applied Crystallography **36**, 791 (2003).

[39] D. de Kort, S. Veen, H. Van As, D. Bonn, K. Velikov, and J. van Duynhoven, *Yielding and flow of cellulose microfibril dispersions in the presence of a charged polymer,* Soft Matter (2016), 10.1039/c1sm05495c.

[40] P. Münüklü and P. Jansens, *Particle formation of an edible fat (rapeseed 70) using the supercritical melt micronization (ScMM) process,* The Journal of Supercritical Fluids **40**, 433 (2007).

[41] F. Maleky and G. Mazzanti, *Lipid Crystal Networks Structured under Shear Flow,* in *Crystallization of Lipids* (John Wiley & Sons, Ltd, Chichester, UK, 2018) pp. 211–239.

[42] T. Nikolaeva, *Manipulation of recrystallisation and network formation of oil- dispersed micronized fat crystals,* Submitted for publication (2019).

[43] R. den Adel, K. van Malssen, J. van Duynhoven, O. O. Mykhaylyk, and A. Voda, *Fat Crystallite Thickness Distribution Based on SAXD Peak Shape Analysis,* European Journal of Lipid Science and Technology **120**, 1800222 (2018).

[44] J. M. Manski, A. J. van der Goot, and R. M. Boom, *Advances in structure formation of anisotropic protein-rich foods through novel processing concepts,* Trends in Food Science & Technology **18**, 546 (2007).

[45] B. Tian, Z. Wang, L. de Campo, E. P. Gilbert, R. M. Dalgleish, E. Velichko, A. J. van der Goot, and W. G. Bouwman, *Small angle neutron scattering quantifies the hierarchical fibrous structure in calcium caseinate,* Macromolecules (2019).

3.4. SUPPLEMENTARY INFORMATION

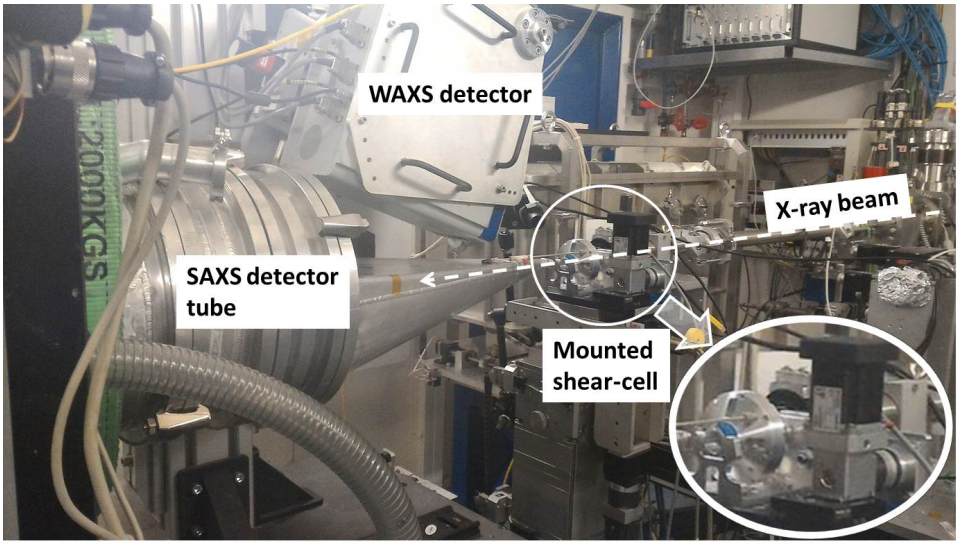

Figure 3.9: An image of the developed shear cell mounted at the SAXS DUBBLE (BM-26) beamline at ESRF.

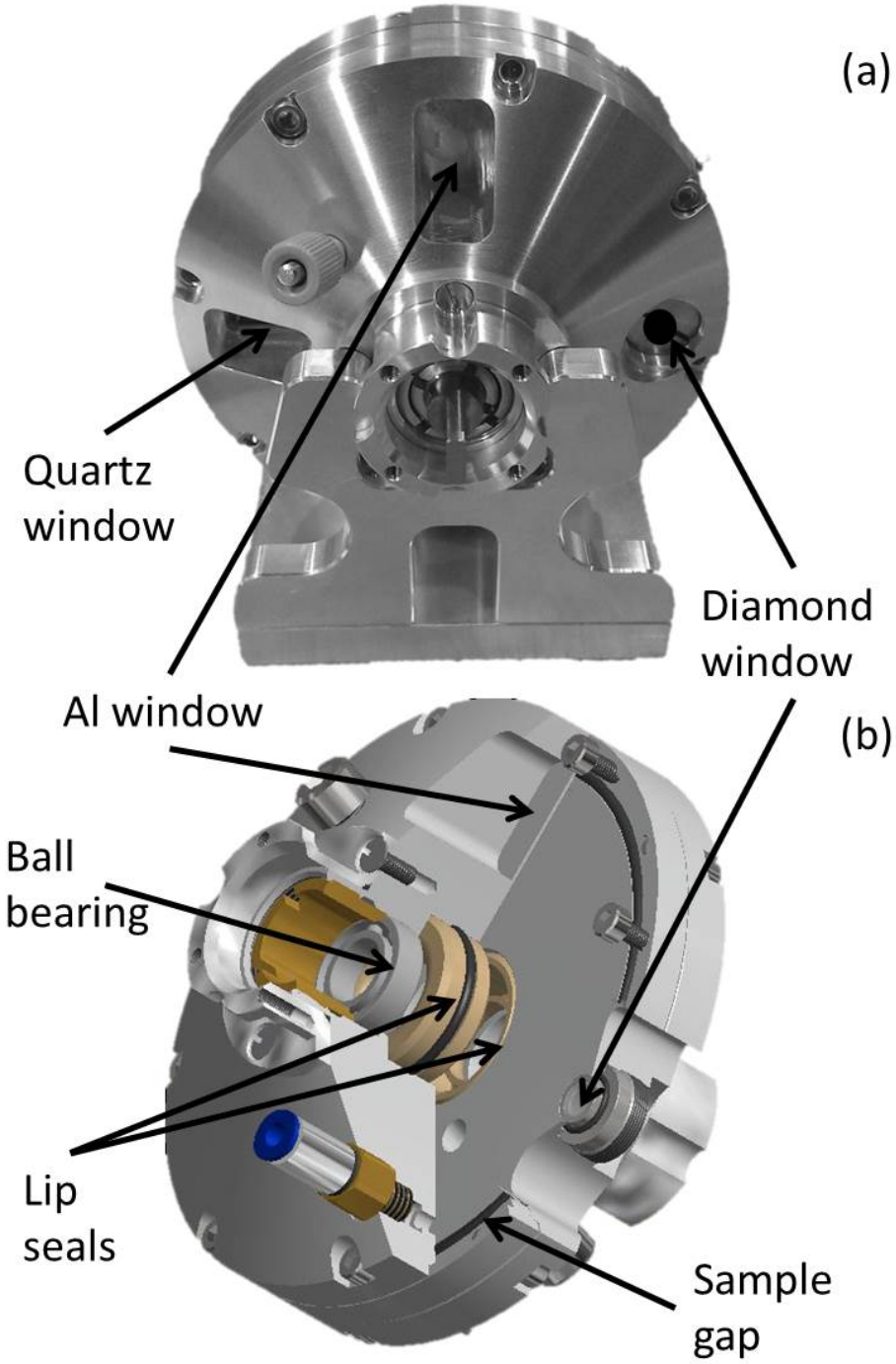

Figure 3.10: A foto (a) and a schematic drawing (b) of the shear-cell, outlining windows and some other construction elements of the cell

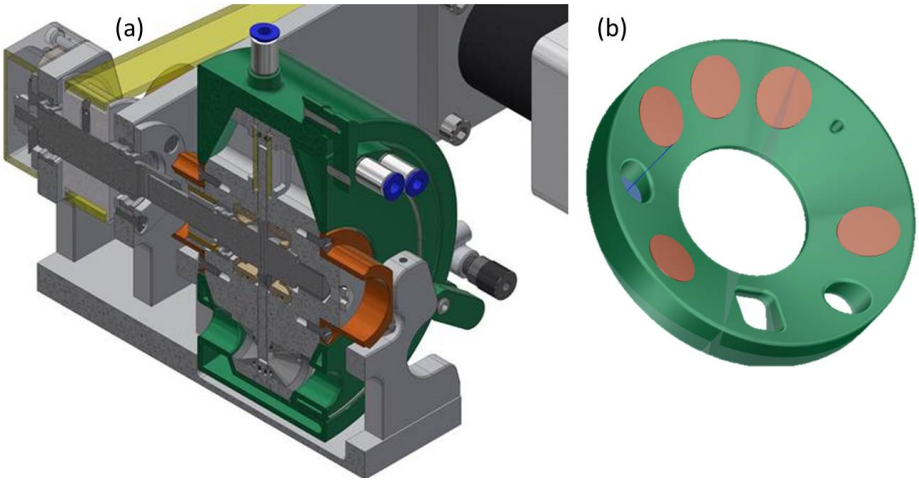

Figure 3.11: A cross section of the cell in thermostatic shell (a) and an internal surface of the shell with copper insertions in it (b)

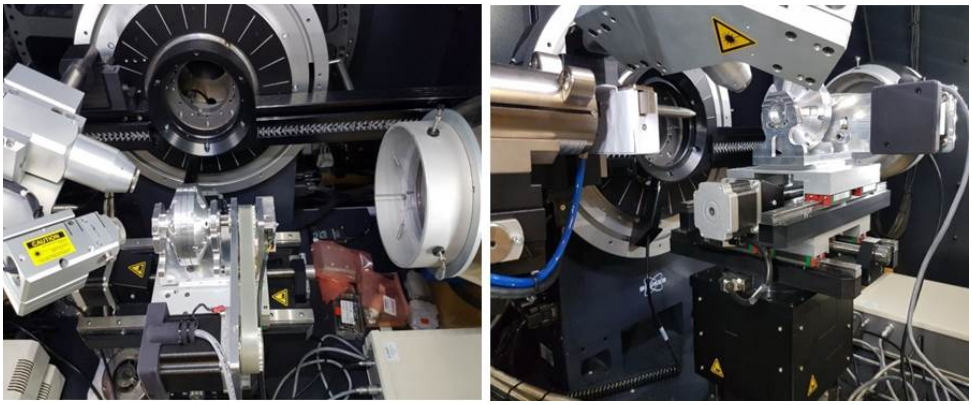

Figure 3.12: An image of the developed Couette shear cell mounted at the lab-scale X-ray diffractometer Bruker D8-Discover

4

STRUCTURE AND STABILITY OF MICROFIBRILLATED CITRUS FIBER UNDER SHEAR

Suspensions of microfibrillated citrus fiber were studied by means of SAXS, rheology, rheo-MRI, and shear-SAXS. The effect of high pressure on the structure of the suspensions was assessed by means of SAXS on the suspensions which were processed several times (from 0 to 4) by a high-pressure homogenizer. Rheo-MRI of the suspensions under mild shear-rates indicated the presence of flocs with sizes about 100 µm. Investigation of the internal structure of the flocs by means of shear-SAXS has shown that they consist of randomly oriented fibers, and homogeneous and stable on the length scales below 300 nm.

This chapter, by Evgenii Velichko, Ruud den Adel, Tatiana Nikolaeva, Raquel Serial, John van Duynhoven, and Wim G. Bouwman, has been prepared for publication in a scientific journal

4.1. INTRODUCTION

Global challenges, such as the growing world population, plastic pollution, climate change, and diminishing fossil resources, forcing humanity to look for renewable materials for production of a variety of daily products. One of the obvious sources of such materials is cellulose, the most abundant biopolymer on the planet. Present in all plants, cellulose is responsible for their mechanical strength and protection from aggressive environments. A series of mechanical and chemical treatments have to be performed in order to extract cellulose from plant cells. After a very high pressure treatment, cellulose pulp can be turned into microfibrillated cellulose (MFC) – a promissing material with a variety of applications, ranging from protective coatings [1], and packaging [2] to food and cosmetics [3].

First obtained in 1983 by Turbak and Herrick [4, 5], MFC has attracted considerable attention of the researchers worldwide. Some of the most remarkable properties of MFC are high theoretical strength and modulus [6, 7], high surface area and water absorption [2], and gel formation at very low concentrations of fibers [8, 9].

One of the most interesting characteristics of microfibrillated cellulose (MFC) suspensions is their peculiar rheological behavior. Due to a very high aspect ratio of cellulose microfibrils, as high as 75, they can form a gel already at concentrations as low as 0.04 wt % [8]. Application of shear disrupts the MFC gel network and starts the flow of flocs of fibrils [10]. A macroscopic mechanism of MFC flocculation under shear was proposed and tested with the aid of imaging [11, 12], ultrasonic speckle velocimetry [13], and MRI [14]. All of the researchers have agreed on the floc formation under shear with average floc sizes in the order of 100 μm with the smaller flocs forming at higher shear rates. However, the internal structure of the flocs is still unknown.

Small-angle scattering of X-rays (SAXS) and Neutrons (SANS) is a powerful tool for studying materials under shear [15, 16]. Main advantages of X-rays and neutrons are the range of studied length-scales, non-destructiveness, ability to penetrate bulky materials, and a possibility to adjust probed sample volume by altering the beam size. Broad research has been published concerning the structure of cellulosic materials from different origins at static conditions [17]. Moreover, fibrin networks, which are similar to MFC, were successfully studied by means of shear-SANS [18]. However, due to specifics of neutron interactions with the matter, it is suggested to use deuterated solvent and/or materials for SANS experiments. It has been shown that replacing hydrogen with deuterium can substantially change interactions in the system and, therefore, affect its structure and rheology. As we wanted to avoid any experimental artifacts, we chose to perform shear-SAXS experiments.

In this work, we have first investigated the effect of the number of passes through a high-pressure homogenizer on the structure of MFC based on citrus fiber, as well as the effect of concentration of the fiber on the structure. Then, we have focused on the flocculation of the MFC and the internal structure of the flocs under shear. Rheo-MRI measurements were performed to probe local flows of citrus fiber MFC and estimate averaged sizes of flocs at different shear rates. Furthermore, a special shear-SAXS cell was designed to probe the internal structure of the flocs at different positions along the shear-gradient direction [16]. We believe, our results to be of interest to both, the progress of fundamental knowledge in the field of non-local rheology, as well as to in-

dustrial use of MFC suspensions.

4.2. MATERIALS AND METHODS

4.2.1. MATERIALS

Two sets of microfibrillated citrus fiber materials were investigated in this study: series of various concentrations obtained from 2% suspension and series of the various number of defibrillation passes. Initial suspension of citrus fiber was prepared from citrus fiber powder by suspending it in demineralized water at concentration 2 or 1% wt. A sample of the initial 1% suspension was saved for later investigation. The suspensions were stirred by a Silverson mixer for 10 minutes and, consequently, pushed through a diamond coated Z-chamber (G10Z) of a high-pressure homogenizer (M-110S microfluidizer). The 2% suspension was pushed through the homogenizer once, while for the 1% suspension a part was saved for later investigation and the rest of material underwent 2, 3, and 4 homogenizing steps, respectively. Thereafter, a 0.08 w% of nipacide was added to the microfibrillated citrus fiber suspensions to prevent the material from deterioration by microorganisms. Ten samples of microfibrillated citrus fiber were prepared by dilution of the 2% suspension to various concentrations (0.05, 0.1, 0.2, 0.3, 0.4, 0.5, 0.8, 1, 1.5, 2%) with demineralized water.

4.2.2. SAXS

The high-brilliance ID02 beamline[19] of the European Synchrotron Radiation Facility (ESRF) was employed for small-angle X-ray scattering measurements. The measurements were performed in a broad range of momentum transfers: $3 \times 10^{-4} \leq Q/\text{Å} \leq 0.7$, where $Q = 4\pi\lambda \cdot \sin(2\theta)$ is the momentum transfer, where θ is a scattering angle and λ the wavelength of the used X-rays (in our experiments λ=0.0996 nm). The samples were placed in a 30 position temperature stage with aluminum sample holders between X-ray mica windows, at a constant temperature of the stage 20°C. Scattering of 2 mm of water between two mica windows was used for a background subtraction for all the measurements. Water reference ($I_{H_2O,20°C} = 1.641 \cdot 10^{-2}\text{cm}^{-1}$) was also used for scaling of the scattering intensities to absolute units [cm^{-1}].

The SAXS data were fitted using SASview package [20] software and applying a two-level scattering model. The model consists of a cylinder form-factor of the cellulose fibrils with polydisperse radii, and a power-law function describing the agglomerates of the fibrils:

$$I(Q) = \frac{sf}{V} \cdot \sum_{R_{cyl}} n(R_{cyl}, \sigma_{R_{cyl}}) \cdot P(q, R_{cyl}, L, \rho_{cyl}, \rho_{solv}) + A \cdot q^{-m}, \tag{4.1}$$

where the first term corresponds to the form factor of a cylinder with polydisperse radii, multiplied by the number density of particles (sf/V), where V is the total volume of the particle, and the second term accounts for the power-law behavior of the network. The model is inspired by the one proposed and successfully applied by Martinez-Sanz et al. [21, 22]. However, for our data treatment, we simplified the model by removing the shell component. We will explain this modification in Sec. 4.3.1. Although most of the works employing the core-shell cylinder model were focused on the characterization of

the individual fibrils [22–25], the power-law term of the model plays an important role in the description of the fibrillar networks. For example, the low-Q power-law dependency of scattering was used to extract a fractal dimension of the fibrin network [26].

4.2.3. RHEOLOGY

Flow curves of the microfibrillated cellulose suspensions were measured on a stress-controlled rheometer (AR 2000, TA Instruments), using a plate-plate geometry (plate diameter 4 cm, gap 1 mm). During the measurements, the shear rate was firstly increased from 0.1 to 500 s^{-1} in 2 min and then decreased back to 0.1s^{-1} in 2 min. Sand-blasted metal plates were used to prevent wall slip. The system was temperature controlled with a Peltier system at a temperature of 20 ± 0.1°C.

4.2.4. RHEO-MRI

TTime-averaged velocity profiles were measured according to procedures by Callaghan et al. [27, 28] on a Bruker Avance II spectrometer at 7.0 T magnetic field strength (resonance frequency 300 MHz for 1H). The magnet was equipped with a Bruker rheo-MRI accessory in combination with a cone-plate (CP) geometry made of PEEK (cone angle 7.0°and cone diameter 1 cm). For all imaging experiments, the field of view was set to 25 mm and profiles of 1024 points were collected, resulting in a spatial resolution of 24 μm. For each shear rate, 64 signal acquisitions were collected and averaged. All velocity profiles were corrected for slippage employing the same approach proposed by de Kort et.al [14].

4.2.5. SHEAR-SAXS

The shear-SAXS measurements were carried out at the BM26 beamline of the European Synchrotron Radiation Source, Grenoble, France [29, 30]. A home-built horizontal Couette shear-cell [16] allowed the X-ray beam to be directed along the vorticity direction of the flow at different positions across the gap between the inner and outer cylinders. A gap of 1 mm with a 38 mm outer radius was used. Rotation speed was applied to the inner cylinder of the shear-SAXS cell. Measurements were performed under constant shear for 10 minutes, after which another shear rate was imposed on the same sample. Shear rates applied on the same sample were 0, 1, 3, 5, 10, 15,20, 30, 40, 50, 100, 300, 100, 50, 40, 30, 20, 15, 10, 5, 3, 1, and 0 s^{-1}. The beam cross-section at the sample position was about 120 μm, which allowed us to measure five different positions across the gap without overlap. We used the Pilatus detector with a resolution of 981×1043 pixels and a pixel size of 172×172 μm^2 positioned at a distance of 6672 mm away from the sample for the SAXS measurements with a wavelength λ = 1.033 Å. The experimental setup gave access to the momentum transfer range of $3.7 \times 10^{-3} \leq Q/Å \leq 0.1$. Standard corrections for sample absorption and background subtraction were applied. The scattering intensities were scaled to absolute units [cm^{-1}] using a water reference ($I_{H_2O,20°C} = 1.641 \cdot 10^{-2} cm^{-1}$).

4.3. RESULTS AND DISCUSSION

4.3.1. STRUCTURAL CHANGES IN CITRUS FIBER SUSPENSIONS DUE TO HIGH PRESSURE HOMOGENIZATION

Multiple studies have shown the effect of high-pressure homogenization on the rheological properties of the MFC [1, 10–12, 31–34]. However, none of these studies could tell how deep the homogenization propagates into MFC structure. In order to bridge this gap, we have performed SAXS measurements on MFC suspensions before and after high-pressure homogenization for up to 4 passes through the homogenizer.

SAXS

Figure 4.1 shows the SAXS scattering curves for the 1% citrus fiber suspension before and after microfibrillation with their respective fitting curves. The curves can be visually separated into two parts: high-Q range (above $\approx 1{\cdot}10^{-2}$Å^{-1}) corresponds to the form-factor of individual fibrils in MFC, while the low-Q region (below $\approx 1{\cdot}10^{-2}$Å^{-1})is related to the fibrillar network. We started our fitting procedures with the core-shell cylinder model described in [21, 22]; however, the fitting algorithm was decreasing the value of shell thickness ($t = R_{shell} - R_{core}$) to the values close to 0 (1×10^{-5}Å). Fixing this parameter to 0 improved the overall quality of fits and substantially decreased computation time. This effect could be explained by the differences in the scattering of neutrons and X-rays. The model is more advantageous for neutron scattering, where scattering contrast between different parts of material could be substantially increased by application of contrast variation technique (based on the difference in the scattering of H and D atoms). In the case of X-ray scattering, there is much less contrast between crystalline, paracrystalline and amorphous cellulose (14.46, 13.65, and 13.38 $\times 10^{10}$ cm^2, respectively), and it cannot be easily altered. Therefore, in the later analysis, we have reduced our model to the sum of polydisperse cylinders form factor and absolute power law, presented by Eq. 4.1.

Table 4.1: Fitting results for the 1% citrus fiber before and after microfibrillation

N passes	ρ_{cyl}* (10^{10} cm^{-2})	ρ_{solv}* (10^{10} cm^{-2})	sf/V	R^{+}_{cyl}, Å	L^*, Å	A	m
0	13.83	9.47	0.0032(5)	14.8(9)	9999	$5.1(4)\cdot10^{-6}$	2.70(5)
1	13.83	9.47	0.0029(5)	15.3(9)	9999	$3.2(4)\cdot10^{-5}$	2.60(5)
2	13.83	9.47	0.0033(5)	14.5(9)	9999	$4.0(4)\cdot10^{-5}$	2.55(5)
3	13.83	9.47	0.0029(5)	15.3(9)	9999	$6.1(4)\cdot10^{-5}$	2.50(5)
4	13.83	9.47	0.0027(5)	15.5(9)	9999	$5.0(4)\cdot10^{-5}$	2.50(5)

* parameters which were fixed in the fitting process

+ polydispersity of radii was fitted with log-normal distribution with a standard deviation of 0.3 fixed for all of the fitting results

As can be seen from the table 4.1, the main changes of the structure due to defibrillation of citrus fiber are on the level of the fibrillar network, scattering of which is described by absolute power law term of the scattering model. As can be seen from figure 4.2, the m parameter decreases with the defibrillation and levels off at a value of 2.5 after

3 passes. In scattering theory [35] values $m < 3$ are attributed to mass-fractal with fractal dimension $D_f \equiv m$ and higher values of m correspond to the higher density of fractal building blocks [36]. Therefore, we can conclude that defibrillation leads to loosening of the fibrillar network.

As can be seen from figure 4.3(a), although radii of the elementary fibrils stay the same at all concentrations of fiber, their volume fraction linearly increases with concentration. From figure 4.3(b) we can see that m parameter of the absolute power law increase with the concentration of fibers. This increase of the fractal dimension can be structurally explained by the increase in the density of fibers and a decrease in the distance between the network nodes with increasing concentration of fibrils. A similar effect was previously reported for the fibrin networks [26].

4.3.2. IMPACT OF LOW SHEAR ON STABILITY OF MICROFIBRILLATED CITRUS FIBER

RHEOLOGY

Figure 4.4 shows flow curves for various concentrations of microfibrillated citrus fiber suspensions. A peculiar property of the curves is some hysteresis in the low shear-rates region. The initial viscosity of the materials is higher than the one after relatively high shear rates. A similar effect was observed previously in MFC [1, 13, 31]. It was suggested that the shear slowly breaks down the no-shear gel structure and the shear thinning effect was attributed to the orientation of the fibrils along the flow direction[31]. The difference between the increasing and decreasing shear-rate curves was explained by the energy transferred to the system at high shear-rates, which allowed for higher mobility of the fibrils. In contrast to the orientation hypothesis by of Iotti *et al.*, other groups have observed flocculation of MFC and attributed the peculiar rheology of MFC to the flocculated flow with decreasing floc sizes with increasing shear-rates [11–14].

RHEO-MRI

In order to address the flocculation of microfibrillated citrus fiber suspensions, we have performed rheo-MRI measurements at various shear-rates. Results of rheo-MRI measurements are presented in figure 4.5. The results are in good agreement with similar experiments performed for bacterial cellulose suspensions by de Kort et al. [14]. The experimental results were fitted with a model proposed by Goyon et al. [37], accounting for nonlocal effects. As a fitting result, length scale parameter ξ was defined at several shear rates. As can be seen from figure 4.5, the non-local model provides a correlation length of app. 100 μm, this is in line with the estimated size of the microfibrillated cellulose flocs. Unfortunately, rheo-MRI could not resolve the internal structure of these inhomogeneities and answer whether the flocs are formed by aligned of randomly oriented fibrils. Therefore, we have designed and performed a shear-SAXS experiment to investigate the structure of MFC under shear.

SHEAR-SAXS

We have had two major hypotheses for the internal organization of MFC flocs in mind: a) isotropic aggregation of randomly oriented microfibrils, and b) local alignment of fibrils inside the flocs. As small angle scattering is very sensitive to the orientation of fibrous

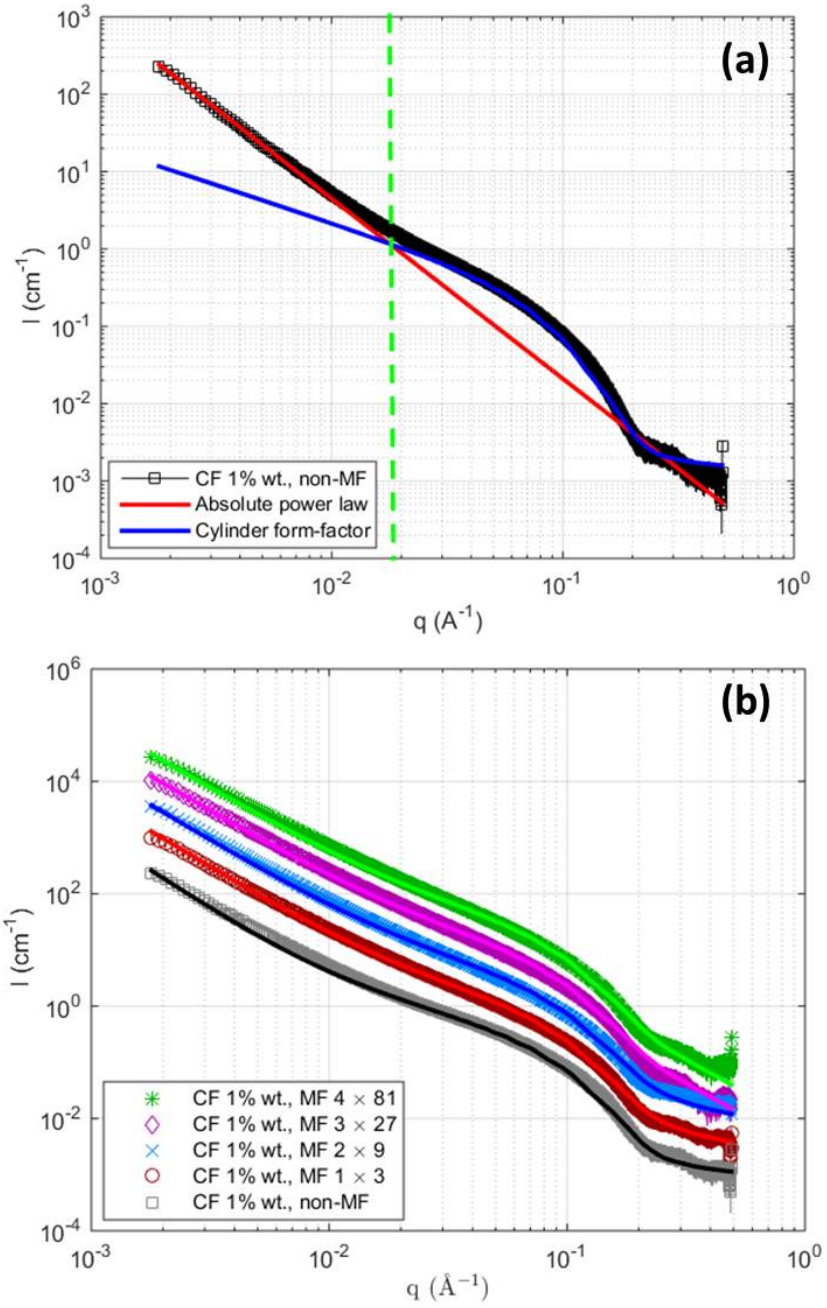

Figure 4.1: (a) Small-angle X-ray scattering curve of 1% suspension of Citrus Fiber before homogenization with individual parts of the scattering model and a division of the measured q range into high- and low-q parts, where either contribution of the model dominate the scattering; (b) measured SAXS curves (symbols) with respective fitting results (solid lines) for 1% suspension of Citrus Fiber before and after going through high-pressure homogenizer several times

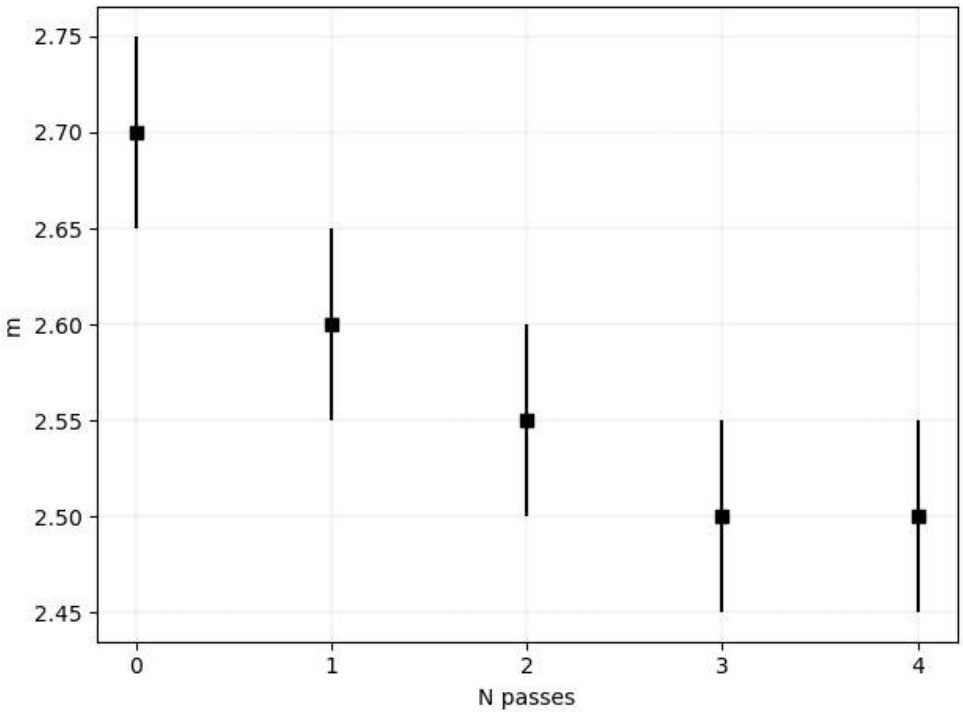

Figure 4.2: Effect of the number of passes through a high-pressure homogenizer on the network structure of 1% suspension of Citrus Fiber. Parameter m corresponds to the fractal dimension of the network ($D_f \equiv m$)

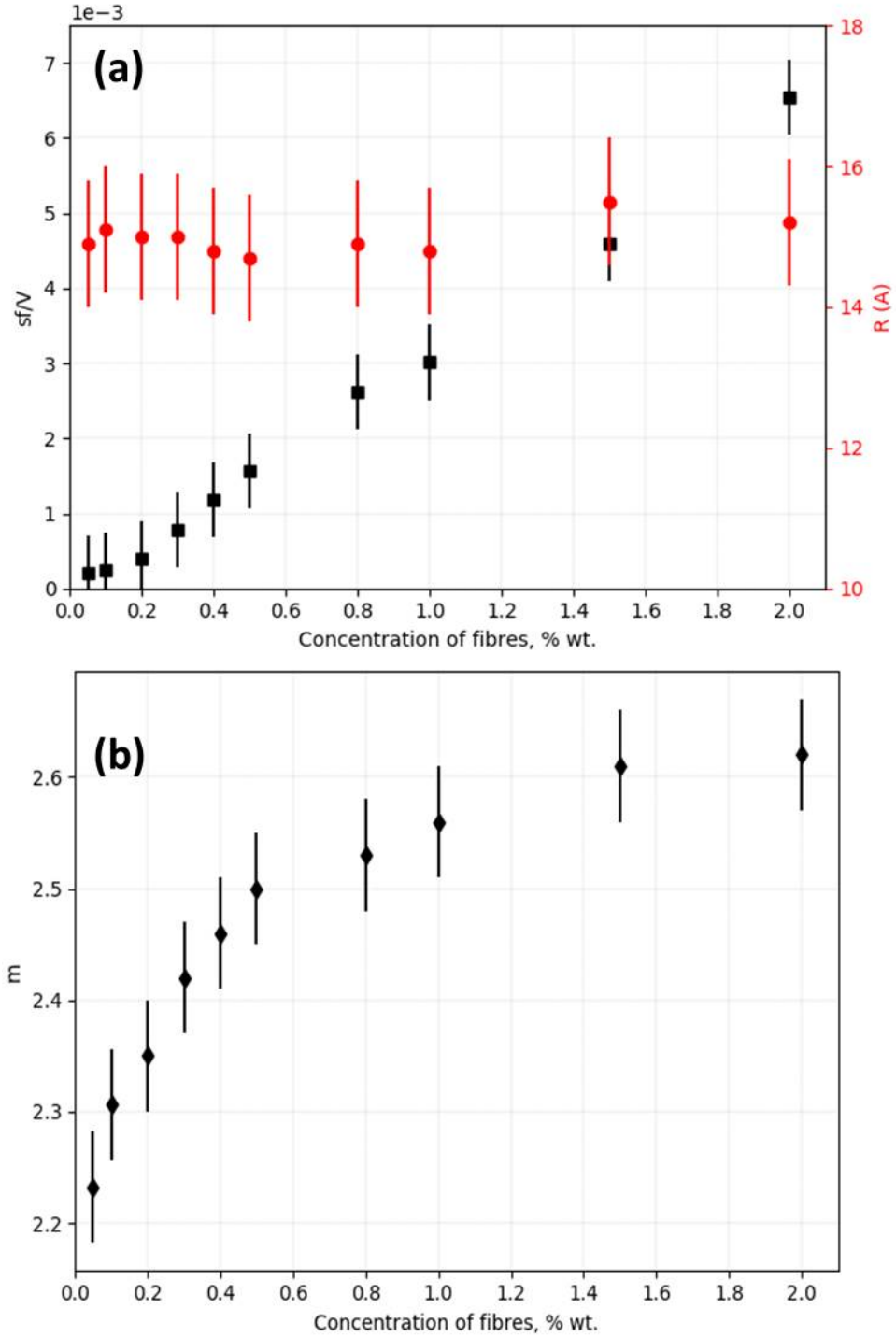

Figure 4.3: Effect of concentration on the structure of microfibrillated Citrus Fiber: (a) radii and volume fractions of elementary fibrils; (b) fractal dimension of the fibular network ($D_f \equiv m$)

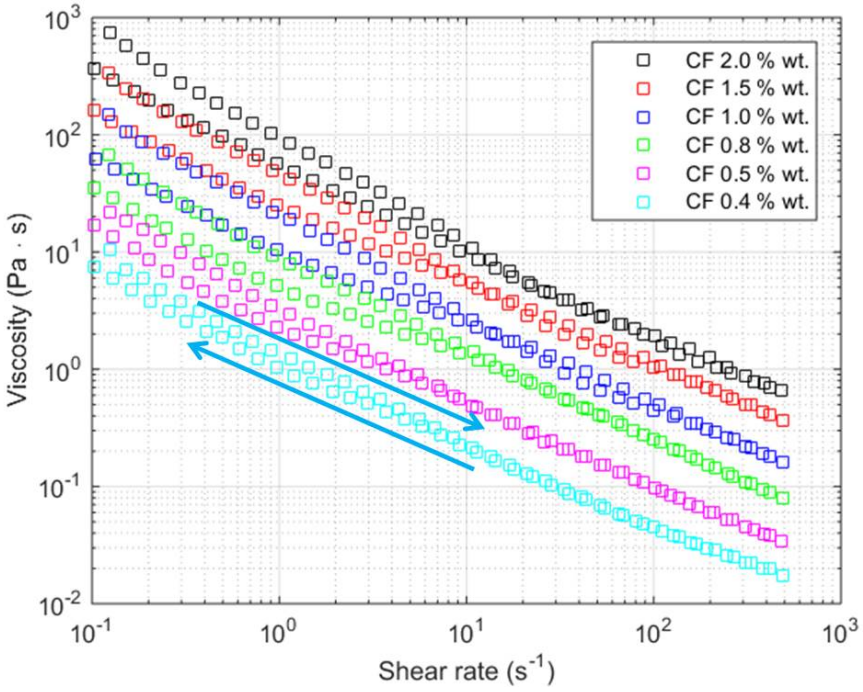

Figure 4.4: Flow curves for various concentrations of microfibrillated citrus fiber suspensions. All of the curves demonstrate shear-thinning behavior of the suspensions with some peculiar hysteresis at shear-rates below $10s^{-1}$: the initial increasing shear-rate curve is above the consecutive decreasing one for all of the samples

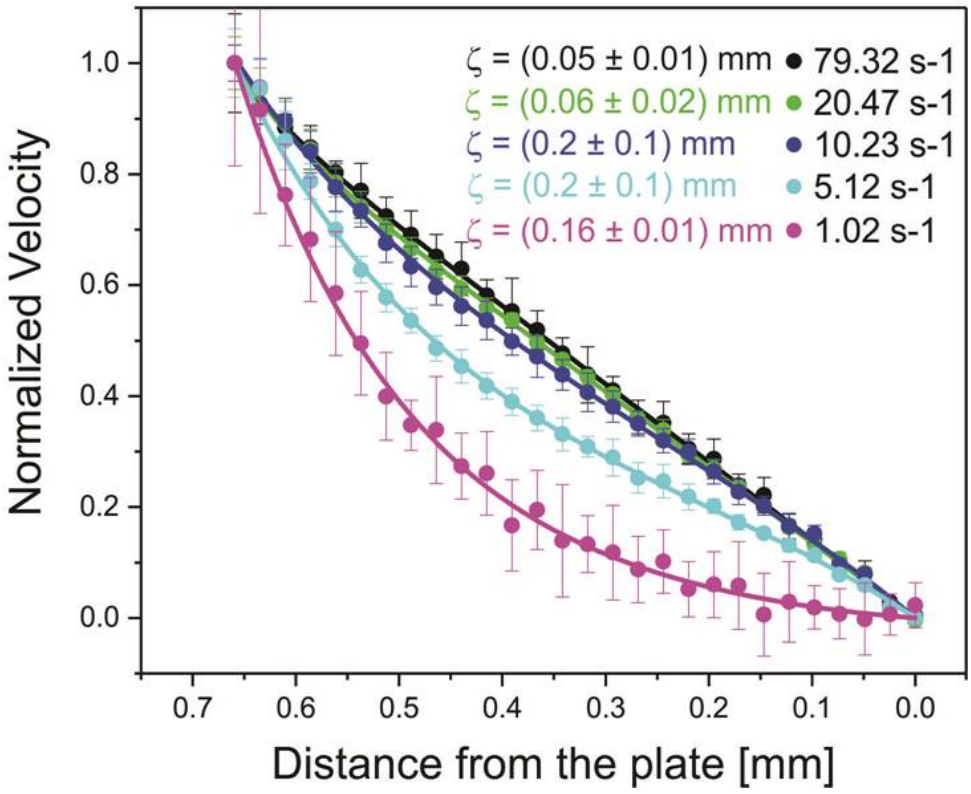

Figure 4.5: Velocity profiles normalized to the cone velocity of the 0.3% microfibrillated citrus fiber suspension in CP geometry. Solid lines are fits to the nonlocal model proposed in [37]. The imaged gap is 0.65 mm wide at the position where the profile was measured. For all profiles, slippage at the plate was corrected employing the approach used by de Kort, et. al [14]

gels [18], we expected to see isotropic scattering patterns as support for the first hypothesis and strongly anisotropic ones in support of the second one.

The first step in the analysis of shear-SAXS results was a visual inspection of the 2D scattering patterns. As can be seen from figure 4.6, no anisotropy of scattering was observed at the experimental conditions. In order to quantify this conclusion, we have performed an anisotropy analysis of the 2D patterns. We have applied a Legendre series expansion to fit our azimuthally averaged scattering curves, as was performed before by Weigandt et al. [18]:

$$F(\varphi) = \Sigma_{n=0}^{\infty} a_n P_{2n}(\cos(\varphi - (\varphi_0 + \pi/2))), \tag{4.2}$$

where φ and φ_0 are an azimuth angle and its shift, the values a_n are fitting coefficients, and the functions P_{2n} are even Legendre polynomials. We used the first eight terms of the series for the fitting. The orientation parameter $\overline{P_2}$ was determined from the $F(q,\varphi)$ dependencies as

$$\overline{P_2} = \frac{a_1}{5}. \tag{4.3}$$

The orientation parameter $\overline{P_2}$ defines the level of fiber alignment, it varies between zero for randomly oriented fibers and unit for the perfectly aligned ones.

Figure 4.7 shows the steps of the analysis. Firstly, the most appropriate q-range was chosen by scanning radial direction of one of the 2D scattering patterns from beam-stop outwards and calculating orientation parameter $\overline{P_2}$ for each detector pixel size step. We found that above $q = 0.014$Å (45 pixel from the beam center) $\overline{P_2}$ drops below 0.01 and below $q = 0.01$Å (32 pixel from the beam center) the azimuthally averaged scattering curves contained many artifacts due to shadow effect from the beam-stop. Therefore, we have limited our q-range for anisotropy analysis to $0.01\text{Å}^{-1} \leq q \leq 0.014\ \text{Å}^{-1}$ (annular ring in figure 4.7(a)). It should be noted that $q \geq 0.02\ \text{Å}^{-1}$ is the region of momentum transfers where scattering from individual fibrils dominates the pattern. Therefore, we can conclude the absence of global alignment of fibrils in the system under applied conditions. Figure 4.7(b) shows an example of azimuthally averaged scattering curves and their respective fits for a suspension of microfibrillated citrus fiber. Figure 4.7(c) shows the orientation parameter as a function of shear rate for a 0.2% citrus fiber suspension. As can be seen, there is very little orientation ($\overline{P_2}$ <0.06), which indicates the absence of the global alignment of fibrils and supports isotropic floc hypothesis. Since no extra information could be extracted from the 2D scattering patterns, the patterns were reduced to 1D I vs. q dependencies, which were used in further analysis.

Figure 4.8 shows typical 1D SAXS dependencies and their fitting curves for 0.2% MFC suspension at 0 and 300 s^{-1} shear-rate. For the fitting of shear-SAXS data, we found out that the parameters of the cylinder form-factor part of the scattering model 4.1 did not vary much in the fitting process. It can be easily explained by the limits of the investigated q range in shear-SAXS experiments: most of the form-factor features fall above $q = 0.1$Åand could not be observed. Therefore, in the analysis, we have fixed these parameters to the values found in section 2.3.4. In this way, we could obtain information

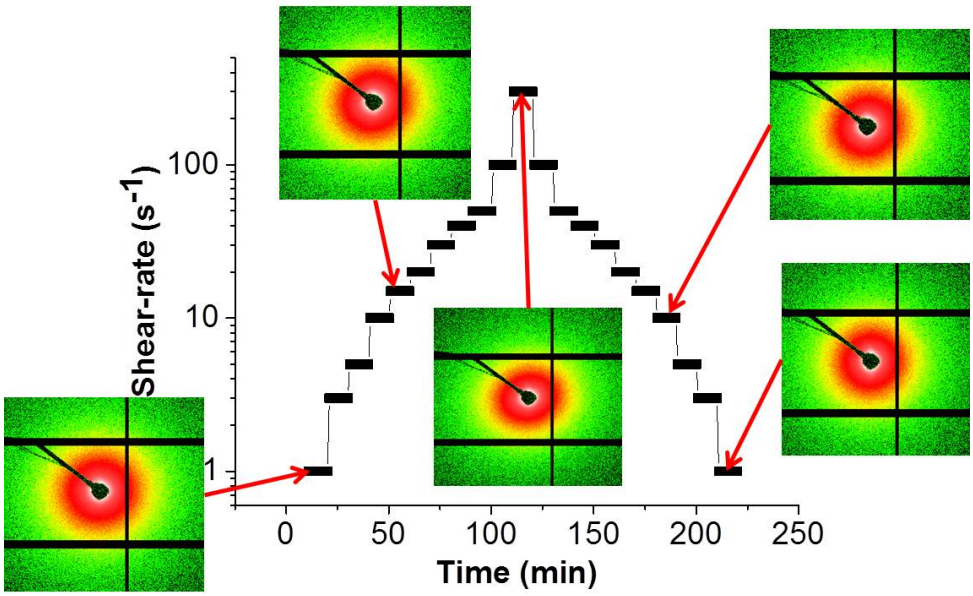

Figure 4.6: Graphical representation of the shear-SAXS measurement protocol and 2D scattering patterns of the 0.2% microfibrillated citrus fiber suspension. Black lines on the 2D patterns appear due to space between different modules of Pilatus detector, and the dark spot in the center is due to beam stop

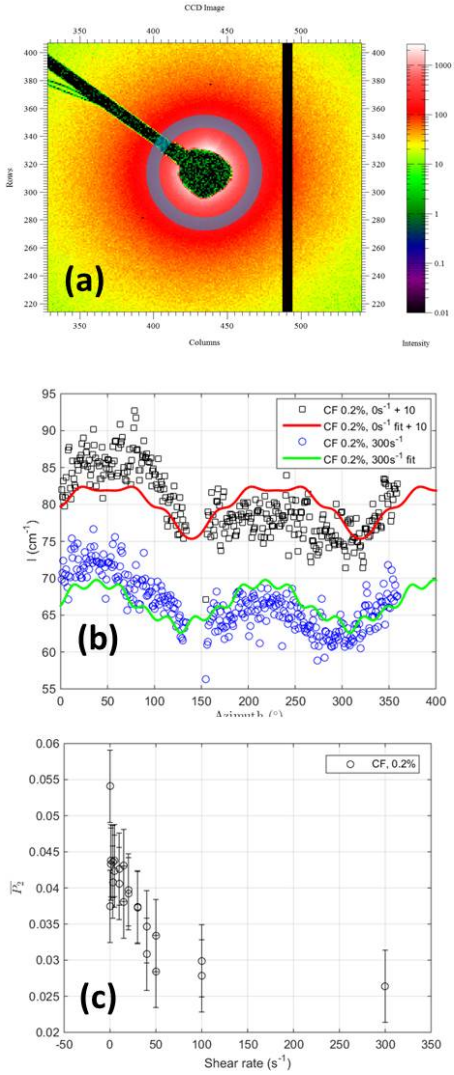

Figure 4.7: Analysis of scattering anisotropy: (a) a typical 2D scattering pattern with an indictaion of the annular ring (0.01Å$\leq q \leq$ 0.014Å) over which I(φ) is calculated, (b) annular intensity averages of 2D scattering profiles for a suspension of microfibrillated citrus fiber at concentration of 0.2% wt. at 0 and 300 s^{-1} shear rates. Lines correspond to the Legendre expansion fits, (c) anisotropy parameter as a function of shear rate for citrus fiber MFC suspension at concentration of 0.2% wt.

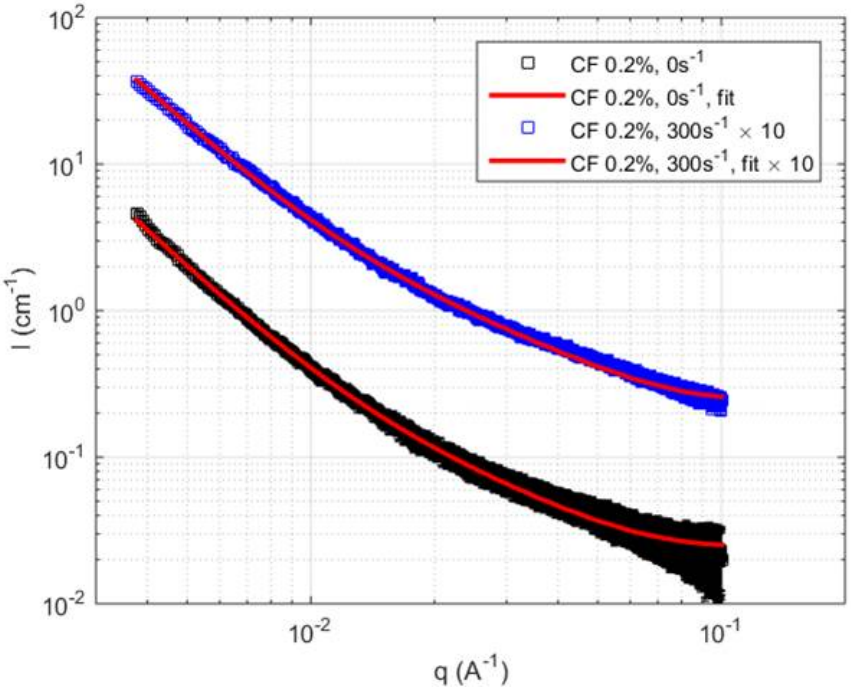

Figure 4.8: Small-angle X-ray scattering curves, measured at 0 and 300 s^{-1} shear-rate for citrus fiber MFC suspension at 0.2% wt. concentration

on the organization of a network of cellulose fibrils under shear expressed in the fractal dimension of the network D_f.

Figure 4.9 demonstrates a typical dependency of D_f on the applied shear-rate for a 0.2% CF suspension. As can be seen, there is no clear dependence of the fractal dimension on the position along the shear-gradient direction of the shear-cell, or on the applied shear rate. Therefore, we conclude that although the overall floc sizes are changing under applied shear, their internal structure remains almost intact in the course of shearing. It could explain hight stability and homogeneity of the studied MFC suspensions.

The dependencies of fitting parameters on the shear-rate and the positions across the gap for the suspensions of microfibrillated citrus fiber do not show any trend. It indicates that the suspensions are homogeneous on the length-scales below 300 nm and that the internal structure of flocs is preserved throughout the entire measured range of shear rates.

DISCUSSION

Our findings indicate the formation of flocs of microfibrillatd cellulose with the typical sizes in the order of 100 μm. No fibril alignment within the flocs was observed at shear-rates up to 300s^{-1}. A slight anisotropy of 2D scattering patterns ($\overline{P_2}$ <0.06) at

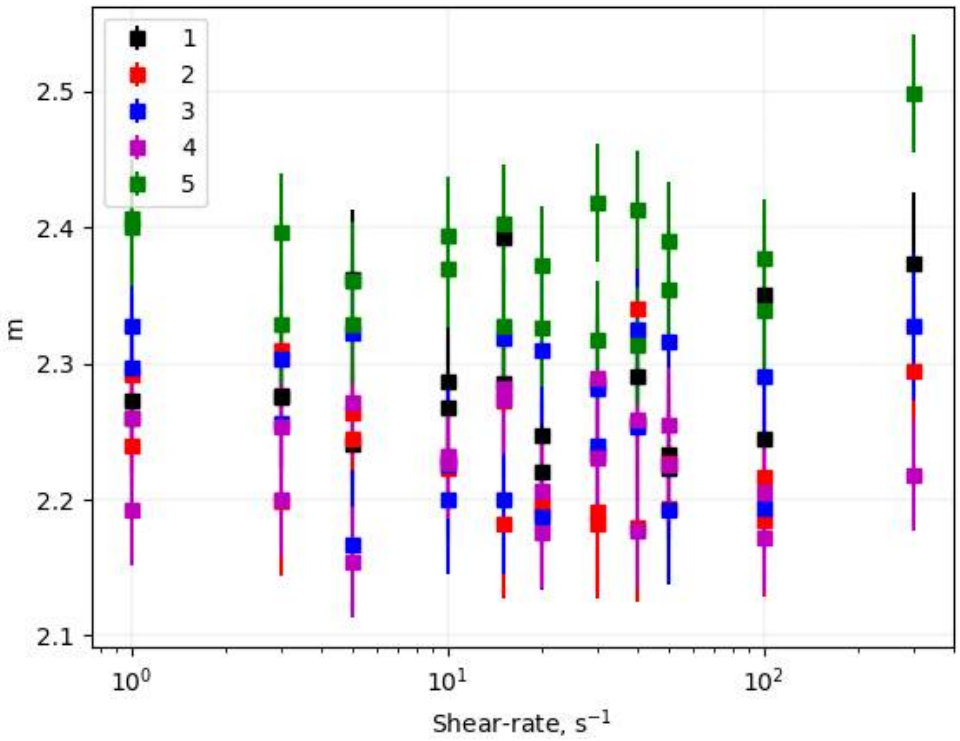

Figure 4.9: Fitting results of the fractal dimension of the MFC network for a 0.2% CF suspension. Line numbers correspond to the beam position within the gap of the shear-cell, 1 bein the closest to rotor, and 5 is closest to stator

$q < 0.014$Åwas attributed to elongation of the flocs. There was no change of radii of microfibrils at different positions across the gap of the shear-cell at all applied shear-rates. This finding indicates that suspensions are quite stable and homogeneous under the applied experimental conditions.

4.4. CONCLUSIONS

Results of this work suggest that even large shear applied on citrus fiber suspensions by high-pressure homogenization does not affect cross-sectional sizes of the elementary fibrils in the system. On a larger scale, on the other hand, it disrupts the microfibrillar network, which is reflected in a decrease in its mass-fractal dimension. Rheo-MRI measurements confirm the appearance of the flocculated flow of MFC already under relatively small shear rates (about 10 s^{-1}). The sizes of flocs are estimated to be about 100 μm. The internal structure of the flocs consists of randomly oriented intertwined fibers. Consistency of the structural parameters of the suspensions at different positions across the gap of shear-cell and at the various shear rates (varied between 1 and 300s^{-1}) suggest that the citrus fiber MFC system is stable and homogeneous under these conditions.

REFERENCES

[1] F. Grüneberger, T. Künniger, T. Zimmermann, and M. Arnold, *Rheology of nanofibrillated cellulose/acrylate systems for coating applications,* Cellulose **21**, 1313 (2014).

[2] K. L. Spence, R. A. Venditti, O. J. Rojas, Y. Habibi, and J. J. Pawlak, *The effect of chemical composition on microfibrillar cellulose films from wood pulps: water interactions and physical properties for packaging applications,* Cellulose **17**, 835 (2010).

[3] D. Klemm, E. D. Cranston, D. Fischer, M. Gama, S. A. Kedzior, D. Kralisch, F. Kramer, T. Kondo, T. Lindström, S. Nietzsche, K. Petzold-Welcke, and F. Rauchfuß, *Nanocellulose as a natural source for groundbreaking applications in materials science: Today's state,* Materials Today **21**, 720 (2018).

[4] A. F. Turbak, F. W. Snyder, and K. R. Sandberg, *Microfibrillated cellulose, a new cellulose product: properties, uses, and commercial potential,* (United States, 1983).

[5] F. W. Herrick, R. L. Casebier, J. K. Hamilton, and K. R. Sandberg, *Microfibrillated cellulose: morphology and accessibility,* (United States, 1983).

[6] D. G. Hepworth and D. M. Bruce, *Method of calculating the mechanical properties of nanoscopic plant cell wall components from tissue properties,* Journal of Materials Science **35**, 5861 (2000).

[7] Y.-C. Hsieh, H. Yano, M. Nogi, and S. J. Eichhorn, *An estimation of the Young's modulus of bacterial cellulose filaments,* Cellulose **15**, 507 (2008).

[8] A. Naderi, T. Lindström, and T. Pettersson, *The state of carboxymethylated nanofibrils after homogenization-aided dilution from concentrated suspensions: a rheological perspective,* Cellulose **21**, 2357 (2014).

[9] S. J. Veen, A. Kuijk, P. Versluis, H. Husken, and K. P. Velikov, *Phase Transitions in Cellulose Microfibril Dispersions by High-Energy Mechanical Deagglomeration,* Langmuir **30**, 13362 (2014).

[10] U. Björkman, *The metarheology of crowded fibre suspensions,* Annual Transactions of the Nordic Rheology Society **14**, 69 (2006).

[11] E. Saarikoski, T. Saarinen, J. Salmela, and J. Seppälä, *Flocculated flow of microfibrillated cellulose water suspensions: An imaging approach for characterisation of rheological behaviour,* Cellulose **19**, 647 (2012).

[12] A. Karppinen, T. Saarinen, J. Salmela, A. Laukkanen, M. Nuopponen, and J. Seppälä, *Flocculation of microfibrillated cellulose in shear flow,* Cellulose **19**, 1807 (2012).

[13] F. Martoïa, C. Perge, P. J. J. Dumont, L. Orgéas, M. A. Fardin, S. Manneville, and M. N. Belgacem, *Heterogeneous flow kinematics of cellulose nanofibril suspensions under shear,* Soft Matter **11**, 4742 (2015).

[14] D. de Kort, S. Veen, H. Van As, D. Bonn, K. Velikov, and J. van Duynhoven, *Yielding and flow of cellulose microfibril dispersions in the presence of a charged polymer,* Soft Matter (2016), 10.1039/c1sm05495c.

[15] A. P. R. Eberle and L. Porcar, *Flow-SANS and Rheo-SANS applied to soft matter,* Current Opinion in Colloid & Interface Science **17**, 33 (2012).

[16] E. Velichko, B. Tian, T. Nikolaeva, J. Koning, J. van Duynhoven, and W. G. Bouwman, *A versatile shear cell for investigation of structure of food materials under shear,* Colloids and Surfaces A: Physicochemical and Engineering Aspects **566**, 21 (2019).

[17] M. Martínez-Sanz, M. J. Gidley, and E. P. Gilbert, *Application of X-ray and neutron small angle scattering techniques to study the hierarchical structure of plant cell walls: A review,* Carbohydrate Polymers **125**, 120 (2015).

[18] K. M. Weigandt, L. Porcar, and D. C. Pozzo, *In situ neutron scattering study of structural transitions in fibrin networks under shear deformation,* Soft Matter **7**, 9992 (2011).

[19] T. Narayanan, O. Diat, and P. Bösecke, *SAXS and USAXS on the high brilliance beamline at the ESRF,* Nuclear Instruments and Methods in Physics Research Section A: Accelerators, Spectrometers, Detectors and Associated Equipment **467-468**, 1005 (2001).

[20] M. Doucet, J. H. Cho, G. Alina, J. Bakker, W. Bouwman, P. Butler, K. Campbell, M. Gonzales, R. Heenan, A. Jackson, P. Juhas, S. King, P. Kienzle, J. Krzywon, A. Markvardsen, T. Nielsen, L. O'Driscoll, W. Potrzebowski, R. Ferraz Leal, T. Richter, P. Rozycko, T. Snow, and A. Washington, *Sasview version 4.2,* (2018).

[21] M. Martínez-Sanz, D. Mikkelsen, B. Flanagan, M. J. Gidley, and E. P. Gilbert, *Multiscale model for the hierarchical architecture of native cellulose hydrogels,* Carbohydrate Polymers **147**, 542 (2016).

[22] M. Martínez-Sanz, D. Mikkelsen, B. M. Flanagan, C. Rehm, L. de Campo, M. J. Gidley, and E. P. Gilbert, *Investigation of the micro- and nano-scale architecture of cellulose hydrogels with plant cell wall polysaccharides: A combined USANS/SANS study,* Polymer **105**, 449 (2016).

[23] M. Martínez-Sanz, P. Lopez-Sanchez, M. J. Gidley, and E. P. Gilbert, *Evidence for differential interaction mechanism of plant cell wall matrix polysaccharides in hierarchically-structured bacterial cellulose,* Cellulose **22**, 1541 (2015).

[24] M. Martínez-Sanz, M. J. Gidley, and E. P. Gilbert, *Hierarchical architecture of bacterial cellulose and composite plant cell wall polysaccharide hydrogels using small angle neutron scattering,* Soft Matter **12**, 1534 (2016).

[25] M. Martínez-Sanz, F. Pettolino, B. Flanagan, M. J. Gidley, and E. P. Gilbert, *Structure of cellulose microfibrils in mature cotton fibres,* Carbohydrate Polymers **175**, 450 (2017).

[26] K. M. Weigandt, D. C. Pozzo, and L. Porcar, *Structure of high density fibrin networks probed with neutron scattering and rheology,* Soft Matter **5**, 4321 (2009).

[27] P. T. Callaghan, *Principles of nuclear magnetic resonance microscopy* (Oxford University Press on Demand, 1993).

[28] P. T. Callaghan, *Rheo-NMR: nuclear magnetic resonance and the rheology of complex fluids,* Reports on Progress in Physics **62**, 599 (1999).

[29] M. Borsboom, W. Bras, I. Cerjak, D. Detollenaere, D. Glastra van Loon, P. Goedtkindt, M. Konijnenburg, P. Lassing, Y. K. Levine, B. Munneke, M. Oversluizen, R. van Tol, and E. Vlieg, *The Dutch–Belgian beamline at the ESRF,* Journal of Synchrotron Radiation **5**, 518 (1998).

[30] W. Bras, I. Dolbnya, D. Detollenaere, R. van Tol, M. Malfois, G. Greaves, A. Ryan, and E. Heeley, *Recent experiments on a small-angle/wide-angle X-ray scattering beam line at the ESRF,* Journal of Applied Crystallography **36**, 791 (2003).

[31] M. Iotti, Ø. W. Gregersen, S. Moe, and M. Lenes, *Rheological Studies of Microfibrillar Cellulose Water Dispersions,* Journal of Polymers and the Environment **19**, 137 (2011).

[32] K. Benhamou, A. Dufresne, A. Magnin, G. Mortha, and H. Kaddami, *Control of size and viscoelastic properties of nanofibrillated cellulose from palm tree by varying the TEMPO-mediated oxidation time,* Carbohydrate Polymers **99**, 74 (2014).

[33] T. Saarinen, M. Lille, and J. Seppälä, *Technical Aspects on Rheological Characterization of Microfibrillar Cellulose Water Suspensions,* Annual Transaction of the Nordic Rheology Society **17**, 121 (2009).

[34] H. Taheri and P. Samyn, *Effect of homogenization (microfluidization) process parameters in mechanical production of micro- and nanofibrillated cellulose on its rheological and morphological properties,* Cellulose **23**, 1221 (2016).

[35] J. Teixeira, *Small-angle scattering by fractal systems,* Journal of Applied Crystallography **21**, 781 (1988).

[36] G. Beaucage, *Small-Angle Scattering from Polymeric Mass Fractals of Arbitrary Mass-Fractal Dimension,* Journal of Applied Crystallography **29**, 134 (1996).

[37] J. Goyon, A. Colin, G. Ovarlez, A. Ajdari, and L. Bocquet, *Spatial cooperativity in soft glassy flows.* Nature **454**, 84 (2008), arXiv:0803.1352 .

5

MESOSTRUCTURE OF BACTERIAL CELLULOSE FROM NATA DE COCO AND FROM THE LAB WITH AND WITHOUT DEUTERATION STUDIED BY SANS

Bacterial cellulose suspensions from two different sources were studied with SANS. One set of materials was prepared from crushed cubes of the commercially available dessert nata de coco, and the second was obtained via microbial synthesis in-house at the Neutron Deuteration Facility at ANSTO. The in-house synthesized cellulose was either completely hydrogenated, or completely deuterated. It was found that mesostructure of hydrogenated bacterial cellulose from two different sources was very similar. However, the mesostructure of the deuterated material was found to be substantially different, which resulted in strong agglomeration and completely altered rheological properties. This shows that contrast variation in SANS is not always possible to determine arrangements of different components.

This chapter, by Evgenii Velichko, Robert Russell, Anna Sokolova, John van Duynhoven, and Wim G. Bouwman, is being prepared for publication in a scientific journal

5.1. INTRODUCTION

Microfibrillated cellulose (MFC) is a promising renewable material which can be used in a variety of applications, ranging from protective coatings [1], and packaging [2] to food and cosmetics [3]. It is obtained from cellulose fibres by high-pressure homogenization [4, 5]. Aqueous dispersions of MFC have to be protected from agglomeration by stabilizers, typically charged soluble polymers [6–8], such as carboxy methyl cellulose. However, the underlying mechanism of this stabilization is still unknown. It has been suggested, that the charged polymer absorbs on the surface of the cellulose microfibrils, increasing the ζ potential of the microfibrils, forming a repulsive shell around them, preventing agglomeration[6]. However, no experimental evidence for such behaviour is available in literature. In the industrial processing MFC undergoes a series of processing steps, most of which apply shear-stress. Under certain shear-rates the MFC starts to agglomerate, despite the presence of stabilizers [9]. Rheo-MRI investigation has shown shear-banding behaviour in such systems [8].

In order to understand the stabilization mechanism of the MFC by charged polymers and the peculiar flow of the MFC suspensions we constructed a special sample cell, which allows for scattering experiments on the materials under shear with spatial resolution across the velocity gradient direction of the cell. The cell design is described in detail in Chapter 3.

Flow-SAXS experiments were performed at DUBBLE beamline at ESRF. No alignment of microfibrills was observed at shear rates from 1 to 300 s^{-1}. The scattering invariant calculation indicated a homogeneous density distribution of cellulose microfibrils across the gap at all applied shear-rates. This implies that no shear induced aggregation and migration of cellulose over the gap occurs. However, due to similar electron densities of cellulose and CMC, SAXS could not give an answer about the role of charged polymers in stabilization and flow of MFC suspensions.

In order to find whether the charged polymer forms a shell around cellulose microfibrils, we have designed a small-angle neutron scattering experiment with different contrasts between cellulose microfibrils and the charged polymer. Contrast variation is a powerful technique for material investigation: It allows to increase the visibility of individual elements in a multi-component system. It can be achieved either by deuteration of the solvent [10] or the cellulose [11, 12]. In our experiment, we have tried both approaches: we have samples of bacterial cellulose prepared from nata de coco dessert in light or heavy water and samples of bacterial cellulose grown in a laboratory at National Deuteration Facility at ANSTO either hydrogenated in light water, or deuterated in heavy water.

Our measurements show, however, that deuteration has a too strong influence on the system. Deuterated bacterial cellulose was too much agglomerated and could not be homogenized. Our SANS measurements suggest that the sizes of microfibrils of deuterated cellulose are considerably larger than maximal sizes accessible in our SANS measurements (250 nm).

5.2. MATERIALS AND METHODS

5.2.1. MATERIALS

In this work we investigated bacterial cellulose suspensions from two different sources. The first set of bacterial cellulose suspensions were obtained from mango flavoured nata de coco dessert (Kara Santan Pertama, Bogor 16964, Indonesia). We have chosen this method since it is a relatively easy method to obtain the bacterial cellulose and our group has performed most earlier experiments on bacterial cellulose using this method. The drawback is that it cannot be used to obtain deuterated bacterial cellulose. Cubes of bacterial cellulose from four cups of the dessert were immersed in 750 ml of nanopure water (Barnstead Nanopure Diamond, resistance of 18 MΩ cm). The cubes were subsequently cut in a blender (Philips avance HR2096/01) and washed. At every washing step the cellulose suspension was filtrated over a vacuum filter (Whatman Schleicher and Schuell 113, wet-strengthened circles, 185 mm in diameter) and re-dispersed in 750 ml of nanopure water in the blender. After 8 washing steps, the filtered water was completely transparent and the cellulose residue had lost all artificial colours, from which we concluded that all of the added chemicals were removed from it. Consequently, the residue was re-dispersed in 200 mL of nanopure water. The weight percentage (wt %) of bacterial cellulose in the resulting suspension was determined by drying a part of it under vacuum over night and was adjusted to 0.4 wt % by adding extra nanopure water. Half of the final suspension was kept for further investigation (we denote it from now on as HBC_{nata} in H_2O), while the solvent in the other half was replaced with D_2O by centrifugation and removal of supernatant and replacement of it with D_2O (HBC_{nata} in D_2O).

The second set of bacterial cellulose suspensions was produced at Neutron Deuteration Facility at ANSTO, Australia, via microbial synthesis as described in [13]. One of the materials was completely hydrogenated in light water (from now on denoted as HBC_{lab} in H_2O) to be compared with the material extracted from the nata de coco to see if we had obtained the same material. The other sample was produced completely deuterated (DBC_{lab} in D_2O) by bio-synthesis in a deuterated medium to at least 95% deuteration, as determined from FT-IR and NMR measurements. Deuterated glucose-d12 and glycerol-d8 for this bio-synthesis were sourced from Sigma-Aldrich (cat. # 616338 and 447498, respectively).

It is important to note that the deuterated material was very agglomerated. Even after several dispersion steps in a blender the agglomerates were present in the form of blobs of cellulose, which were blocking any nozzle with a diameter below 2 mm. Fig. 5.1 shows the photo of the deuterated bacterial cellulose suspension filled in the experimental cell for SANS measurements. Due to this strong agglomeration of the material, it was not possible to perform high-pressure homogenization on it.

5.2.2. SANS

Small-angle neutron scattering measurements were performed at BILBY, [14] the SANS instrument at the high-flux reactor Opal in Lucas Heights, Australia. The scattering was measured in a q-range of 0.0025 to 1 $Å^{-1}$, where the magnitude of the scattering vector is defined as $q = (4\pi/\lambda \sin(\theta)$, where λ is the wavelength of the neutron and 2θ its scatter-

Figure 5.1: Photo of the deuterated bacterial cellulose suspension filled in the experimental cell for SANS measurements.

ing angle. The instrument was operated in the time-of-flight mode with λ in the range from 2 to 16 Åand two sets of detectors at 15 and 18 m distance from the sample, respectively. All data are corrected for sample cell background, transmission, normalised to an absolute scale and radially averaged. The incoherent background scattering from the solvent has been subtracted.

5.3. RESULTS AND DISCUSSION

5.3.1. COMPARISON OF MESOSTRUCTURE OF BACTERIAL CELLULOSE FROM NATA DE COCO AND THE LAB

The measurements of the bacterial cellulose prepared from nata de coco and from ANSTO are compared in Fig. 5.2. The shape of the measurements are very similar. There seems to be a Guinier regime at low q, followed by a power law decay and a background. The differences in intensity are proportional to the differences in scattering length density contrast and differences in concentration. To obtain a quantitative description of the measurements, the data are fitted with the generalised Guinier-Porod model [15]. For the mathematical details and symbols we refer to the original article [15]. The parameters

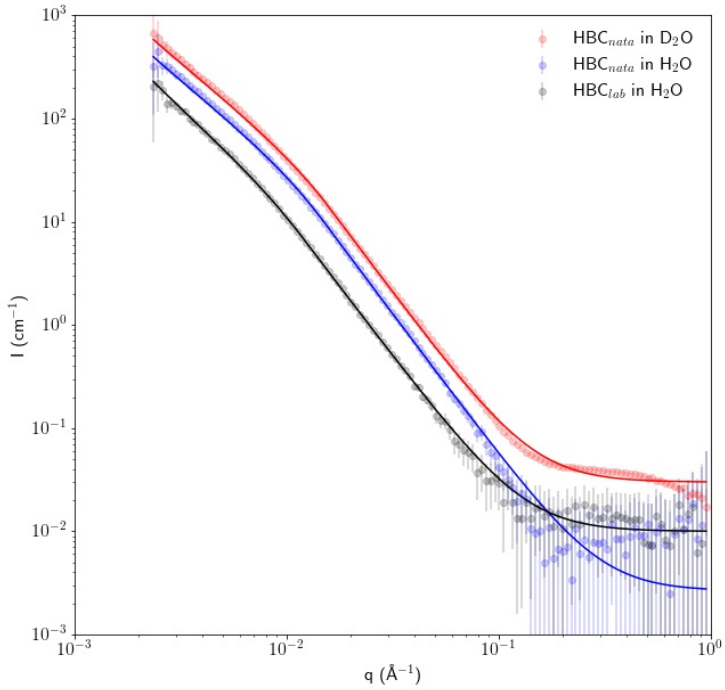

Figure 5.2: Normalised SANS measurements of the bacterial cellulose from nata de coco and as prepared in the lab in H_2O or D_2O. The data are fitted with the Guinier-Porod model and a background.

describing this model are the radius of gyration, R_g and the dimensionality s describing the dimension of these objects, the Porod power d and the scale G. The dimension of G depends on the value of d. The results are presented in Tab. 5.1. The value for the radius of gyration R_g had in all cases a value of some 60 Å, which corresponds to the size expected for the radius of the bundles of micro-fibrils in bacterial cellulose [16]. The corresponding dimension s has a value of 1.7, which is in between 1 for needles and 2 for platelets. This is a value we can expect, since it is known of bacterial cellulose that the micro-fibrils are produced by the bacteria in the shape of ribbons [16–18]. The value of the Porod exponent is 2.7, which is in line with previously observed values for pure bacterial cellulose and complexes of bacterial cellulose with other cell-wall polysacharides [19–21]. The bundles are composed of the micro-fibres yielding a roughness of the interface of the ribbons which indeed should be described with a Porod exponent lower than 4. The left over background will be due to imperfections in the subtraction of the solvent background and the incoherent scattering of the hydrogen in the cellulose itself.

Table 5.1: Fitting results for the studied suspensions of bacterial cellulose

Sample	scale	background [cm^{-1}]	R_g [Å]	s	d
HBC$_{nata}$ in D_2O	0.026(3)	0.030(1)	56(3)	1.6(1)	2.7(1)
HBC$_{nata}$ in H_2O	0.008(1)	0.010(1)	50(3)	1.8(1)	2.7(1)
HBC$_{lab}$ in H_2O	0.003(1)	0.010(1)	61(3)	1.8(1)	2.7(1)
DBC$_{lab}$ in D_2O	0.000024(3)	0.010(1)	–	–	2.8(1)

5.3.2. DEUTERATED CELLULOSE

The scattering data from the biodeuterated bacterial cellulose look rather different. They can be described by a single power law with an exponent with a value of 2.8 as shown in Fig. 5.3. This value for the Porod regime is similar as to the non-deuterated cellulose samples, which indicates that the interface properties are similar. Apparently, the aggregates of the micro-fibrils are larger than can be resolved with SANS. This explains why the samples are so much more viscous compared to the non-deuterated cellulose samples.

5.4. CONCLUSIONS

From the scattering data it is clear that the mesostructure of bacterial cellulose extracted from commercial nata de coco is the same as bacterial cellulose grown directly in the lab. The mesostructure is also independent on using H_2O or D_2O as a solvent. However, biodeuteration of bacterial cellulose has a dramatic effect on the mesostructure of bacterial cellulose. The biodeuteration results in much larger aggregates of the micro-fibrils of cellulose. This is likely also the cause for a much more viscous dispersion of this cellulose in water. So biodeuteration is not a viable method to resolve how a charged polymer influences the rheology of bacterial cellulose. As has been found before, deuteration is not always such an innocent method to create contrast in SANS [22]. The difference in zero-point vibrational energy of hydrogen and deuterium bonds [23] could be the cause for the significant effect deuteration has on the rheological properties of polysaccharides [24].

REFERENCES

[1] F. Grüneberger, T. Künniger, T. Zimmermann, and M. Arnold, *Rheology of nanofibrillated cellulose/acrylate systems for coating applications,* Cellulose **21**, 1313 (2014).

[2] K. L. Spence, R. A. Venditti, O. J. Rojas, Y. Habibi, and J. J. Pawlak, *The effect of chemical composition on microfibrillar cellulose films from wood pulps: water interactions and physical properties for packaging applications,* Cellulose **17**, 835 (2010).

[3] D. Klemm, E. D. Cranston, D. Fischer, M. Gama, S. A. Kedzior, D. Kralisch, F. Kramer, T. Kondo, T. Lindström, S. Nietzsche, K. Petzold-Welcke, and F. Rauchfuß, *Nanocellulose as a natural source for groundbreaking applications in materials science: Today's state,* Materials Today **21**, 720 (2018).

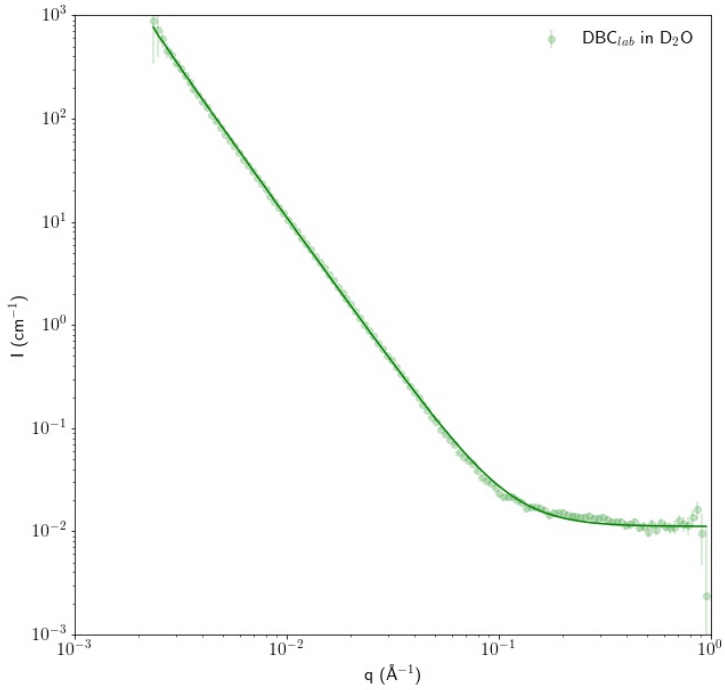

Figure 5.3: Normalised SANS measurements of the bacterial cellulose from nata de coco and as prepared in the lab in H_2O or D_2O. The data are fitted with the Guinier-Porod model and a background.

[4] A. F. Turbak, F. W. Snyder, and K. R. Sandberg, *Microfibrillated cellulose, a new cellulose product: properties, uses, and commercial potential,* (United States, 1983).

[5] F. W. Herrick, R. L. Casebier, J. K. Hamilton, and K. R. Sandberg, *Microfibrillated cellulose: morphology and accessibility,* (United States, 1983).

[6] S. J. Veen, A. Kuijk, P. Versluis, H. Husken, and K. P. Velikov, *Phase Transitions in Cellulose Microfibril Dispersions by High-Energy Mechanical Deagglomeration,* Langmuir **30**, 13362 (2014).

[7] S. J. Veen, P. Versluis, A. Kuijk, and K. P. Velikov, *Microstructure and rheology of microfibril–polymer networks,* Soft Matter **11**, 8907 (2015).

[8] D. de Kort, S. Veen, H. Van As, D. Bonn, K. Velikov, and J. van Duynhoven, *Yielding and flow of cellulose microfibril dispersions in the presence of a charged polymer,* Soft Matter (2016), 10.1039/c1sm05495c.

[9] E. Saarikoski, T. Saarinen, J. Salmela, and J. Seppälä, *Flocculated flow of microfibrillated cellulose water suspensions: An imaging approach for characterisation of rheological behaviour,* Cellulose **19**, 647 (2012).

[10] M. Martínez-Sanz, F. Pettolino, B. Flanagan, M. J. Gidley, and E. P. Gilbert, *Structure of cellulose microfibrils in mature cotton fibres,* Carbohydrate Polymers **175**, 450 (2017).

[11] J. Su, V. S. Raghuwanshi, W. Raverty, C. J. Garvey, P. J. Holden, M. Gillon, S. A. Holt, R. Tabor, W. Batchelor, and G. Garnier, *Smooth deuterated cellulose films for the visualisation of adsorbed bio-macromolecules,* Scientific Reports **6**, 36119 (2016).

[12] S. Bhagia, Y. Pu, B. R. Evans, B. H. Davison, and A. J. Ragauskas, *Hemicellulose characterization of deuterated switchgrass,* Bioresource Technology **269**, 567 (2018).

[13] R. A. Russell, C. J. Garvey, T. A. Darwish, L. J. R. Foster, and P. J. Holden, *Biopolymer Deuteration for Neutron Scattering and Other Isotope-Sensitive Techniques,* in *Methods in Enzymology*, Vol. 565 (Elsevier Inc., 2015) 1st ed., pp. 97–121.

[14] A. Sokolova, A. E. Whitten, L. de Campo, J. Christoforidis, A. Eltobaji, J. Barnes, F. Darmann, and A. Berry, *Performance and characteristics of the BILBY time-of-flight small-angle neutron scattering instrument,* Journal of Applied Crystallography **52**, 1 (2019).

[15] B. Hammouda, *A new Guinier-Porod model,* Journal of Applied Crystallography **43**, 716 (2010).

[16] O. M. Astley, E. Chanliaud, a. M. Donald, and M. J. Gidley, *Structure of Acetobacter cellulose composites in the hydrated state.* International journal of biological macromolecules **29**, 193 (2001).

[17] M. Iguchi, S. Yamanaka, and A. Budhiono, *Bacterial cellulose - a masterpiece of nature's arts,* Journal of Materials Science **35**, 261 (2000), arXiv:bk-12 .

[18] K. Zhang, *Illustration of the development of bacterial cellulose bundles/ribbons by Gluconacetobacter xylinus via atomic force microscopy,* Applied Microbiology and Biotechnology **97**, 4353 (2013).

[19] M. Martínez-Sanz, M. J. Gidley, and E. P. Gilbert, *Hierarchical architecture of bacterial cellulose and composite plant cell wall polysaccharide hydrogels using small angle neutron scattering,* Soft Matter **12**, 1534 (2016).

[20] M. Martínez-Sanz, D. Mikkelsen, B. Flanagan, M. J. Gidley, and E. P. Gilbert, *Multiscale model for the hierarchical architecture of native cellulose hydrogels,* Carbohydrate Polymers **147**, 542 (2016).

[21] M. Martínez-Sanz, D. Mikkelsen, B. M. Flanagan, C. Rehm, L. de Campo, M. J. Gidley, and E. P. Gilbert, *Investigation of the micro- and nano-scale architecture of cellulose hydrogels with plant cell wall polysaccharides: A combined USANS/SANS study,* Polymer **105**, 449 (2016).

[22] B. Tian, V. Garcia Sakai, C. Pappas, A. J. van der Goot, and W. G. Bouwman, *Fibre formation in calcium caseinate influenced by solvent isotope effect and drying method – A neutron spectroscopy study,* Chemical Engineering Science **207**, 1270 (2019).

[23] S. Scheiner and M. Čuma, *Relative Stability of Hydrogen and Deuterium Bonds,* Journal of the American Chemical Society **118**, 1511 (1996).

[24] L. Yu, G. E. Yakubov, M. Martínez-Sanz, E. P. Gilbert, and J. R. Stokes, *Rheological and structural properties of complex arabinoxylans from Plantago ovata seed mucilage under non-gelled conditions,* Carbohydrate Polymers **193**, 179 (2018).

SUMMARY

Humanity needs to increase use of renewable sources of materials and energy. As further discussed in Chapter 1, biomass can be used for both of these needs. Cellulose is the main component of biomass. Understanding the multi-level hierarchical structure of cellulose holds the key to multiple applications of this material.

One of the promising applications of lignocellulsic biomass is the production of bio-ethanol as a replacement for fossil fuels. Yearly production of biomass could potentially supply enough bio-ethanol to completely replace gasoline. However, it would require dramatic increase in the efficiency of the bioethanol production. The main obstacle to the development of bioethanol production into a sustainable process is the recalcintrance of cellulose which was developed throughout entire plant evolution. In order to overcome this obstacle an important step was incorporated into the process, i.e. pretreatment of biomass. A multitude of pretreatments have been developed and applied to disrupt the structure of lignocellulosic biomass. However it is still not clear, which structural parameters are responsible for the success of a certain pretreatment technique.

Chapter 2 demonstrates a structural study of poplar biomass before and after acid pretreatment. In order to comprehend all levels of organizations within the material, we have applied a range of techniques, including microscopy, small-angle scattering and diffraction of X-rays. The structural studies were supported by the investigation of the performance of the biomass in the conversion of cellulose into glucose. The main parameters responsible for the efficiency of biomass conversion are specific surface area, which is mostly defined by the microscopic particle sizes of the materials, and the biomass crystallinity. Our findings suggest that an increase in specific surface area makes the material better accessible for enzymes, while decrease in crystallinity makes it easier to digest by enzymes.

Microfibrillated cellulose, obtained by disruption of cellulose fibers, can be applied for production of low-caloric food. Since food materials undergo multiple mixing and shearing steps during production and consumption, it is important to ascertain stability of the MFC material under such conditions. In order to investigate the structure of MFC under shear, we have designed a shear-SAXS experiment.

In Chapter 3 we discuss current developments in the sample environment for small-angle scattering X-ray and neutron experiments on the materials under shear. In our search for a sample environment which would satisfy our experimental needs we have discovered that not a single piece of equipment designed before could be used for both X-ray and neutron experiment. Moreover, most of the shear-cell could not be used for experiment with spatial resolution along the shear gradient direction of the cell. In order to avoid creating multiple devices for each specific experiment, we have designed our Shear-SAS cell in such a way that it can be used for both, X-ray and neutron scattering experiments, and be easily modified to accommodate several different rheological geometries.

An application of the shear-cell for investigation of microfibrillated citrus fiber is described in Chapter 4. The first question which was answered in this study was whether MFC would align in the shear field. The performed experiment has clearly shown random orientation of the microfibrils under shear rates up to 300 s^{-1}. The second question was concerning compaction of the cellulose fibrils in the flocs formed under shear and the possibility of agglomeration of the fibrils. The flocs did not substantially change their fractal dimension at all the applied shear-rates and at all the positions across the gap. It suggests that the material is very stable and can be readily used under the applied experimental conditions.

A possibility for application of contrast variation in combination with small-angle neutron scattering was considered in Chapter 5. It was found that mesostructure of hydrogenated bacterial cellulose from different sources is very similar. However, the mesostructure of the deuterated material is found to be substantially different, which results in strong agglomeration and completely altered rheological properties. This shows that contrast variation in SANS is not always possible to determine arrangements of different components.

SAMENVATTING

De mensheid moet meer gebruik maken van hernieuwbare bronnen van materialen en energie. Zoals nader besproken in hoofdstuk 1, kan biomassa voor beide doeleinden worden gebruikt. Cellulose is het hoofdbestanddeel van biomassa. Inzicht in de hiërarchische structuur van cellulose op meer niveaus is de sleutel tot meerdere toepassingen van dit materiaal.

Een van de veelbelovende toepassingen van lignocellulosebiomassa is de productie van bio-ethanol als vervanging voor fossiele brandstoffen. De jaarlijkse productie van biomassa kan mogelijk voldoende bio-ethanol opleveren om benzine volledig te vervangen. Het zou echter een dramatische toename van de efficiëntie van de productie van bio-ethanol vergen. Het belangrijkste obstakel voor de ontwikkeling van de productie van bio-ethanol tot een duurzaam proces is de recalcitrantie van cellulose die gedurende de hele evolutie van de plant is ontwikkeld. Om dit obstakel te overwinnen werd een belangrijke stap in het proces opgenomen: voorbehandeling van de biomassa. Er is een groot aantal voorbehandelingen ontwikkeld en toegepast om de structuur van lignocellulosebiomassa te verbreken. Het is echter nog steeds niet duidelijk welke structuurparameters verantwoordelijk zijn voor het succes van een bepaalde voorbehandelingstechniek.

Hoofdstuk 2 demonstreert een onderzoek naar de structuur van populierbiomassa voor en na voorbehandeling met zuur. Om alle niveaus van organisatie binnen het materiaal te begrijpen, hebben we een aantal technieken toegepast, waaronder microscopie, kleine hoekverstrooiing en diffractie van röntgenstralen. De studies naar de structuur werden ondersteund door het onderzoek naar de prestaties van de biomassa bij de omzetting van cellulose in glucose. De belangrijkste parameters die verantwoordelijk zijn voor de efficiëntie van biomassaconversie zijn soortelijk oppervlak, dat meestal wordt bepaald door de microscopische deeltjesgroottes van de materialen, en de kristalliniteit van de biomassa. Onze bevindingen suggereren dat een toename in soortelijk oppervlak het materiaal beter toegankelijk maakt voor enzymen, terwijl afname in kristalliniteit het gemakkelijker te verteren maakt door enzymen.

Microfibrillaire cellulose, verkregen door het opbreken van cellulosevezels, kan worden toegepast voor de productie van caloriearm voedsel. Omdat voedingsmaterialen tijdens het productieproces en tijdens consumptie meerdere meng- en vervormingstappen ondergaan, is het belangrijk om de stabiliteit van het MFC-materiaal onder dergelijke omstandigheden te bepalen. Om de structuur van MFC onder afschuiving te onderzoeken, hebben we een shear-SAXS-experiment ontworpen.

In hoofdstuk 3 bespreken we de huidige ontwikkelingen in de monsteromgeving voor röntgen- en neutronenexperimenten met kleine hoekverstrooiing aan materialen onder afschuiving. Bij onze zoektocht naar een omgeving die aan onze experimentele behoeften zou voldoen, hebben we ontdekt dat geen enkel eerder-ontworpen apparaat kon worden gebruikt voor zowel röntgen- als neutronenexperimenten. Bovendien kon het

grootste deel van de afschuifcel niet worden gebruikt voor experimenten met ruimtelijke resolutie in de richting van het afschuifgradiënt in de cel. Om te voorkomen dat er voor elk specifiek experiment meerdere apparaten worden gemaakt, hebben we onze Shear-SAS-cel zo ontworpen dat deze kan worden gebruikt voor zowel röntgen- als neutronenverstrooiingsexperimenten en eenvoudig kan worden aangepast om tegemoet te komen aan verschillende reologische geometrieën.

Een toepassing van de afschuifcel voor onderzoek naar microfibrillaire citrusvezels wordt beschreven in hoofdstuk 4. De eerste vraag die in deze studie werd beantwoord, was of MFC zou uitlijnen in het afschuifveld. Het uitgevoerde experiment heeft duidelijk een willekeurige oriëntatie van de microfibrillen getoond bij afschuifsnelheden tot 300 s^{-1}. De tweede vraag had betrekking op de verdichting van de cellulosefibrillen in de onder afschuiving gevormde vlokken en de mogelijkheid van agglomeratie van de fibrillen. De vlokken veranderden hun fractale dimensie niet wezenlijk bij alle toegepaste afschuifsnelheden en bij alle posities over de opening heen. Het suggereert dat het materiaal zeer stabiel is en gemakkelijk kan worden gebruikt onder de toegepaste experimentele omstandigheden.

5

De mogelijkheid contrastvariatie toe te passen in combinatie met kleine-hoekneutronenverstrooiing werd overwogen in hoofdstuk 5. Het bleek dat de mesostructuur van gehydrogeneerde bacteriële cellulose uit verschillende bronnen erg op elkaar lijkt. De mesostructuur van het gedeutereerde materiaal blijkt echter aanzienlijk te verschillen, hetgeen resulteert in sterke agglomeratie en volledig veranderde reologische eigenschappen. Dit laat zien dat contrastvariatie in SANS niet altijd mogelijk is teneinde de rangschikking van de verschillende componenten te bepalen.

Краткое изложение

Человечество должно расширить использование возобновляемых источников материалов и энергии. Как более подробно обсуждается в главе 1, биомасса может использоваться для обеих этих потребностей. Целлюлоза является основным компонентом биомассы. Понимание многоуровневой иерархической структуры целлюлозы является ключом к разнообразным применениям этого материала.

Одним из перспективных применений лигноцеллюлозной биомассы является производство биоэтанола в качестве замены ископаемого топлива. Ежегодное производство биомассы может потенциально обеспечить достаточное количество биоэтанола для полной замены бензина. Тем не менее, это потребует резкого повышения эффективности производства биоэтанола. Основным препятствием для превращения производства биоэтанола в энергетически эффективный процесс является устойчивость целлюлозы к воздействиям внешней среды, которая развивалась на протяжении всей эволюции растений. Чтобы преодолеть это препятствие, в процесс был включен важный шаг – предварительная обработка биомассы. Множество способов предварительной обработки было разработано и применено для разрушения структуры лигноцеллюлозной биомассы. Однако до сих пор не ясно, какие структурные параметры ответственны за успех определенной методики предварительной обработки.

Глава 2 демонстрирует структурное исследование биомассы тополя до и после предварительной обработки кислотой. Чтобы понять все уровни организации в материале, мы применили целый ряд методов, включая микроскопию, малоугловое рассеяние и дифракцию рентгеновских лучей. Структурные исследования были подтверждены исследованием продуктивности биомассы в реакции конверсии целлюлозы в глюкозу. Основными параметрами, определяющими эффективность преобразования биомассы, являются удельная площадь поверхности, которая в основном определяется размерами микроскопических частиц материалов и кристалличностью биомассы. Наши результаты показывают, что увеличение удельной поверхности делает материал более доступным для ферментов, а снижение кристалличности облегчает его усвоение ферментами.

Микрофибриллированная целлюлоза, полученная путем разрушения целлюлозных волокон, может применяться для производства низкокалорийной пищи. Поскольку пищевые материалы подвергаются многочисленным стадиям смешивания и резки во время производства и потребления, важно установить стабильность материала МФЦ в таких условиях. Чтобы исследовать структуру МФЦ при сдвиговой деформации, мы разработали эксперимент по малоугловому рассеянию рентгеновских лучей на материалах находящихся под воздействием сдвиговой деформации.

В главе 3 мы обсуждаем текущие разработки в области экспериментальных ячеек для малоуглового рассеяния рентгеновских и нейтронных экспериментов на материалах при сдвиге. В нашем поиске ячейки, которая бы удовлетворяла нашим экспериментальным потребностям, мы обнаружили, что ни одна описанная ячейка из разработанный ранее, не может быть использована как для рентгеновского, так и для нейтронного эксперимента. Кроме того, большая часть описанных ячеек не может использоваться для эксперимента с пространственным разрешением вдоль направления градиента сдвига ячейки. Чтобы избежать создания нескольких устройств для каждого конкретного эксперимента, мы спроектировали нашу ячейку для малокглового рассеяния на материалах находящихся под действием сдвиговой деформации таким образом, чтобы ее можно было использовать как для экспериментов по рентгеновскому и нейтронному рассеянию, так и для ее легкой модификации с учетом нескольких различных реологических геометрий.

Применение сдвиговой ячейки для исследования микрофибриллированного цитрусового волокна описано в главе 4. Первый вопрос, на который был дан ответ в этом исследовании, заключался в том, будут ли волокна МФЦ выстраиваться вдоль направлению сдвига. Проведенный эксперимент четко показал случайную ориентацию микрофибрилл при скоростях сдвига до 300 $с^{-1}$. Второй вопрос касался уплотнения целлюлозных фибрилл в хлопьях, образованных при сдвиге, и возможности агломерации фибрилл. Хлопья существенно не изменили свой фрактальный размер при всех приложенных скоростях сдвига и во всех точках вдоль градиента сдвига. Это говорит о том, что материал очень стабилен и может быть легко использован в условиях эксперимента.

Возможность применения вариации контраста в сочетании с малоугловым рассеянием нейтронов рассматривалась в главе 5. Было обнаружено, что мезоструктура гидрогенизированной бактериальной целлюлозы из разных источников очень похожа. Однако обнаружено, что мезоструктура дейтерированного материала существенно отличается, что приводит к сильной агломерации и полностью измененным реологическим свойствам. Это показывает, что изменение контраста в SANS не всегда позволяет определить расположение различных компонентов.

ACKNOWLEDGEMENTS

I would like ot thank a number of people for their contributions to this thesis.

First of all, I would like to thank my supervisor and a good friend of mine, Wim Bouwman, without whom this thesis would not have been possible. Wim, thank you for the opportunity to work on this project and for your trust in my ability to finish it. It was an honor to be guided into science by you. I admire your ability to keep a healthy work-life balance, your unlimited patience and your passion for teaching.

Secondly, I would like to thank Bei Tian, who has been in the same boat with me for the last four years. It was always interesting to talk with you, since we could disagree even on the matters which I have never considered questionable. I have learned so much from our discussions that I have enough material for a thesis on cultural differences, should I ever consider starting such a venture again.

Thirdly, I am greatful to our industrial partners from DSM, Unilever, TNO, and NIZO: Margot Schooneveld-Bergmans, John van Duynhoven, Ruud den Adel, Mazhar Nazim, Kees Van Malssen, Adrian Voda, Arjen Bot, Adriana Carvalho de Souza, Loes Bevers, Joost van 't Hoff, Joyce Heuvink, Maaike Nieuwland, Hans Tromp. Margot and John actively participated in planning, design and discussions of the results of my experiments, Ruud had helped me to get started with SAXS experiments and data treatment and shared many interesting thoughts about work and life in general. Adrian, Arjen, Maaike and Hans were very attentive and full of ideas during our projcet meetings.

We had a very fruitful collaboration with people from Wageningen University and Research: Tatiana Nikolaeva, Erik van der Linden, Paul Venema, Atze Jan Van Der Goot, Daan de Kort, Jinfeng Peng, and Harry Baptist. Thank you Tatiana for keeping optimistic atmosphere during sleepless nights at ESRF, endless drive through some side roads in the middle of England, and even after finding out about measurements with closed shutter.

Also, I would like to thank all the colleagues from RID: Ad van Well, Adrie Laan, Aldo Hennik, Alexandros Vasileiadis, Andrei Kuzmin, Anton Lefering, Ashutosh Pati, Beien Wang, Ben Harrison, Bert Zwart, Bowei Huang, Catherine Pappas, Chris Duif, Denis Bykov, Dimitrios Bessas, Ekkes Brück, Ernst van der Wal, Fahad Al-Sayyari, Fulvio Bertocchi, Giacomo Borghi, Henk Schut, Henk van Doorn, Ignatz de Schepper, Ilse van der Kraaij, Jaen Ocadiz Flores, Jeroen Koning, Jeroen Plomp, Jouke Heringa, Jurrian Bakker, Kees Goubitz, Koos van Kammen, Lambert van Eijck, Lars Bannenberg, Maarten Plokker, Maik Butterling, Marco Tiberga, Marnix Wagemaker Martijn de Boer, Matteo Gamarino, Michael Maschek, Michel Steenvoorden, Michel Thijs, Minh Phuong Nguyen, Nicole Banga, Niek de Klerk, Niels van Dijk, Paul Gubbens, Peter-Paul Harks, Robin de Kruijff, Sara Mastromarino, Stephan Eijt, Steven Parnell, Swapna Ganapathy, Theo Rekveldt, Tomas Verhallen Trudy Beentjes, Valentina Valori, Violetta Arszelewska, Viviam Marques Pereira, Walter Legerstee, Weronika Wolszczak, Wicher Kraan, Xinmin You, Xue-Fei Miao, Yifan Fu, Zhaolong Li, Zhou Zhou, and Zoltan Perko. Thank you, Katia, your trust in my abilities and for providing me with every opportunity to stay out of my comfort zone.

Thank you, Chris, for your hospitality and enthusiasm which you shed on me ever since I first came to Delft for my first SESANS experiments. Thank you, Denis, for pulling me over the first threshold on the way to Delftian society and lifestyle. Thank you, Henk and Koos, for always keeping a bottle of Paulaner for me in 't Koepeltje and for introducing me to the rich Dutch beer culture. Thank you, Ignatz, for your help with calculation of scattering models, your experience in such calculations is really impressive. Ilse and Nicole, thank you for taking care of paperwork related to my project, stay and trips, and for your patience and persistence in improving my Dutch. Thank you, Jeroen for your help in acquiring and maintaining my race bike. Jouke, thank you for your help with all of my computer-related issues and with translations. Lambert and Lars, thank you for being a great company in the office, in the bar and in various swimming reservoirs. Thank you, Wicher, for your eager interest in my work and life and for keeping me updated on development of my previous project.

While working on this thesis I have got to supervise some amazing bachelor students: Fieneke van der Voort, Sebastian Wendt, Lisa de Kluijver. It was a deep pleasure to work with you. I am happy to have been able to contribute to your education and am grateful for the help and support I have got back from you.

Most of the experiments described in this thesis were performed at various international facilities. Success of these experiments was largely determined by support from local scientists at the facilities. I am grateful to Adam Washington, Najet Mahmoudi, Rob Dalgleish, Sarah Rogers, and Stephen King from ISIS Neutron and Muon Source, Anna Sokolova, Elliot Paul Gilbert, Jamie Schulz, Jitendra Mata, and Norman Booth from Australian Nuclear Science and Technology Organisation, Daniel Hermida Merino Michael Sztucki, Theyencheri Narayanan, Vadim Dyadkin, and Wim Bras from European Synchrotron Radiation Facility.

Large part of my expertise in scattering of neutrons and X-ray is based on the knowledge and experience I had gained during my time Petersburg Nuclear Physics Institute. I am grateful to people who introduced me to these techniques: Leonid Axelrod, Sergey Grigoriev, Vladimir Zabenkin, and Yurii Chetverikov. Thank you, Sergey, for noticing my potential and giving me the opportunity to enter this field.

Last, but not least I would like to thank the people who were around me outside working hours and who did their best to keep me sane especially during the toughest times in the last four years: Aldo Hennik, Caroline Ryzhkouskaya, Denis Rusakovich, Fahad Al-Sayyari, Jan Chau, John Eriksson, Koos van Kammen, Maaike Jantine van Veldhuizen, Maikel Lourenssen, Michael Rein, Milen Stefanov, Mikhail Alekhin, Mikhail Shipilin, Natalia Velichko, Nikos Poulopoulos, Olga Foin, Pavlo Bazilinskyy, Rody Saito-Snijder, Sara Mastromarino, Sharida Wekker, Tatiana Velichko, and Viktoria Kim. It is always great to meet and do some sports, or share a drink/food/trip with you. Thanks to all of you, I have always had some nice distractions from work, which resulted in increase of my long-term productivity.

I am a very lucky person to have met such a large number of incredibly good people. Without any doubt, not all of these who deserve to be acknowledged have been, and I sincerely apologize for it. Should you have been unjustly not mention – come and claim a compensation in beer- or coffee equivalent.

CURRICULUM VITÆ

Evgenii VELICHKO

17-10-1988 Born in Nizhny Tagil, USSR.

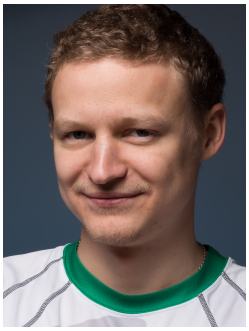

EDUCATION AND EMPLOYMENT

1995–2005	Ordinary school #64 in Nizhny Tagil
2005–2009	Bachelor of Science in Chemistry URAL STATE UNIVERSITY
2005–2006	Sales promoter COMMERCIAL NETWORK KUPETS
2006–2007	Passenger car attendant RUSSIAN RAILWAYS
2008–2011	Laboratory assistant URAL STATE UNIVERSITY
2009–2011	Master of Science in Chemistry URAL FEDERAL UNIVERSITY
2011–2014	Senior laboratory assistant PETERSBURG NUCLEAR PHYSICS INSTITUTE
2014–2015	Junior researcher PETERSBURG NUCLEAR PHYSICS INSTITUTE
2015-2019	PhD candidate DELFT UNIVERSITY OF TECHNOLOGY

Thesis: Small-angle scattering by cellulose. Structural changes in cellulosic materials under chemical and mechanical treatments

Promotor: Dr. W. G. Bouwman

List of Publications

11. **Evgenii Velichko**, Bei Tian, Tatiana Nikolaeva, Jeroen Koning, John van Duynhoven, and Wim G. Bouwman *A versatile shear cell for investigation of structure of food materials under shear*, Colloids and Surfaces A: Physicochemical and Engineering Aspects **566**, 21-28 (2019).

10. Tatiana Nikolaeva, Ruud den Adel, **Evgenii Velichko**, Wim G. Bouwman, Daniel Hermida-Merino, Henk van As, Adrian Voda, and John van Duynhoven *Networks of micronized fat crystals grown under static conditions*, Food & Function **9**, 2102-2111 (2018).

9. **Evgenii Velichko**, Aleksandr Buyanov, Natalia Saprykina, Yurii Chetverikov, Chris Duif, Wim G. Bouwman, and Ruslan Smyslov *High-strength bacterial cellulose–polyacrylamide hydrogels: Mesostructure anisotropy as studied by spin-echo small-angle neutron scattering and cryo-SEM*, European Polymer Journal **88**, 269-279 (2017).

8. Ekaterina Iashina, **Evgenii Velichko**, Mikhail Filatov, Wim G. Bouwman, Chris Duif, Annie Brulet, and Sergei Grigoriev *Additive scaling law for structural organization of chromatin in chicken erythrocyte nuclei*, Physical Review E **96**, 012411 (2017).

7. Konstantin Pavlov, **Evgenii Velichko**, Vladimir Zabenkin, Wicher Kraan, Chris Duif, Wim G. Bouwman, Zoia Michailovskaya, Elena Buyanova, and Sergei Grigoriev *Investigation of the Closed Porosity of Functional Ceramic Materials by Spin-Echo Small-Angle Neutron Scattering*, Journal of Surface Investigation: X-ray, Synchrotron and Neutron Techniques **11**, 92-98 (2017).

6. Alexandr Ostroushko, Lidiya Adamova, Ekaterina Eremina, Kirill Grzhegorzhevskii, **Evgenii Velichko**, Savva Bogdanov, and Aleksei Pirogov *Thermodynamics of acetone sorption from vapor phase by Keplerate and toroid polyoxomolybdate nanoclusters*, Russian Journal of Physical Chemistry A **91**, 1313-1318 (2017).

5. Viktor Ukleev, Reda Moubah, Dmitrii Baranov, Sergei Gastev, Boris Krichevtsov, **Evgenii Velichko**, Nikita Kulesh, Yurii Chetverikov, and Sergei Grigoriev *Imprinted Magnetic Anisotropy and Zigzag Domain Structure of Amorphous TbCo Films*, Journal of Superconductivity and Novel Magnetism **28**, 3571-3577 (2015).

4. Wicher Kraan, Leonid Akselrod, Yurii Chetverikov, Sergei Grigoriev, Evgenii Moskwin, Vasily Piyadov, Kyaw Thu Set, Arsen Sumbatyan, **Evgenii Velichko**, and Vladimir Zabenkin *Present status and prospects for Spin-Echo Small-Angle Neutron Scattering (SESANS) at PIK neutron source*, Journal of Surface Investigation. X-ray, Synchrotron and Neutron Techniques **8**, 1035-1043 (2014).

3. **Evgenii Velichko**, Yurii Chetverikov, Leonid Akselrod, Vladimir Zabenkin, Vasily Piyadov, Arsen Sumbatyan, Wicher Kraan, and Sergei Grigoriev *Spin-echo small-angle neutron scattering device: Test experiment using SiO2 colloidal particles*, Journal of Surface Investigation. X-ray, Synchrotron and Neutron Techniques **7**, 401-406 (2013).

2. **Evgenii Velichko**, Zoia Mikhailovskaya, Maria Morozova, Elena Buyanova, Yulia Emel'yanova, Sofia Petrova, and Vladimir Zhukovskii *Synthesis, region of existence, structural characteristics, and conductivity of BI(CR, FE)VOX solid solutions*, Russian Journal of Electrochemistry **47**, 563-568 (2011).

1. Yulia Emel'yanova, Maria Morozova, Zoia Mikhailovskaya, **Evgenii Velichko**,Elena Buyanova, and Vladimir Zhukovskii *Synthesis processes and transport properties of solid solutions in the Bi2O3-GeO2-V2O5 system*, Russian Journal of Electrochemistry **45**, 382-387 (2009).